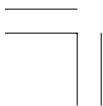
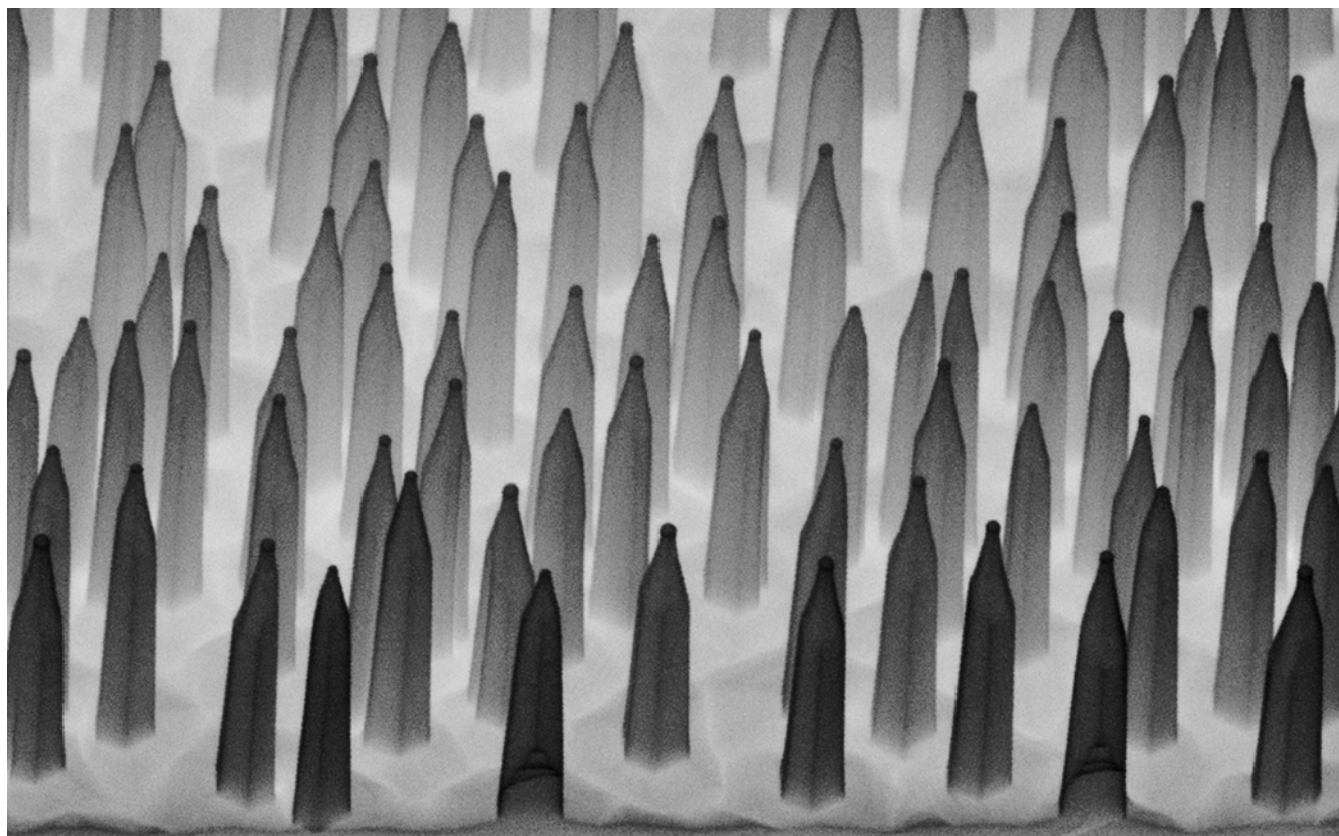


# **Scientific report 2014-2015**

 **CNRNANO**  
ISTITUTO NANOSCIENZE CONSIGLIO NAZIONALE DELLE RICERCHE





# **Scientific report 2014-2015**

 **CNRNANO**  
ISTITUTO NANOSCIENZE CONSIGLIO NAZIONALE DELLE RICERCHE

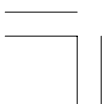
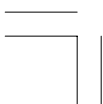




Table of contents

foreword	3
organization	5
highlights	7
publications	85
projects & grants	95
Cnr Nano life	101
people	107
contacts	112
credits	113



## Foreword

This is the third biennial report of the Istituto Nanoscienze of the Italian National Research Council (Cnr Nano). It shows some scientific highlights, that are representative of our main research areas: from the fundamental understanding of matter and materials at the nanoscale to frontier quantum technologies, from nanodevices and nanosystems to emerging phenomena and applications of relevance in biology and medicine as well as ICT, energy, and manufacturing sectors.

A signature of the Institute is its multidisciplinary approach and the convergence of scientists endowed with different and complementary backgrounds. This cultural richness reflects in the variety of technologies and instruments present in the Institute and by the broadness of the spectrum of research covered. The close interaction between experimental, theoretical and computational components continues to be a special strength of Cnr Nano. The impact of our research shows in the large number of publications in high profile journals.

A further achievement in 2014-2015 was a significant increment in the external funding obtained for our research. The dynamic attitude of Cnr Nano researchers led to a large number of highly competitive individual projects such as the European ERC grants (starting, consolidator, and advanced). In particular, three consolidator ERC grants have been granted to CNR Nano during the last call.

Moreover, in the framework of the Horizon 2020 program, several projects have been funded such as Ultraqcl (FET-Open), two Marie Curie fellowships (Supermag and Graflex), and the e-Infra Centre of excellence MaX, coordinated by Cnr Nano. A strategic activity of Cnr Nano is also the participation in the Graphene Flagship which will continue in its second phase. The Institute is now well integrated in regional and local research networks of relevance for the local economic environment: in the last two years several projects have been granted by Regione Toscana and Regione Emilia Romagna and by the Fondazione Cassa di Risparmio di Modena.

A large number of young researchers could join the Institute to work on these national and international projects. Prominent in Cnr Nano is in fact the presence of many postdocs and fixed-term scientists. At the beginning of 2016 the Institute has 66 staff members and about 42 researchers with doctoral and post-doctoral fellowships, in addition to associated scientists and PhD students.

The following pages report information on staff, published papers, funded projects, and the events organized by Cnr Nano in this period. In 2015, a reorganization of Cnr Nano took place, and most of the researchers of the Lecce unit moved to a newly established Cnr site. This transformation offered the opportunity to reshape the research activities of the Nano Institute in the new configuration: the research highlights presented in the following are a good way to represent our research lines.

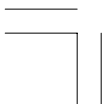
I would like to thank Carmela Iannotta, Elisabetta Narducci, Luisa Neri, Maddalena Scandola, Fabio Della Sala, Stefan Heun, and Paola Luches for their help in making this Report.

A handwritten signature in blue ink that reads "Lucia Sorba".

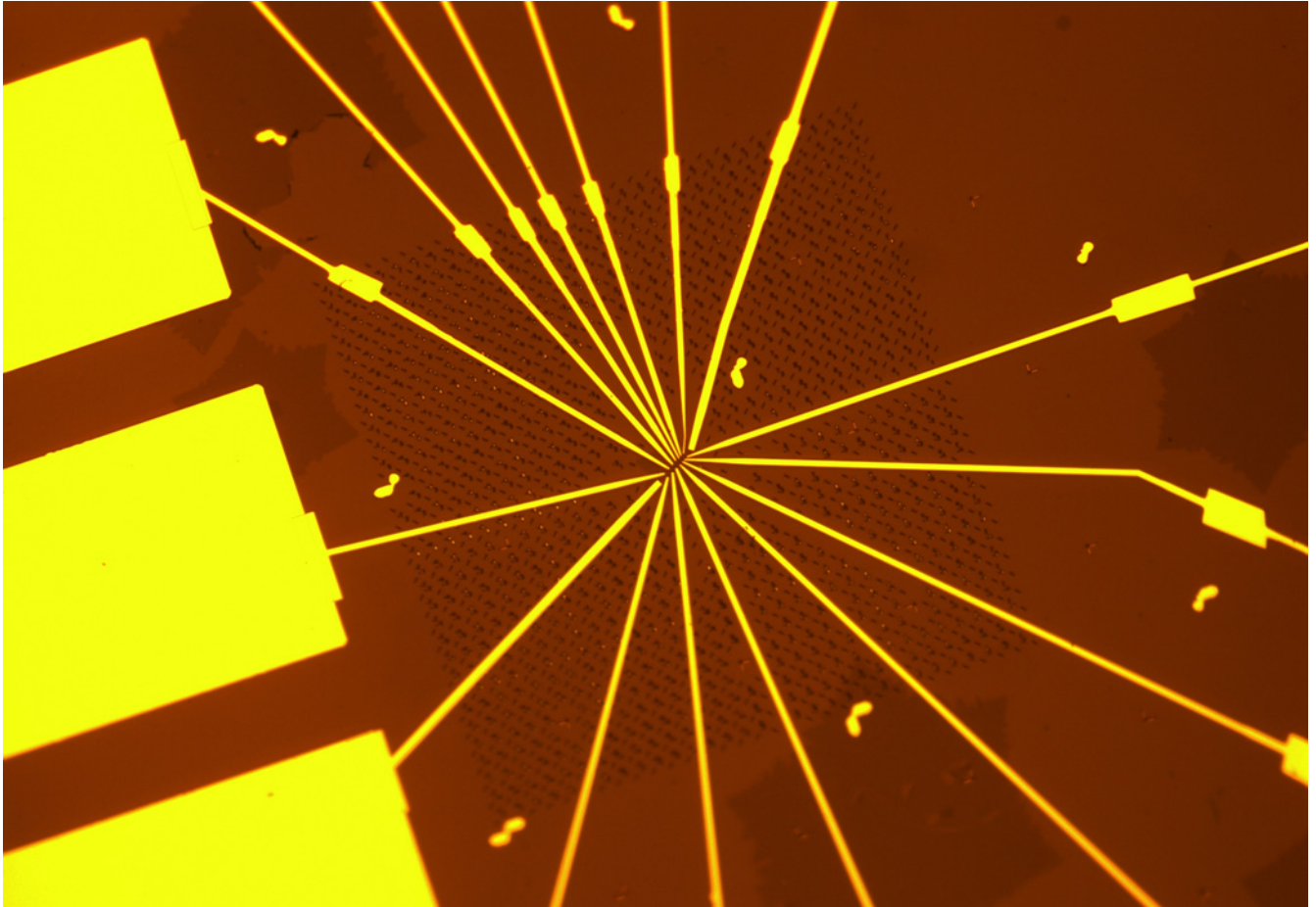
Lucia Sorba  
Director of Institute Nanoscience

## Organization

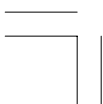
institute director	Lucia Sorba
supervisors of units	Lecce: Dario Pisignano Modena: Elisa Molinari Pisa: Lucia Sorba
administrative director	Maria Grazia Angelini
executive board	Cnr researchers: Giorgia Brancolini, Fabio Della Sala, Stefan Heun, Paola Luches, Gian Michele Ratto, Massimo Rontani  Cnr technical/administrative staff: Luisa Neri  Affiliated researchers: Andrea Alessandrini, Elisa Molinari, Dario Pisignano, Alessandro Tredicucci







# **Highlights Nanotechnology**



## Introduction to Nanotechnology

The main research activities of Cnr Nano in **Nanotechnologies** include:

**Transport:** Quantistic and spin control transport in low dimensional systems, such as nanowires, quantum dots, nanoribbons, quantum Hall systems, are explored in depth. In particular, experimental and theoretical research lines are dedicated to transport phenomena at the nanoscale. Electron transport in nanodevices based on semiconductor, superconductor, 2D (graphene and phosphorene) and hybrid materials is investigated to clarify the peculiar quantum effects at this scale. Heat interference and heat diffraction studies in Josephson-based superconducting circuits and non-equilibrium dynamics are also deeply investigated.

**Advanced photonics and optoelectronics:** The development of innovative and fundamental elements for emission (quantum cascade lasers, light-emitting polymer nanofibers), propagation and detection of light (nanowires, graphene and 2D materials-based sensors) in the visible and THz frequency range; nano-optics; advanced lithographies and three-dimensional additive manufacturing methods on organic materials and nanocomposites, all are well developed and established research activities of the Institute.

**Optomechanics:** The use of electromagnetic radiation, for exploring the possibility to employ the “optical forces” for the observation of quantum effects in macroscopic objects, is a recent research activity. Devices based on double-metal and III-V heterostructured semiconductor layers are fabricated and allow the emission wavelength of THz lasers to be tuned and controlled, through modulation at the frequency of mechanical eigenmodes, ranging from kHz to tens of MHz.

**Polaritronics:** Controlling the way light interacts with material excitations is at the heart of cavity quantum electrodynamics (cavity QED). Waveguide structures are investigated in the regime from weak to ultrastrong light-matter interaction, where a novel class of extremely non-adiabatic phenomena becomes observable, and coherent photon population can be monitored while converting to cavity polaritons during abrupt switching

## OPTICAL PROPERTIES OF ORGANIC NANOWIRES

Organic nanowires are emerging as novel building blocks for photonic devices and circuits. Their integration in fully functional systems requires the development of both individual organic wires and complex arrays based on them, with tailored optical properties. We have investigated the optical properties of composite organic wires and filaments embedding various species of chromophores, including self-assembling rotaxane-type molecular systems. These composite materials are relevant for applications in optical amplifiers, lasers, chemical sensors and environmentally responsive materials.

Miniaturized photonics is acquiring a prominent role in many applications, where the exploitation of the properties of light interacting with nanostructured materials (such as field enhancement and optical scattering) may significantly improve the performance of the produced devices compared to macroscopic systems. In this context, the use of organic nanowires is particularly advantageous, allowing for tailoring optical properties by engineering their molecular components, their individual geometry, and the architecture of macroscopic arrays based on them.

An example of optically-active nanowires developed in our group is shown in Figure 1a-c, where near-infrared (NIR) emitting organic wires were realized by embedding light-emitting molecules in polymer fibers, obtaining optical gain up to  $5\text{ cm}^{-1}$ . The gain properties of macroscopic arrays made by many filaments can be tailored by controlling their assembly

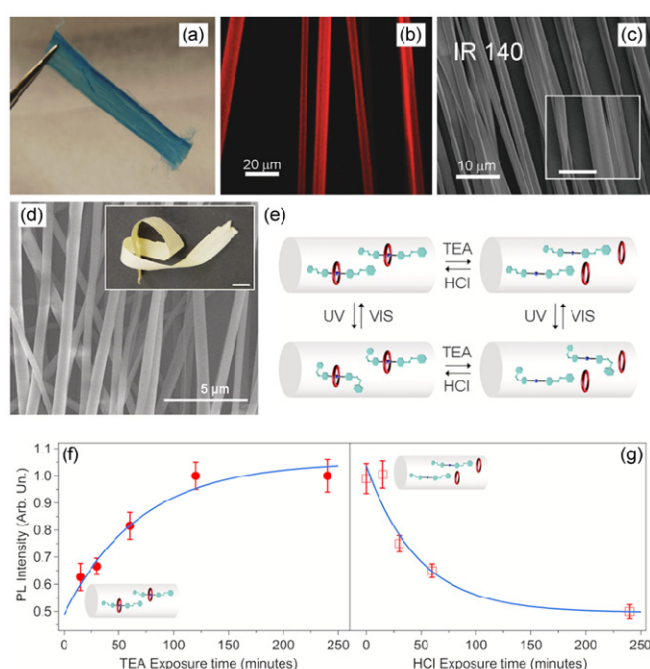


Figure 1.

(a) Photograph and (b) fluorescence confocal micrograph of an array of polymer wires doped with a NIR-emitting dye. (c) Scanning electron microscopy (SEM) images of polymer wires doped with a NIR-emitting dye. Inset scale bar =  $10\text{ }\mu\text{m}$ . Adapted with permission from Ref. [1]. © 2014 WILEY-VCH Verlag GmbH & Co. (d) SEM micrographs of polymer filaments doped with rotaxane-type molecular systems. Inset: photograph of an array made of such wires. Scale bar =  $1\text{ cm}$ . (e) Schematics of the photo-isomerization processes of the azobenzene end-units of the axle and of the chemically-induced dethreading/rethreading processes of the axle and ring molecular components. Photo-isomerization processes occur upon exposure to ultraviolet (UV) and visible (Vis) light, whereas the dethreading/rethreading processes are induced by exposure to base/acid vapours (triethylamine, TEA,

and HCl, respectively). (f)-(g) Photoluminescence (PL) intensity of polymer nanowires doped with molecular motors vs. base (f) and acid (g) vapours exposure times. These data evidence the reversible dethreading/rethreading processes that the axle and ring molecular components undergo inside polymer wires, upon chemical stimulation. Adapted from Ref. [2]. © 2014 American Chemical Society. This is an unofficial adaptation of an article that appeared in ACS publications. ACS has not endorsed the content of this adaptation or the context of its use.

and mutual alignment.

Other examples include stimuli-responsive nanowires, realized by embedding a molecular motor in a polymer matrix (Figure 1d-e). Exposure to base and acid vapors induced the dethreading and rethreading of the molecular components in the solid wires (Figure 1f-g). The light-induced photo-isomerization of the azobenzene molecules was also demonstrated in solid wires, making such composite systems responsive to both optical and chemical external stimuli. Interestingly, the dethreading of the axles from the rings enhanced significantly the Young's modulus of arrays made of aligned wires. These findings demonstrate the possibility of tailoring the macroscopic properties of such composite materials, by controlling the behavior of the molecular constituents at the nanoscale.

The research leading to the most recent of these results has received funding from the European Research Council under the European Union's Seventh Framework Programme (FP/2007-2013)/ERC Grant Agreement n. 306357 (ERC Starting Grant "NANO-JETS").

### Contact person

Andrea Camposeo (andrea.camposeo@nano.cnr.it)

### References

- [1] *Optical gain in the near infrared by light-emitting electrospun fibers*. G. Morello, M. Moffa, S. Girardo, A. Camposeo, and D. Pisignano. *Adv. Funct. Mater.* 24, 5225-5231 (2014).
- [2] *Organic nanofibers embedding stimuli-responsive threaded molecular components*. V. Fasano, M. Baroncini, M. Moffa, D. Iandolo, A. Camposeo, A. Credi, and D. Pisignano. *J. Am. Chem. Soc.* 136, 14245-14254 (2014).

## MOLECULAR SPINTRONICS: GRAPHENE-MEDIATED EXCHANGE COUPLING BETWEEN MOLECULAR NANOMAGNETS AND MAGNETIC SUBSTRATES

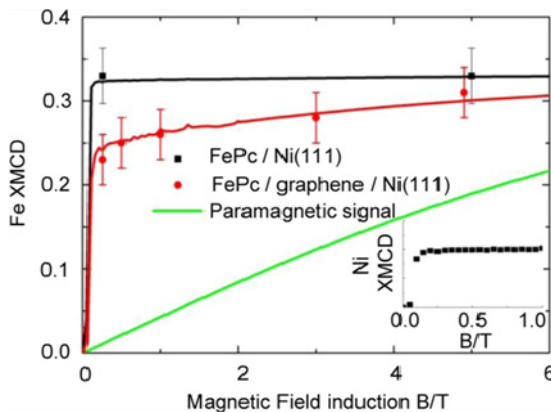
Exploiting the spin of molecular materials holds great promise in a number of possible future applications, ranging from memories for magnetic data storage to quantum computing. In this growing field, the so-called molecular spintronics, one of the key points is the control of the spin properties of the interface between the molecular units and their environment. The mutual interaction between the molecules and a proper substrate can be tuned by, for instance, doping and/or intercalation at the interface and can lead to novel properties and functionalities. In this context we studied, by means of X-ray Magnetic Circular Dichroism (XMCD) and Density Functional Theory (DFT) calculations, the effect of the insertion of a graphene layer between magnetic molecules and a magnetic substrate, addressing the specific role of graphene in the transmission of the spin information at the nanoscale.

We have studied the magnetic exchange coupling between molecular magnets (FePc iron phthalocyanine molecules) and Ni(111) substrates with and without the presence of a graphene layer in between the molecules and the metal surface [1]. Graphene is grown on top of a Ni(111) single crystal in ultra-high vacuum conditions and the molecules are then sublimated in situ. The system is structurally characterized by XPS and STM and its magnetic properties are studied by field-dependent XMCD at low temperature (8 K) at synchrotron facilities. The experimental observations are further analyzed in combination with DFT calculations. We have found that the FePc molecules are strongly modified by the interaction with the Ni surface when they are absorbed directly on the metal substrate. On the other hand, the presence of the graphene interlayer helps in recovering the electronic properties of the pristine molecular units. More interesting, we observed a sizeable magnetic-exchange interaction between the FePc molecules and the magnetization of the Ni substrate with and without the graphene layer. This is visualized by the field-dependent XMCD measurements reported in Figure 1. The role of graphene, which prevents a strong electronic interaction between the molecules and the substrate but at the same time preserve the magnetic coupling, is highlighted in Figure 2: the Carbon  $\pi$ -orbitals hybridize with the underlying Nickel spin-polarization and extend through the interface towards the FePc molecules.

It is interesting to compare these results with a related study we have performed on a

Figure 1.

Field-dependent XMCD intensity at the Fe  $L_3$ -edge for FePc directly on Ni(111) and on graphene/Ni(111). Solid lines are the fitting curves assuming a ferromagnetic coupling between the molecules and the Ni substrate. For comparison, the curve corresponding to a paramagnetic signal (i.e., without coupling) is also shown in solid green. Inset: magnetization of the Ni(111) single crystal substrate. The experimental data evidence the presence of an exchange interaction between the FePc molecules and the Ni substrate which is of ferromagnetic nature both when the molecules are in direct contact with Ni and when a graphene spacer layer is inserted in between.





similar system made of Co-porphyrin (CoP) molecules on the same graphene/Ni(111) substrate [2]. In both systems an interaction of ferromagnetic nature is found when the molecules are directly in contact with the substrate, but the insertion of the graphene layer preserve the sign of the coupling for the case of FePc while it flips to an antiferromagnetic coupling for the CoP molecules. This evidences the role of the graphene orbitals as a “spin filter” combined with the specific spin states of the molecular unit, showing that graphene at the hybrid interface between molecules and metal substrates is a unique platform to study and engineer the spin coupling.

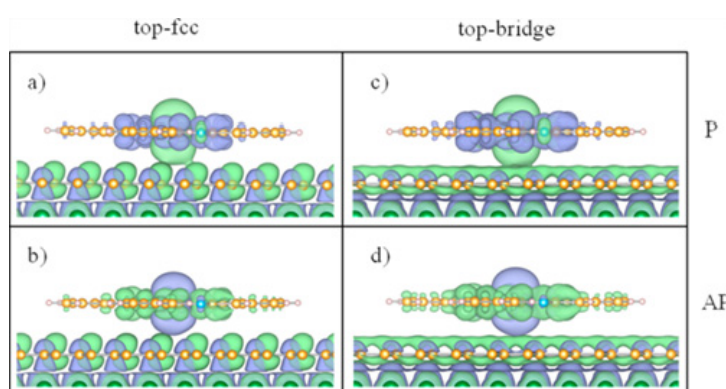


Figure 2.

Three-dimensional contour plots of the spin density distribution at the FePc/graphene/Ni(111) interface for top-fcc (a, b) and top-bridge (c, d) stacking, as calculated by DFT; (a) and (c) are for the parallel, (b) and (d) for the antiparallel coupling between the Fe and Ni spin moments. Light green (light blue) colour refers to an excess of spin up/majority (down/minority) electrons. Our finding suggest that the parallel/graphene orbitals with spin up

ferromagnetic coupling is favoured for both configurations as the graphene orbitals with spin up polarization tend to be closer to the Fe spin state in the FePc molecule.

### Contact person

Andrea Candini (andrea.candini@nano.cnr.it)

### References

- [1] *Ferromagnetic Exchange Coupling between Fe Phthalocyanine and Ni(111) Surface Mediated by the Extended States of Graphene*. A. Candini, V. Bellini, D. Klar, V. Corradini, R. Biagi, V. De Renzi, K. Kummer, N. B. Brookes, U. del Pennino, H. Wende, and M. Affronte. *J Phys Chem C* 118, 17670–17676 (2014).
- [2] *Field-regulated switching of the magnetization of Co-porphyrin on graphene*. D. Klar, S. Bhandary, A. Candini, L. Joly, P. Ohresser, S. Klyatskaya, M. Schleberger, M. Ruben, M. Affronte, O. Eriksson, B. Sanyal, and H. Wende. *Phys Rev B* 89, 144411 (2014).

## SINGLE MOLECULE COOLERS

Proving the preservation of functionality at the molecular scale is still a major challenge, both for the choice of suitable derivatives and protocols and for the employed experimental tools and methods. By using a combined scanning probe (AFM, STM) and spectroscopic methodology (XPS, XAS, XMCD) we show that  $Gd_4M_8$  derivatives (with  $M=Zn^{2+}$ ,  $Ni^{2+}$ ) are robust molecular units which preserve their electronic, magnetic, and thermodynamic properties when deposited on a metallic surface. Namely we measured entropy variation  $\Delta S=[S(6T)-S(0T)]$  exceeding  $8R$  ( $20 \text{ J kg}^{-1} \text{ K}^{-1}$ ) at  $4K$  in isolated  $Gd_4Ni_8$  molecules adsorbed on  $Au(111)$  surface showing a viable route to exploit large magnetocaloric effect at single molecule level.

The changes of thermal properties in magnetic materials upon the application of a magnetic field are known as magnetocaloric effects (MCE). Of particular interest for applications are substances for which the magnetic entropy decreases when a magnetic field is applied. In these cases, an adiabatic demagnetization process provokes a temperature drop, that is a cooling process driven by the magnetic field. The interest for applications is obviously focused on substances with large entropy variation upon application of relatively small magnetic fields. Paramagnetic impurities in alloys or salts are used as coolers at cryogenic temperatures. Unfortunately these materials cannot be simply efficiently scaled at the nanometer size. Nanomagnets and in particular magnetic molecules emerged in the last decade as an alternative route for refrigeration at cryogenic temperatures since they may offer high magnetization and large values of entropy change.

Using an appropriate deposition protocol and combined experimental techniques (STM, AFM, XPS on campus, XAS and XMCD at SOLEIL synchrotron), we show that the  $Gd_4M_8$  ( $M=Zn$ ,  $Ni$ ) molecules remain intact and fully preserve their magneto-thermal properties when dispersed on gold and graphite substrates. The sub-monolayer of  $Gd_4M_8$  ( $M=Zn$ ,  $Ni$ ) molecules have been obtained by immersing  $Au(111)$  or HOPG (Highly Oriented Pyrolytic Graphite) surfaces in a solution of  $Gd_4M_8$  ( $M=Zn$ ,  $Ni$ ). From the isothermal-magnetization curves derived by the dichroic signal at the  $Ni-L_{2,3}$  and  $Gd-M_{4,5}$  edges (Figure 1c), we measured a remarkable magnetocaloric effect, namely  $\Delta S= S(6T) - S(0T)$  exceeds  $8R$  ( $20 \text{ J kg}^{-1} \text{ K}^{-1}$ ) for the whole  $Gd_4Ni_8$  at  $4K$ . These results demonstrate that it is possible by exploiting the magnetic properties of individual molecular units, i.e., paramagnetic

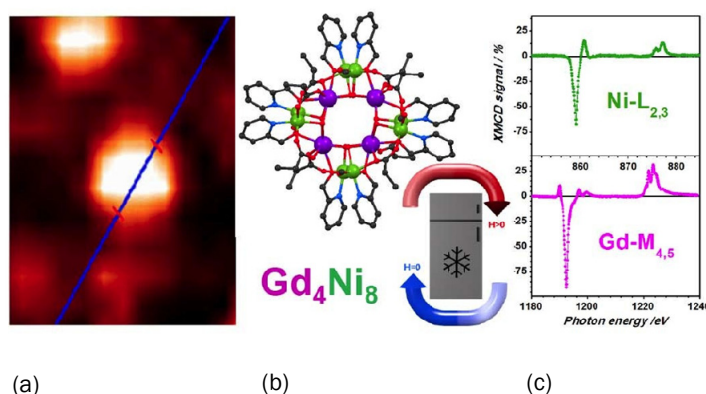


Figure 1.  
(a) STM image and (b) molecular structure of the  $Gd_4M_8$  cluster [colour scheme: Gd, large purple circles; M ( $=Zn$ ,  $Ni$ ), green; O, red; N, blue; C, black]. (c) The XMCD spectra at the  $Ni-L_{2,3}$  and  $Gd-M_{4,5}$  edges, taken at SOLEIL synchrotron at low temperature ( $4K$ ) and in magnetic field ( $6T$ ) on a molecular sub-monolayer, allowed to directly evaluate the magnetic entropy variation -and therefore the magnetocaloric effect- on individual molecule.

organometallic molecules with enhanced magneto-caloric effect, to make them excellent refrigerants at cryogenic temperatures. We found that  $Gd_4Ni_8$  fully retains its features and it exhibits record MCE values. This opens the way to miniaturize devices or composite materials where such a molecule can be used to cool down the whole system.

### Contact people

Valdis Corradini (valdis.corradini@nano.cnr.it)

Marco Affronte (marco.affronte@unimore.it)

### Reference

[1] *Surface investigation on  $Gd_4M_8$  ( $M=Zn, Ni$ ) Single Molecule Coolers*. V. Corradini, A. Ghirri, A. Candini, R. Biagi, U. del Pennino, V. De Renzi, G. Dotti, E. Otero, T. N. Hooper, R. Inglis, E. K. Brechin, and M. Affronte. *Adv. Funct. Mater.* 24, 4782-4788 (2014). Also selected for the Synchrotron SOLEIL Highlights 2014.

## NANOSCALE MANIPULATION OF ELECTRONIC HEAT CURRENTS WITH SUPERCONDUCTING HYBRID DEVICES

The ability to master heat currents at the nanoscale has become an essential request in many fields of nanoscience, including solid state cooling, radiation detection and quantum information. Research activities at Cnr Nano Nest Pisa led to the realization of two fundamental building blocks towards this end: an efficient hybrid thermal diode and a balanced Josephson heat modulator. The first device is able to provide differences of more than two orders of magnitude between the amplitude of heat currents transmitted in the forward and reverse configurations, while the second offers the full control over the phase-coherent component of the thermal current flowing through a Josephson junction.

The evolution of modern electronics has been boosted by the introduction of non-linear elements like interferometers, diodes and transistors. In the last five years, our research group has demonstrated that superconducting hybrid structures at cryogenic temperatures represents an ideal platform to realize the thermal counterpart of these non-linear devices. For instance, a simple normal metal-insulator-superconductor (NIS) junction (see Figure 1a) offers a sizeable asymmetry in the thermal transport due to the temperature dependence of the energy gap in the superconducting density of states. This asymmetry can be increased by connecting the N electrode to a thermalizing cold finger and it can be exploited to realize a thermal diode, i.e., a device that allows heat to flow preferentially in one direction.

A highly efficient thermal diode should provide a difference of at least one order of magnitude between the heat current transmitted in the forward temperature (T) bias configuration ( $J_{fw}$ ) and that generated with T-bias reversal ( $J_{rev}$ ), leading to  $R = J_{fw}/J_{rev} \gg 1$  or  $\ll 1$ .

In previous experiments, a maximum  $R \approx 1.4$  was reported in phononic devices.

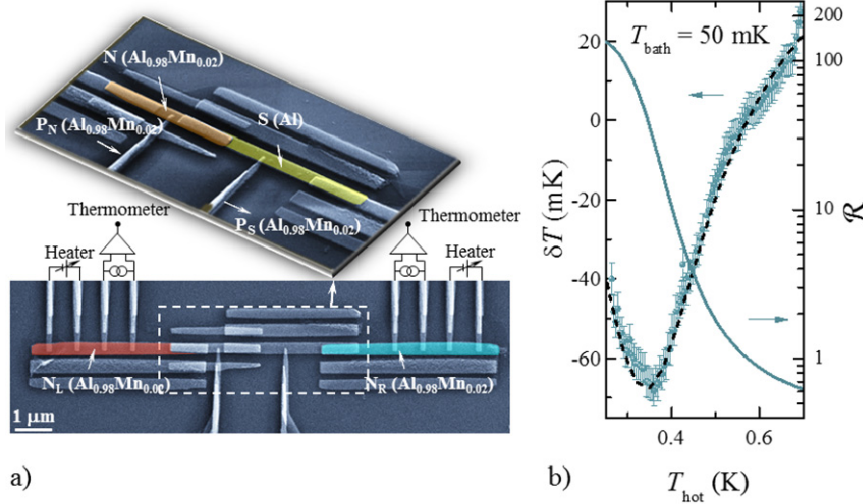


Figure 1.  
a) False-colour scanning electron micrograph of the hybrid thermal diode. Top: core of the device, which is composed of a NIS junction, where N stands for a normal metal (orange), I for a thin insulating layer and S for a superconductor (yellow). The probe  $P_N$  acts as a cold finger for

the N electrode. Bottom: the NIS junction is inserted between two right and left N electrodes (red and blue), which act as thermal reservoirs and are connected to heaters and thermometers. b) Experimental output temperature difference  $\delta T$  between the forward and reverse configurations versus the bias temperature  $T_{hot}$  (scatter, left axes) measured at a bath temperature of 50 mK. Black dashed lines are the theoretical results from the thermal model of the device. The solid line is the corresponding thermal rectification coefficient  $R$  (right axes, logarithmic scale).

Our structure showed a maximum difference of more than 60 mK between the output temperatures in the forward and reverse configurations, together with unprecedentedly high values of  $R \approx 140$  at a bath temperature of 50 mK (see Figure 1b).

On the other hand, it has been shown that the heat current flowing through a temperature-biased Josephson junction (JJ) has a coherent component that depends on the phase difference of the macroscopic condensates in the superconductors. This component can be manipulated at will by using a double-loop superconducting quantum interference device (SQUID) with three JJs in parallel (see Figure 2a). The heat modulator proved to be robust against unavoidable structure asymmetries and to provide exotic interference patterns of the output temperature, with large oscillation amplitude (reaching a maximum of 40 mK) and enhanced sensitivities to variations of the magnetic flux threading the loops (up to 200 mK per flux quantum). Foremost, the interferometer demonstrated the perfect correspondence between charge and heat currents (see Figure 2b), breaking ground for advanced caloritronic nanodevices such as thermal splitters, heat pumps and time-dependent electronic engines.

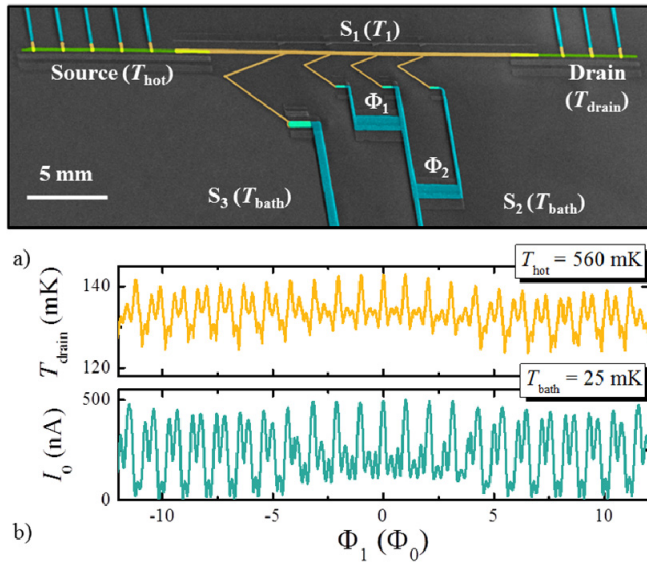


Figure 2.

a) False-colour scanning electron micrograph of the double-loop Josephson heat modulator. Source and drain N electrodes, depicted in green, are connected to the superconducting island  $S_1$  (represented in orange) and to a set of heaters or thermometers (dark cyan).  $S_1$  is tunnel-coupled to the superconducting lead  $S_2$  (dark cyan) by means of three parallel JJs forming the double-loop SQUID and to a superconducting probe  $S_3$  (dark cyan). b) Top: output drain temperature  $T_{\text{drain}}$  versus magnetic flux  $\Phi_1$  for a bias temperature  $T_{\text{hot}} = 560$  mK. Bottom: magnetic flux modulation of the SQUID critical current  $I_0$ . Both the curves were measured at a bath temperature of 25 mK.

### Contact person

Francesco Giazotto (francesco.giazotto@nano.cnr.it)

### Reference

[1] *Rectification of electronic heat current by a hybrid thermal diode*. M. J. Martínez-Pérez, A. Fornieri, and F. Giazotto. *Nature Nanotechnology* 10, 303-307 (2015).

## Pb/InAs NANOWIRE JOSEPHSON JUNCTION WITH HIGH CRITICAL CURRENT AND MAGNETIC FLUX FOCUSING

We have studied mesoscopic Josephson junctions formed by highly n-doped InAs nanowires (NWs) and superconducting Ti/Pb source and drain leads. The current-voltage properties of the system are investigated by varying temperature and external out-of-plane magnetic field. Superconductivity in the Pb electrodes persists up to 7 K and with magnetic field values up to 0.4 T. Josephson coupling at zero backgate voltage is observed up to 4.5 K and the critical current is measured to be as high as 615 nA. The supercurrent suppression as a function of the magnetic field reveals a diffraction pattern that is explained by a strong magnetic flux focusing provided by the superconducting electrodes forming the junction.

The coupling of superconducting electrodes by a weak link can result in the formation of a Josephson junction (JJ), where a dissipationless supercurrent is induced due to the proximity effect, i.e., the penetration of superconducting correlations in the non-superconducting link resulting from Andreev reflection. JJs realized with semiconductor have shown a high potential in different types of nanoscale devices which benefit from the tunable charge density by means of a gate. Yet, small dimensions of NWs also make them a promising choice for studying fundamental phenomena such as the quantum interference and Majorana fermions.

The vast majority of the studies of NW based JJs relies on Al superconducting electrodes limiting the operation to maximum 1.2 K, which corresponds to the critical temperature ( $T_c$ ) of the superconducting leads. In this work we report an exhaustive study of the response of InAs NW JJs with Pb ( $T_c=7.2$  K) superconducting leads as a function of the temperature and in the presence of an external perpendicular magnetic field ( $B$ ).

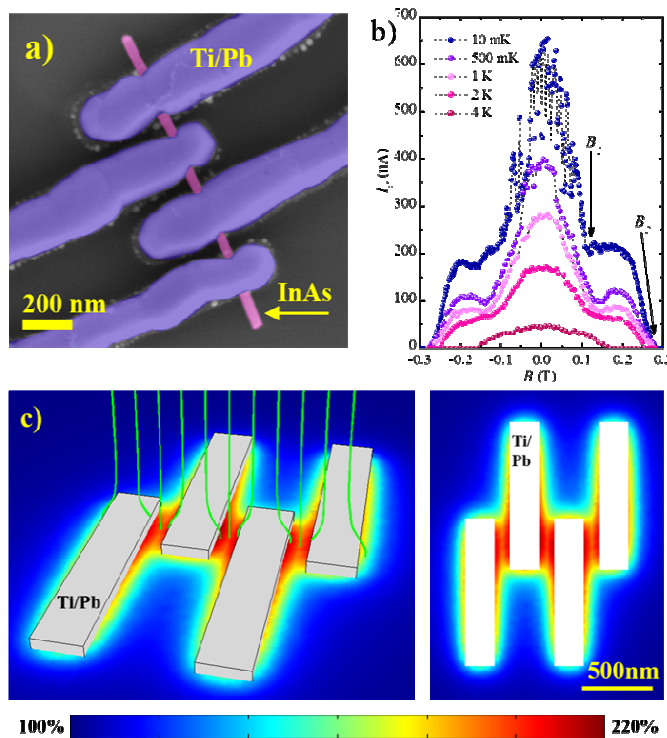


Figure 1.

a) False colored electron micrograph of our typical InAs NW-based JJ. The nanowire appears in pale pink whereas the Ti/Pb leads in blue. b) Evolution of the critical current as a function of perpendicular magnetic field for different temperatures from 10 mK to 4 K. Each point represents one current-voltage measurement where the magnetic field and temperature have been kept constant. The beginning and the end points of the shoulder structure  $B_1=0.13$  T and  $B_2=0.28$  T are indicated by arrows. c) A COMSOL simulation results showing the strength of perpendicular magnetic field in the system depending on the position. The appearance of the magnetic flux focusing is predominant at the interelectrode spacing, thus, at the InAs NW-based weak-link.



We have fabricated mesoscopic Pb/InAs-NW/Pb Josephson junctions with 100 nm interelectrode spacing (see Figure 1a) by a room-temperature Pb evaporation. Devices show excellent properties in terms of a high critical current ( $I_c$ ) exceeding 600 nA and an observable Josephson current at temperatures up to 4.5 K and magnetic fields up to 0.4 Tesla.

Unlike the expected behaviour in narrow JJs, we observe a marked diffraction pattern of the critical current as a function of B. The evolution of the maximum critical current  $I_c$  as a function of the perpendicular-to-the-plane B is displayed in Figure 1b. For temperatures as high as 2 K, the supercurrent survives up to 0.28T, a value much higher than the critical magnetic field of pure Pb bulk superconductor (0.08T). A remarkable feature is the presence of a shoulder starting at a magnetic field value  $B=0.13$ T which is consistent with a Fraunhofer-like diffraction pattern occurring in the JJ. This unconventional diffraction pattern can be explained by the presence of a strong magnetic flux focusing provided by the superconducting Pb-based electrodes, which repel the external B. The existence of a strong magnetic flux focusing has been supported by theoretical simulations as sketched in Figure 1c.

#### Contact person

Francesco Giazotto (francesco.giazotto@nano.cnr.it)

#### Reference

[1] *Pb/InAs Nanowire Josephson Junction with High Critical Current and Magnetic Flux Focusing*. J. Paajaste, M. Amado, S. Roddaro, F. S. Bergeret, D. Ercolani, L. Sorba, and F. Giazotto. Nano Lett. 15, 1803-1808 (2015).

## ATOMIC SCALE INSIGHT INTO THE CeO<sub>2</sub>/Pt INTERFACE

The structure and charge configuration at the interface between cerium oxide and platinum is studied by aberration-corrected scanning transmission electron microscopy and ab-initio density functional theory calculations, using model systems made of ultrathin cerium oxide films grown on the Pt(111) surface. Local modifications of the registry between the cerium oxide and platinum lattices, and the occurrence of nanometric platinum islands at the interface are detected. The system adopts a specific adsorption geometry which minimizes the interfacial oxygen-platinum distance. The presence of a non-negligible concentration of Ce<sup>3+</sup> ions at the interface is rationalized in terms of interfacial charge transfer.

An accurate atomic scale description of the technologically relevant interface between cerium oxide and platinum is very important for a complete understanding of the interactions which determine the properties of the combined material, in view of its optimization for different applications in energy conversion and catalysis. We investigated the structure and charge configuration of the interface between cerium oxide and platinum by aberration-corrected scanning transmission electron microscopy (STEM) and electron energy loss spectroscopy (EELS). A cerium oxide film was grown by reactive molecular beam epitaxy on a Pt(111) single crystal and processed using a focused ion beam into a cross sectional lamella. The study allowed clarifying important aspects that determine the nature of the interaction between the two materials. In particular a definite, though locally variable, registering is established between the oxide and the metal. The preferential absorption geometry for the oxide has been identified by comparing STEM images in the annular bright field mode (ABF) and simulated images using the atomic positions, evaluated by DFT+U calculations using a model made of three cerium oxide layers supported on a Pt slab. The film adopts the interfacial adsorption geometry indicated by theory to be the most stable one, having the maximum number of short Pt-O bonds. The charge configuration at the interface and within the film was investigated by STEM in the EELS mode. Maps of Ce<sup>3+</sup> concentration were obtained by fitting the local Ce M<sub>4,5</sub> spectra with reference spectra from samples containing only Ce<sup>4+</sup> and Ce<sup>3+</sup>. A non-negligible fraction of cerium atoms at the interface are reduced to the 3+ oxidation state. A comparison with the charge

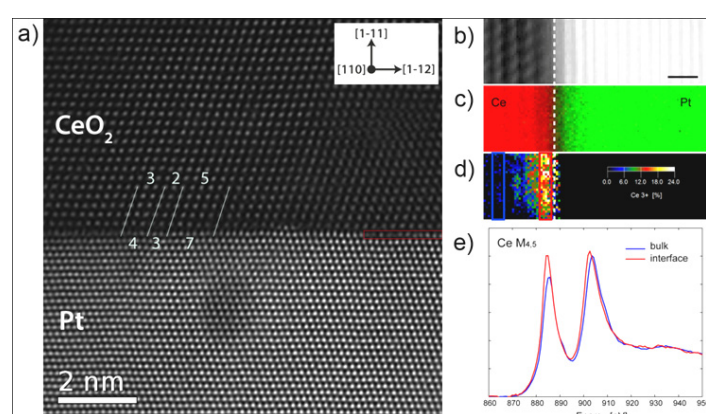


Figure 1.

a) Cross sectional HAADF (High Angle Annular Dark Field)-STEM image of the CeO<sub>2</sub>/Pt(111) interface along the [110] zone axis. The blue lines indicate the interface coincidence registry, which varies locally from 3:4 to 2:3 and 5:7. b) HAADF-STEM image of a portion of the interface where also a Ce/Pt chemical map has been acquired by STEM-EELS at the Ce M<sub>4,5</sub> edge. c); d) map of Ce<sup>3+</sup> concentration at the interface obtained by fitting the local Ce M<sub>4,5</sub> edge spectra with spectra from

reference samples containing Ce only in the 3+ (CeF<sub>3</sub>) and in the 4+ (CeO<sub>2</sub>) oxidation states; e) Ce M<sub>4,5</sub> edge spectra acquired at the interface (red line, average of the spectra measured in the area enclosed by the red rectangle in d) and in the CeO<sub>2</sub> film bulk (blue line, average of the spectra measured in the area enclosed by the blue rectangle in d).

configurations predicted by DFT calculations indicates that interfacial reduction is induced by a charge transfer from the Pt substrate. The obtained results are of help for a correct description of the functionality of cerium oxide based materials based on the atomic scale description of the interface.

#### Contact person

Paola Luches (paola.luches@nano.cnr.it)

#### Reference

[1] *Atomic Scale Structure and Reduction of Cerium Oxide at the Interface with Platinum*. P. Luches, L. Giordano, V. Grillo, G. C. Gazzadi, S. Prada, M. Campanini, G. Bertonni, C. Magen, F. Pagliuca, G. Pacchioni, and S. Valeri. *Adv. Mater. Interfaces* 2, 1500375 (2015).

## MULTIFUNCTIONAL NANOFIBERS

New species of nano-materials are realized by electrospinning methods, and characterized in terms of their morphological, optical and electrical properties. Active polymer nanofibers and nanowires, in the form of individual nanostructures or complex assemblies, exhibit better performances compared to conventional film-based materials and coatings, as demonstrated by single-fiber distributed feedback lasers and flexible, piezoelectric nanogenerators. In addition, nanofibers can be produced with high throughput, making these technologies highly promising for a large variety of applications.

Electrospinning is based on electrified jets of polymer solutions, which have to exhibit significant molecular entanglements, and it is nowadays the most promising method for producing organic nanofibers and nanowires due to its operational simplicity, low cost, and chemical versatility. Solutions are accelerated concomitantly to solvent evaporation, to deposit nanofiber-based coatings on solid surfaces, or to realize free-standing membranes. Electrospinning is being developed in our group in order to realize new, active nanofibrous materials with applications in different scientific fields and technologies.

Examples include the generation of optically-pumped solid-state lasers, based on individual light-emitting nanofibers, which are textured by nanoimprint lithography. Single-fiber distributed feedback lasers can be realized by Bragg gratings (with 400 nm - 600 nm period), imprinted directly onto the active nanowires.

These devices show a threshold excitation fluence ( $750 \text{ mJ cm}^{-2}$ ) reduced by 40–50% with respect to nanopatterned, thin-film lasers made of the same molecular material, due to the higher field confinement which leads to correspondingly higher photonic density inside the active filaments. Analogously, electrospun piezoelectric nanofibers outperform thin films, in terms of self-poling capability and conformability to many surfaces. Aligned arrays of these nanofibers in mutual contact exhibit improved voltage output due to electromechanical

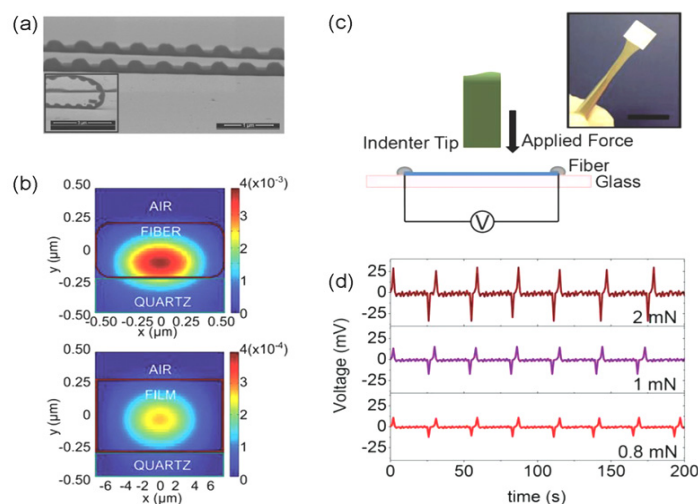


Figure 1.

(a) Scanning electron micrograph of nanopatterned polymer fibers for lasing. Inset: bent patterned fibers. (b) Modelling of light propagating in the distributed feedback lasers. The maps show the normalized, real part of the Poynting vector component along the sample in-plane, longitudinal direction, calculated on a cross-section of a patterned fiber (top) and film (bottom), respectively. For the fiber, fields are much more confined in the transversal direction (see the different horizontal scales for the two maps). The fundamental transverse electric (TE) is calculated by Finite-Difference Time-Domain

(FDTD) simulations. Adapted with permission from Ref. [1]. © 2014 WILEY-VCH Verlag GmbH & Co. KGaA, Weinheim. (c) Scheme of a developed set-up for force-indentation measurements on piezoelectric electrospun nanofibers (photograph in the inset). (d) Measured output voltages under various, repeatedly applied stresses. Adapted with permission from Ref. [2]. © 2014 The Authors. Published by WILEY-VCH Verlag GmbH & Co. KGaA, Weinheim.

coupling of multiple filaments, together with large areas (up to tens of cm<sup>2</sup>) and light weight, and they can be repeatedly bent and twisted without fracture. These features make functional polymer nanofibers very appealing for application in the fields of self-powered systems, smart wearables and body sensor networks, and ambient-assisted living.

The research leading to the most recent of these results has received funding from the European Research Council under the European Union's Seventh Framework Programme (FP/2007-2013)/ERC Grant Agreement n. 306357 (ERC Starting Grant "NANO-JETS").

### Contact person

Luana Persano (luana.persano@nano.cnr.it)

### References

- [1] *Distributed Feedback Imprinted Electrospun Fiber Lasers*. L. Persano, A. Camposeo, P. Del Carro, V. Fasano, M. Moffa, R. Manco, S. D'Agostino, and D. Pisignano. *Adv. Mater.* 26, 6542-6547 (2014).
- [2] *Cooperativity in the Enhanced Piezoelectric Response of Polymer Nanowires*. L. Persano, C. Dagdeviren, C. Maruccio, L. De Lorenzis, and D. Pisignano. *Adv. Mater.* 26, 7574-7580 (2014).

## ADVANCED NANOPATTERNING TECHNOLOGIES FOR RANDOM LASERS AND METAL-ENHANCED FLUORESCENCE ARCHITECTURES

Next-generation patterning technologies will enable the development of entirely new concepts in nanophotonics and nanoelectronics, exploiting the flexibility and functions of biological systems and active organic molecules and nanostructures, and their capability to effectively interface with the human body and the environment. We continuously develop novel nanopatterning tools for biopolymers, organic semiconductors, and nanoparticles to embed them in improved device architectures at nano- and microscale. Here reviewed examples include distributed feedback and random lasers based on DNA, and metal-enhanced fluorescent systems with emission in the near-infrared.

Biopolymers, organic semiconductors, and their complexes involving inorganic nanoparticles have an enormous potential for the realization of new and exotic devices for nano-photonics and electronics. To exploit at best this potential, however, conventional nanofabrication technologies are often inadequate, leading to irreversible degradation of active properties in molecular systems. Instead, dedicated nanopatterning tools need to be developed, hopefully combining chemical flexibility as enabled by soft lithographies, and accuracy in spatial resolution.

We have developed various nanopatterning technologies for the realization of unconventional photonic devices, featuring a resolution down to 100 nm. Room-temperature nanoimprinted, DNA-based distributed feedback lasers, which dissolve in water, have been realized, with operation at 605 nm and 0.3 nm line width. In addition, at high excitation densities, the emission of untextured dye-doped DNA is characterized by a broad emission peak with an overall line width of 12 nm and superimposed narrow peaks, characteristic of random lasing. The localized surface plasmon resonances of metallic

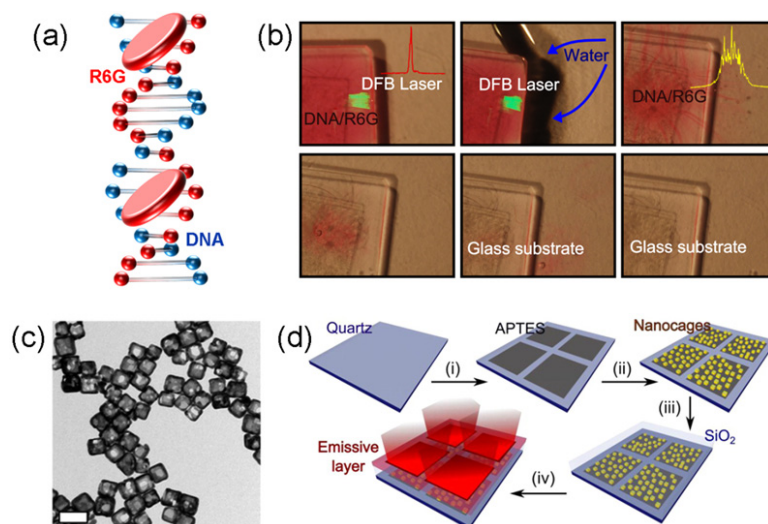


Figure 1. (a) Scheme of R6G binding to DNA helix. (b) Micrographs displaying a DNA-R6G distributed feedback pattern (green region) while dissolving in water. The pattern completely dissolves in water in a few tens of seconds. The top-right panel also shows a single-shot emission spectrum from a DNA-R6G films, above the threshold for random lasing. Adapted from Ref. [1]. © 2014 American Chemical Society. (c) A transmission electron micrograph of Au nanocages. Scale bar: 100 nm. (d) Schematics of the

fabrication of metal-enhanced fluorescent substrates through (i) microcontact printing of (3-aminopropyl) triethoxysilane (APTES), (ii) immobilization of Au nanocages on the APTES regions, (iii) SiO<sub>2</sub> deposition, and (iv) deposition of an emissive layer. The emission in the near-infrared is enhanced only in regions corresponding to the microprinted Au nanocages underneath. Adapted from Ref. [2]. © 2015 American Chemical Society. These are unofficial adaptations of articles that appeared in ACS publications. ACS has not endorsed the content of these adaptations or the context of their use.



nanoparticles can also be helpful in this framework, to amplify the absorption of excitation light and assist in radiating molecular fluorescence to the far-field. By patterning Au nanocages, we have demonstrated metal-enhanced fluorescence from near-infrared light-emitting molecules, which have been investigated experimentally. In addition, the field enhancement and modified radiation and absorption rates have been modeled in detail. The combination of these methods with electrospun fibers is being explored, to develop new nanoscale systems encoding optical or diagnostic information. These new concepts, including physically-transient photonics, might have strong impact on optics, medical diagnostics, and biotechnologies.

The research leading to these results has received funding from the European Research Council under the European Union's Seventh Framework Programme (FP/2007-2013)/ERC Grant Agreement n. 306357 (ERC Starting Grant "NANO-JETS").

### Contact person

Dario Pisignano (dario.pisignano@unisalento.it)

### References

- [1] *Physically Transient Photonics: Random versus Distributed Feedback Lasing Based on Nanoimprinted DNA*. A. Camposeo, P. Del Carro, L. Persano, K. Cyprych, A. Szukalski, L. Sznitko, J. Mysliwiec, and D. Pisignano. ACS Nano 8, 10893-10898 (2014).
- [2] *Metal-Enhanced Near-Infrared Fluorescence by Micropatterned Gold Nanocages*. A. Camposeo, L. Persano, R. Manco, Y. Wang, P. Del Carro, C. Zhang, Z.-Y. Li, D. Pisignano, and Y. Xia. ACS Nano 9, 10047-10054 (2015).

## CONTROLLING SINGLE SPIN EFFECTS IN NANOSCALE MULTI-DOT SYSTEMS

The control of orbitals and spin states of single electrons in solid state devices is a key ingredient for quantum information processing and is of great relevance for spintronics. Recent experiments at Cnr Nano demonstrate a conceptually new technique for the control of a multi-dot system. The method eludes some of the key technical limitations that prevent an aggressive scaling of these devices, which is necessary to increase their typically very low operation temperature (well below 1K). We demonstrate single electron devices based on InAs/InP nanowires that display a strong spin blockade beyond 10K.

Pauli exclusion principle and spin conservation in tunnel-coupled multiple quantum dot systems provide the physical basis for the spin blockade effect. In suitably designed solid-state devices, this effect can yield an all-electric single-spin manipulation. Spin blockade can thus have an important impact on quantum computing architectures and on single-spin filters and detectors. Unfortunately, when the quantum dot dimensions and relative distance are scaled down to a few nanometers, or even to the atomic scale, independent control of two quantum dots is viewed as increasingly challenging and ultimately impossible, since it is expected to require the fabrication of local electrostatic “gates” with different capacitive coupling to the two quantum dots and thus with dimensions on the order of the inter-dot distance.

Our work demonstrates that this is not necessarily the case and we describe an alternative architecture that makes it possible to control the filling of each individual electronic island of a double quantum dot system using large scale gates (see Fig. 1). These gates – thanks to a mechanism mimicking Stark effect in real atoms – can shift the energies of trapped electrons in a very different way, depending on their orbital states in the two islands, despite being much larger in size than the dot system. Hence, our approach eludes complex

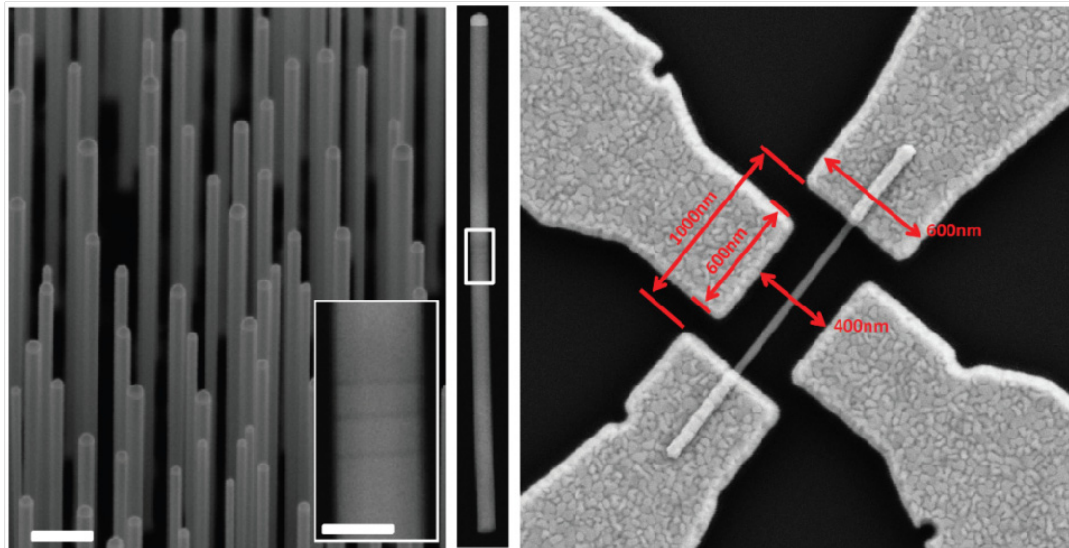


Figure 1.

From left to right: scanning electron micrograph of standing nanowires (scale bar 200nm); scanning tunnel electron microscope image of an InAs/InP heterostructured nanowire, which is nominally identical to the one used for the studied devices (inset scale bar 50nm); top view of one of the fabricated devices with quoted scales.

alignment and scaling issues that become simply prohibitive in the case of local gating on nanoscale single-electron systems. Differently, our gating architecture is in principle scalable down to atom-scale devices. The full control of the multi-dot system is demonstrated by the observation of clear bias triangles (see Fig. 2) and of a strong spin blockade effect, which in our prototypes could be detected at temperatures up to about 10K.

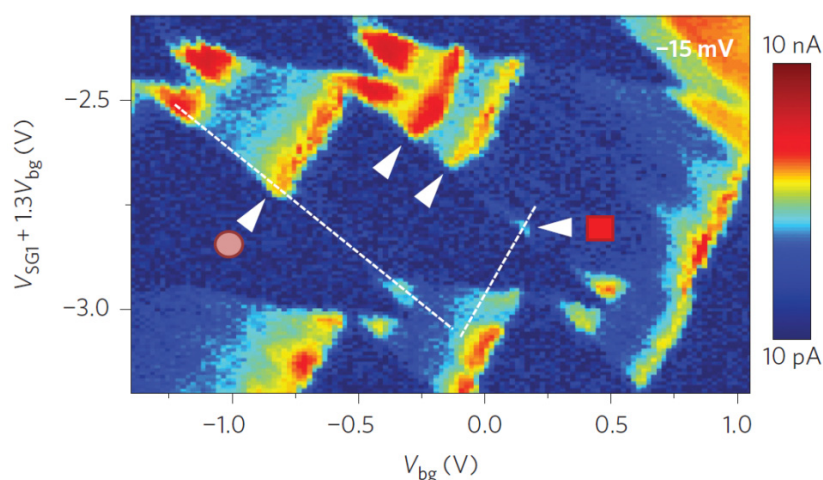


Figure 2. Current map through the multiple dot device at a bias of -15mV and as a function of the gating configuration (backgate and side gates). Despite the field-effect electrodes are much larger in size than the dot system, they can independently control the filling of two dots which are separated by a 5nm-thick InP epitaxial barrier. Bias triangles and excited states resonances (indicated by white triangles) are visible in the color plot.

#### Contact person

Stefano Roddaro (stefano.roddaro@nano.cnr.it)

#### Reference

[1] *Nanoscale spin rectifiers controlled by the Stark effect*. F. Rossella, A. Bertoni, D. Ercolani, M. Rontani, L. Sorba, F. Beltram, and S. Roddaro. *Nature Nanotech.* 9, 997 (2014).

## TERAHERTZ PHOTODETECTORS BASED ON 1D AND NOVEL 2D NANOMATERIALS AND ULTRAFAST THz NANO-SPECTROSCOPY

The ability to convert light into an electrical signal with high efficiencies and controllable dynamics is a major need in photonics and optoelectronics. In the Terahertz (THz) frequency range, with its exceptional application possibilities in high data rate wireless communications, security, night-vision, biomedical or video-imaging and gas sensing, detection technologies providing efficiency and sensitivity performances, that can be “engineered” from scratch, remain elusive. These key priorities prompted in the last decade a major surge of interdisciplinary research, encompassing the investigation of different technologies in-between optics and microwave electronics, different physical mechanisms and a large variety of material systems offering ad-hoc properties to target the expected performance and functionalities. We here provide an overview on our recent developments on THz photodetectors based on novel and fascinating 2D material systems as black phosphorus (BP) and topological insulators (TI).

By exploiting the inherent electrical and thermal in-plane anisotropy of a flexible thin flake of black-phosphorus (BP), we devised plasma-wave, thermoelectric and bolometric nano-detectors with a selective, switchable and controllable operating mechanism. All devices operate at room-temperature and are integrated on-chip with planar nanoantennas, which provide remarkable efficiencies through light-harvesting in the strongly sub-wavelength device channel. The achieved selective detection (5-8 V/W responsivity) and sensitivity performances (signal-to-noise ratio of 500) are here exploited to demonstrate the first concrete application of a phosphorus-based active THz device, for pharmaceutical and quality control imaging of macroscopic samples, in real-time and in a realistic setting.

As a very intriguing alternative, we explored TIs which represent a novel quantum state of matter, characterized by edge or surface-states, showing up the topological character of the bulk wave-functions. Investigation of topological surface states (TSS) is conventionally hindered by the fact that, in most of experimental conditions, the TSS properties are mixed up with those of bulk-states. We devised a novel tool to unveil TSS and to probe related plasmonic effects. By engineering  $\text{Bi}_2\text{Te}_{(3-x)}\text{Se}_x$  stoichiometry, and by gating the surface of nanoscale field-effect-transistors, exploiting thin flakes of  $\text{Bi}_2\text{Te}_{2.2}\text{Se}_{0.8}$  or  $\text{Bi}_2\text{Se}_3$ , we recently provided the first demonstration of room-temperature THz detection mediated by over-damped plasma-wave oscillations on the “activated” TSS of a  $\text{Bi}_2\text{Te}_{2.2}\text{Se}_{0.8}$  flake.

One-dimensional nanostructure devices are at the frontline of studies on future electronics, although issues like massive parallelization, doping control, surface effects, and compatibility with silicon industrial requirements are still open challenges. The recent progresses in atomic to nanometer scale control of materials morphology, size, and composition including the growth of axial, radial and branched nanowire-based heterostructures, make the nanowire (NW) an ideal building block for implementing rectifying diodes or detectors that could be well operated into the THz, thanks to their typical achievable attofarad-order capacitance. We demonstrated room temperature operation of InAs or InAs/InSb NW-based field effect transistors (FETs) in the 0.3-3 THz range with over 100V/W responsivity and  $< 1\text{nW/Hz}^{1/2}$  noise equivalent powers, showing that our devices can already be used in realistic settings, enabling large-area, fast imaging of macroscopic samples.

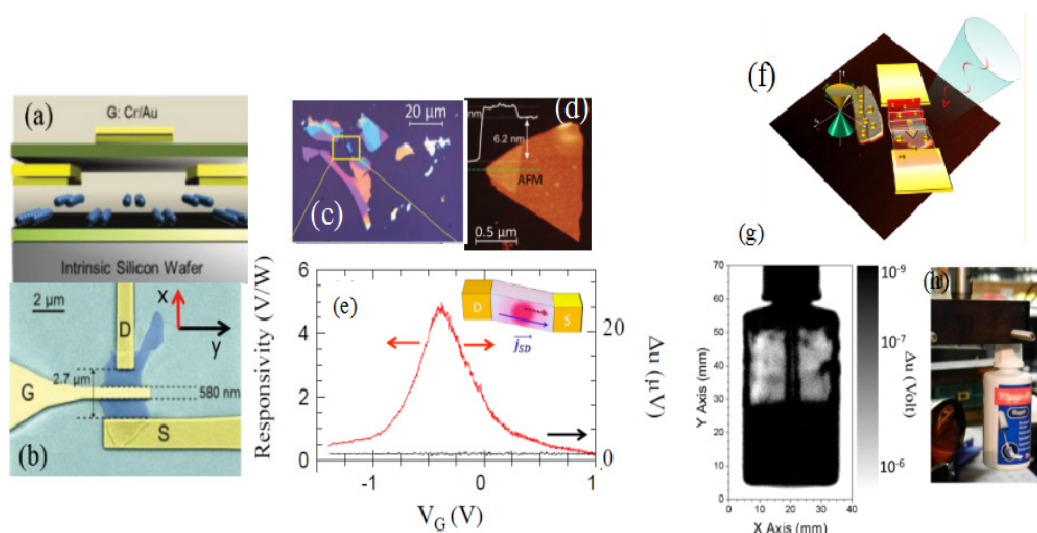


Figure 1.

(a) Sketch of a black phosphorus (BP) photodetector device structure (vertical section). (b) False colors SEM image of the BP-based FET. The channel length ( $L_c$ ) is 2.7  $\mu\text{m}$ , the gate length ( $L_g$ ) is 530 nm. (c) Optical image of exfoliated flakes of BP. (d) Atomic force microscopy topographic image of an individual BP flake with thickness 6.2 nm. A topographic line profile, acquired along the dashed green line is shown. (e) Gate bias dependence of the experimental room temperature responsivity. The red line was measured by impinging the THz beam on the detector surface; the black line was measured while blanking the beam with an absorber (considering unaltered the incident power). Inset: schematics of the over-damped plasma-wave dynamics. (f) Schematic sketch of a THz detection process mediated by topological insulator surface states. (g) Room temperature, large area THz imaging obtained while impinging the 332.6 GHz radiation a topological insulator THz detector, mounted on a XY stage, with an acquisition time of 20 ms/pixel. For visible light illumination the contents cannot be seen, either by naked eye or by the CCD camera used to take the picture. The detection of THz transmitted radiation gives information about the jar content. (h) Photograph of the glue jar.

### Contact person

Miriam Serena Vitiello (miriam.vitiello@nano.cnr.it)

### References

- [1] *Photodetectors based on graphene, other two-dimensional materials, and hybrid systems*. F. H. L. Koppens, T. Mueller, Ph. Avouris, A. C. Ferrari, M. S. Vitiello, and M. Polini. *Nature Nanotech.* 9, 780 (2014).
- [2] *Black Phosphorus Terahertz Photodetectors*. L. Viti, J. Hu, D. Coquillat, W. Knap, A. Tredicucci, A. Politano, and M. S. Vitiello. *Adv Mater* 27, 5567–5572 (2015).

## PHOTONIC ENGINEERING OF TERAHERTZ QUANTUM CASCADE LASERS

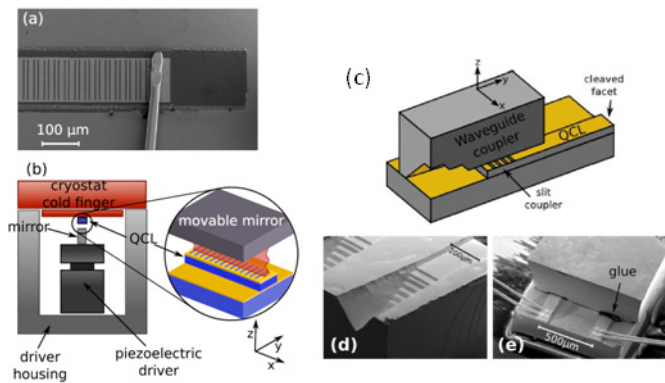
Recent technological innovation in photonics and nanotechnology is now enabling Terahertz frequency research to be applied in an increasingly widespread range of fields, such as information and communications technology, sensing, medical diagnostics, global environmental monitoring, homeland security, quality and process controls. Most of these applications need systems with targeted sensitivity and specificity exploiting advanced quantum devices, novel materials and technologies. To address the above application requirements, high-power, widely-tunable sources with controlled and directional beam profiles need to be developed. We here provide an overview on our recent technological developments in the field of 2D and 1D THz photonic laser resonators, microcavity-coupled continuous tunable sources and waveguide adapters for efficient THz radiation out-coupling.

Tunable oscillators are a key component of almost all electronic and photonic systems. Yet, a technology capable of operating in the terahertz (THz)-frequency range and fully suitable for widescale implementation is still lacking. This issue is significantly limiting potential THz applications in gas sensing, high-resolution spectroscopy, hyper-spectral imaging and optical communications. The THz quantum cascade laser (QCL) is arguably the most promising solution in terms of output power and spectral purity. In order to achieve reliable, repeatable and broad tunability, we exploited the strong coupling between two different cavity mode concepts: a distributed feedback one-dimensional photonic resonator (providing gain), and a mechanically actuated wavelength-size microcavity (providing tuning). The result is a continuously tunable, single-mode emitter covering a 162 GHz spectral range, centered on 3.2 THz with a few tens of MHz resolution and an unprecedented compact and simple architecture (Fig. 1a-b).

We also recently developed a novel approach to couple THz radiation from a double-metal QCL into an on-chip hollow rectangular waveguide feeding a triangular horn, with the specific aim of optimizing the optical beam divergence. The conceived novel extractor is composed of three parts: a series of slits patterned at the end of the laser top contact (slit coupler), a metallic waveguide section (feeder) assembled on top of the laser itself, and an adiabatic expansion of the feeder, forming a horn that radiates into an optical fiber or, alternatively, into free space (Fig. 1c-e). The developed waveguide component is capable of efficiently shaping the output beam profile from a double-metal THz QCL simultaneously

Figure 1.

(a) Scanning electron microscope image of a dual-slit DFB QCL. The absorbing boundary is visible around the grating. (b) Schematic diagram of the external cavity arrangement. The movable mirror was milled from an aluminum block and was then laid on top of the piezoelectric actuator. (c) Device schematics: yellow areas indicate metallized surfaces, gray area correspond to GaAs. (d) Scanning electron microscope (SEM) image of the cleaved chip containing two waveguide couplers; (e) SEM image of the final assembly, taken from the cleaved facet side.





reducing the facet reflectivity opening the way to the realization of more complex systems such as QCL amplifiers or external cavity tuners for multi-spectroscopy applications, injection seeding and metrological approaches across the far-infrared.

We also optimized the extraction efficiently and collimation of the output radiation of our THz QCLs by developing quasi-crystalline resonators, in which the distinction between symmetric (vertically radiative, but low quality factor,  $Q$ ) and antisymmetric (non-radiative, high  $Q$ ) modes is fully overcome, therefore elegantly circumventing any power cancellation issue in the far-field. Our 2D photonic quasicrystal THz QCLs based on a Penrose P2 (kite and dart) tiling with a five-fold rotational symmetry, reached 0.1-0.2% wall-plug efficiencies and 65mW peak output powers with characteristic surface-emitting conical beam profiles, result of the rich quasi-crystal Fourier spectrum (Figure 2a-b).

Photonic engineering solutions to control the emission frequency and the output beam direction of DFB THz QCLs independently have been also developed. The spatial refractive index modulation of the gratings necessary to provide optical feedback at a fixed frequency and, simultaneously, a far-field emission pattern centered at controlled angles, was designed through use of an appropriate wavevector scattering model (Figure 2c-d). Single-mode THz emission at angles tuned by design between  $0^\circ$  and  $50^\circ$  was realized, leading to an original phase-matching approach, lithographically independent, for highly collimated THz QCLs.

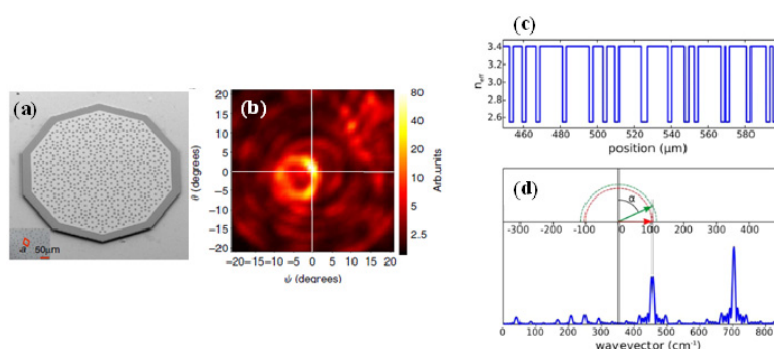


Figure 2.

(a) SEM image of a prototype quasi-crystal resonator device. The lattice spatial length scale have been lithographically designed at each vertex of a Penrose pattern and imprinted into the top Cr/Au metallization of the THz QCL (see inset). (b) Far-field measured from the device with  $a=21 \mu\text{m}$ ; (c) Spatial dependence of the effective

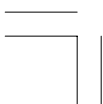
refractive index of a bi-periodic DFB THz QCL (d) Spatial spectra of the grating of panel (c). Two light cones (dashed lines) are drawn, corresponding to the two bandgap modes of a first order grating with spatial periodicity of  $712 \text{ cm}^{-1}$ . The two modes are predicted to be at 3.1 THz (red, inner circle) and 3.35 THz (green, outer circle), and to radiate at different angles, as indicated by the arrows.

### Contact person

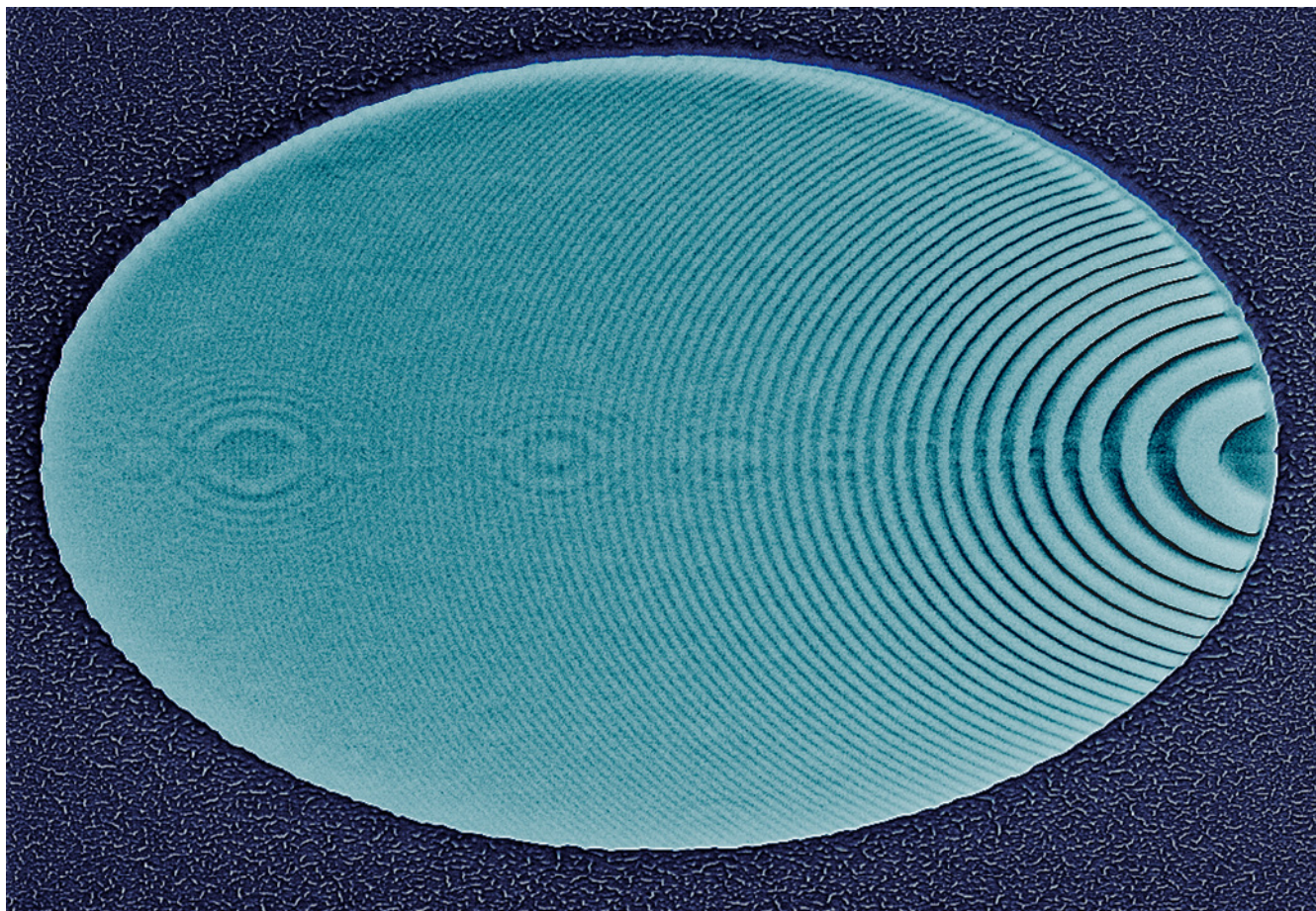
Miriam Serena Vitiello (miriam.vitiello@nano.cnr.it)

### References

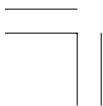
- [1] *Photonic quasi-crystal THz lasers*. M. S. Vitiello, M. Nobile, A. Ronzani, A. Tredicucci, F. Castellano, V. Talora, L. Li, E. H. Linfield, and A. G. Davies. *Nature Communications* 5, 5884 (2014).
- [2] *Tuning a microcavity-coupled terahertz laser*. F. Castellano, V. Bianchi, L. Li, J. Zhu, A. Tredicucci, E. H. Linfield, A. G. Davies, and M. S. Vitiello. *Appl. Phys. Lett.* 107, 261108 (2015).







## **Highlights Nanoscience**



## Introduction to Nanoscience

The separation between nanotechnology and nanoscience activities is not very sharp and several highlights could be classified in both sectors. The activity involves both experimental and theoretical work, and focuses on systems that also have an applicative perspective such as:

- nanostructured graphene
- organic and organic/inorganic photovoltaics and light-emitting materials
- plasmonic nanostructures.

**Nanotribology:** The investigation of friction at the nanoscale is relevant for any application involving relative movements of nanoscale objects, and is also pivotal for unravelling the origin of macroscopic friction. At Cnr Nano, friction at the nanoscale is investigated experimentally and by means of atomistic simulations.

**Nanomagnetism:** The study of magnetic phenomena in nanosystems is investigated by considering a variety of systems (e.g., molecular magnets on surfaces and graphene nanostructures) via different experimental and theoretical approaches (such as scanning probe microscopies and first principle calculations, respectively).

**Energy conversion and storage:** The fundamental understanding and design of metal/oxide materials with optimized properties has strong impact on catalysis, energy conversion, and magnetism. This research is focused on the study of ultrathin films of metals, metal nanoparticles on oxide surfaces and core-shell nanoparticles. Moreover, innovative hydrogen storage materials, such as graphene, are investigated. In particular the interaction between hydrogen and graphene by chemical functionalization of the material, thus enabling fine tuning of the adsorption/desorption properties of hydrogen on graphene, is theoretically and experimentally explored.

Furthermore, thermoelectricity is explored from multiple perspectives: characterization via nano-thermoelectric devices; development of the underlying quantum theory; use of first-principle simulations to understand and to predict thermoelectric properties of materials. Analogously, piezoelectricity, namely the conversion of mechanical deformation in electrical energy and vice versa, is studied in polymer nanostructures to design and realize new energy harvesting and smart wearable materials.

**Development of simulative approaches, and the implementation of the related high-performance computing software** for molecules and materials at the nanoscale. Methods developed and applied include:

- first-principles approaches for molecules, small nanoparticles and materials; atomistic and coarse-grained molecular dynamics simulations for (bio)molecules and their interaction with nanostructured inorganic materials;
- effective mass approaches for semiconductor nanostructures;
- density functional theory approaches to study nanosystems and molecules, to achieve two dimensional charge distribution in transition metals, or to derive electrical currents through polymer nanostructures;
- multiscale methods that bridge length and time scales in complex systems are also actively developed and applied.

**Advanced instrumentation development:** transmission electron microscopy activities are

carried out in two main directions: nanostructure characterization and microscopy methodological development. Methodological research has been devoted to extract quantitative information on strain, composition, and morphology at the atomic scale. The main technical developments have been in Convergent Beam Electron Diffraction, Scanning Transmission Electron Microscopy with an annular dark field detector (STEM-ADF), and High resolution phase contrast TEM (HRTEM). Engineering the quantum nature of the electron beam via phase holograms built by Focused Ion Beam (FIB), is an on-going activity that may also open-up novel electron microscopy investigation techniques.

## PLASMONIC FIELD-ENHANCEMENT IN MOLECULAR SYSTEMS

Using first-principles TDDFT calculations we studied the electric field enhancement in polyacene molecules, proposed as prototypical nano-plasmonic systems. We demonstrated that optical transitions may generate oscillating dipolar response charge, giving rise to an induced electric field near the molecule, which thus acts as a plasmon-like nanoantenna. While the field amplification in the vicinity of single acenes is rather small and decreases when the size of the system is increased, it may be selectively enhanced in the case of acene's assemblies.

Localized surface plasmon resonances are collective electronic excitations, which strongly couple with light allowing the confinement of electromagnetic energy below the diffraction limit. Their high oscillator strength and field enhancement have made plasmons of paramount importance for a variety of applications ranging from surface-enhanced spectroscopies, to nanoantennas and light harvesting. Despite the efforts deployed so far, an unambiguous description of what a plasmon is at the molecular scale is still a controversial issue. While in large nanosystems ( $\sim 100$  nm) optical and plasmonic properties are generally well described by semiclassical models of the dielectric function, when the system size reaches a few nanometers, quantum finite-size effects become important, semiclassical descriptions fail, and purely atomistic approaches become mandatory.

Due to the ambiguities in the definition of plasmons at the molecular scale, here [1] we focus on a typical plasmonic effect: the electric field-enhancement. We consider purely molecular systems that exhibit optical transitions upon illumination. These transitions may cooperate constructively, in a collective way leading to relatively intense absorption peaks, which can be thought of as “plasmonic” since they may enhance an external electric field.

We considered polyacenes with an increasing number of rings (1-50). Their optoelectronic properties and the local electric field enhancement are investigated through first-principles (TD)DFT approaches. We investigated also the field amplification due to light excitation of pairs of acenes at different distances. Our results [1] show a small but not negligible field enhancement cooperation effect between molecules. This proof of concept suggests that, even though the amplification properties of single acenes are generally too small for any realistic application, their supramolecular coupling may provide a tunable and controlled way to realize realistic nanoantenna.

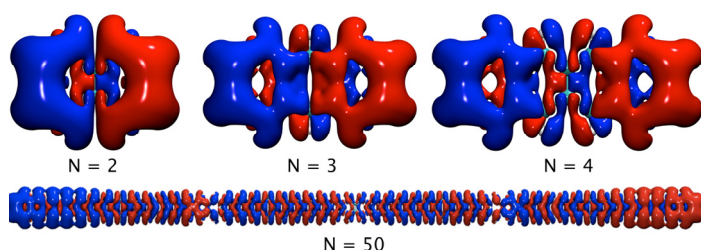


Figure 1. Light-induced response charge densities for selected polyacenes with increasing number ( $N$ ) of C-rings. The spatial separation between positive (blue) and negative (red) contributions remarks the dipolar nature of the optical transition.

### Contact person

Arrigo Calzolari (arrigo.calzolari@nano.cnr.it)

### Reference

[1] *Light-Induced Field Enhancement in Nanoscale Systems from First-Principles: The Case of Polyacenes*. L. Bursi, A. Calzolari, S. Corni, and E. Molinari. ACS Photonics 1, 1049 (2014).



## ENGINEERING THE ELECTRONIC STATES OF CORE-SHELL NANOWIRES

Semiconductor nanowires are filamentary structures whose nanometric thickness exposes quantum mechanical effects. They proved to be versatile building blocks for several nanoelectronic, nanophotonic and photovoltaic devices. Recent technological advancements unlocked the possibility to modulate their composition both in the longitudinal and radial directions: quantum structures of different dimensionality, such as dots, wires, rings and tubes, may coexist, with highly engineerable carrier localization, electronic structure, optical spectra. Predictive numerical modelling of such complex structures is challenging, yet it is pivotal to design novel devices resting upon the interplay of 1D and 2D quantum-confined states.

We study numerically the optical spectra of GaAs/AlGaAs core-(multi)shell nanowires (CSNWs) in a 3D real-space multi-subband density functional approach, which accounts for the complex geometry and composition of the structure, the Coulomb field of excess electrons and holes, and the doping profile. The quantum equation of motion is solved self consistently together with the Hartree potential generated by the free carriers and the static doping. The numerical method relies on a spatial mesh whose symmetry matches the NW crystal. Indeed, it has been proven that the NW free carrier gas substantially deviates from the cylindrical shape, which one could be tempted to use in modeling quantum-well tubes, and accounting for the polygonal section of NWs is fundamental for quantitative results (Figure 1) Furthermore, due to the large computational effort needed to model realistic samples, the simulation software has been adapted to take advantage from the massively

parallel computers available at the Institute through CINECA.

Based on the self-consistent carrier states, we compute two kinds of optical response functions and compare theoretical predictions with experimental data from partner groups. (i) Inelastic light scattering cross section of prototypical GaAs/AlGaAs CSNWs hosting a remotely doped coaxial shell is obtained, assuming nonresonant conditions, via the dynamic response functions of the excess electrons. Calculations of charge and spin density collective-excitations allowed us to understand density fluctuations occurring

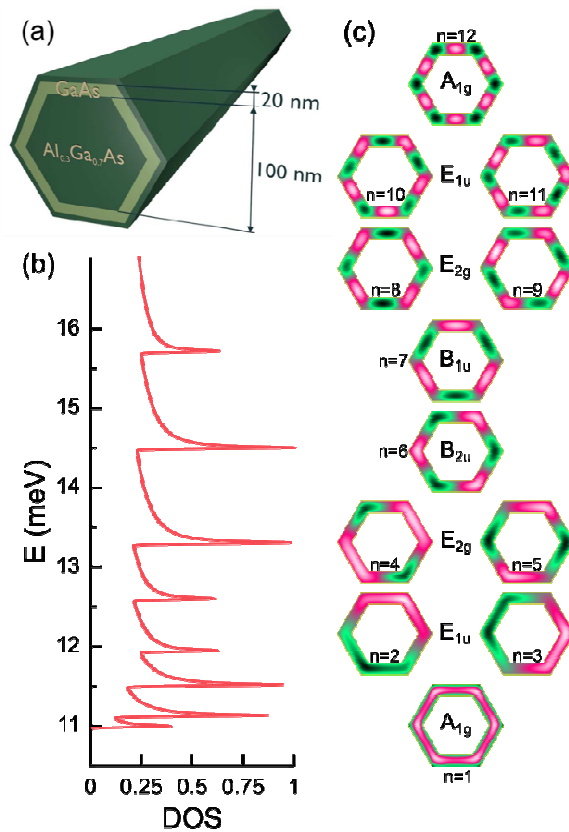


Figure 1. (a) Core-shell nanowire with hexagonal section able to confine electrons in the prismatic tubular GaAs shell. (b) Single-particle density of states spectrum. (c) Envelope function of the 12 lowest states, exposing specific symmetries stemming from the section geometry. This leads to symmetry-induced selection rules of collective excitations [1].

in the azimuthal, radial, or longitudinal directions of the CSNW, to rationalize complex absorption spectra, and to derive specific light-scattering selection rules stemming from the sample symmetry. (ii) Photoluminescence spectra of GaAs/AlAs CSNWs have proved the quantum confinement of carriers at the core-shell interface due to unintentional p-doping of the sample, paving the way towards a high mobility free-hole gas with tubular shape (Figure 2) Magnetic phases and Aharonov-Bohm oscillations of the free carrier gas have also been addressed.

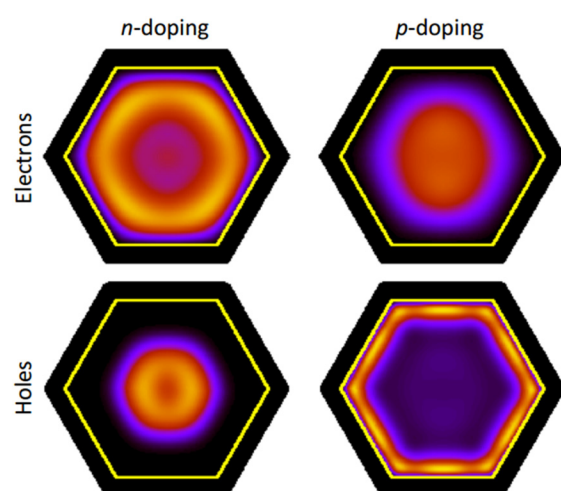


Figure 2. Free electron (top) and hole (bottom) density of n (left) and p (right) doped core-multishell samples with a GaAs core, subject to a transverse magnetic field of 2 T. While minority carriers tend to localize in the core, majority carriers form a tubular high-mobility gas [3].

### Contact person

Andrea Bertoni (andrea.bertoni@nano.cnr.it)

### References

- [1] *Symmetries in the collective excitations of an electron gas in core-shell nanowires*. M. Royo, A. Bertoni, and G. Goldoni. Phys. Rev. B 89, 155416 (2014).
- [2] *Unintentional High-Density p-Type Modulation Doping of a GaAs/AlAs Core-Multishell Nanowire*. J. Jadcak, P. Plochocka, A. Mitioglu, I. Breslavetz, M. Royo, A. Bertoni, G. Goldoni, T. Smolenski, P. Kossacki, A. Kretinin, H. Shtrikman, and D. K. Maude. Nano Lett. 14, 2807 (2014).
- [3] *Magnetophotoluminescence in GaAs/AlAs core-multishell nanowires: A theoretical investigation*. F. Buscemi, M. Royo, A. Bertoni, and G. Goldoni. Phys. Rev. B 92, 165302 (2015).

## KINETIC ENERGY DENSITY FUNCTIONAL

Kohn-Sham (KS) Density Functional Theory (DFT), the most used computational method in quantum chemistry and solid-state physics, typically scales cubically with system size, due to the introduction of KS orbitals: large-scale applications are thus out-of-reach. To that end, orbital-free-DFT and subsystem-DFT, are recently attracting large and renewed interest. However, their accuracy largely depends on approximations for the non-interacting kinetic energy (KE) functional, which is a big challenge in DFT. Here, we present two studies relevant for the development of KE functionals: the application of the Laplacian of the density in subsystem-DFT and the behaviour of the exact KE density at the nuclear cusp.

While the accuracy of KS-DFT depends on the approximations for the exchange-correlation (XC) energy as a functional of the electronic density ( $\rho$ ), orbital-free (OF) and subsystem-DFT calculations require even more essential approximations for the non-interacting kinetic energy (KE) functional. In OF-DFT the total KE needs to be approximated, whereas in subsystem-DFT only its non-additive part (i.e., the difference between the total interacting system and the sum of its non-interacting subsystems) is required. In both cases the development of accurate KE density functionals is a big challenge in DFT. Here, we present two recent advances in this direction.

i) We developed KE functionals which depend on the Laplacian of the density (namely on  $q$ , the reduced Laplacian) for subsystem-DFT. Previously, only KE functionals based on the Generalized-Gradient Approximation (GGA), i.e., depending only on the reduced gradient ( $s$ ), have been considered. Mean absolute errors for the total energy and the density obtained with different approximations are shown in Figure 1A. In particular, earlier functionals (MGE4, MGGA) yield very large errors, instead our new developed LO.4 functional shows an accuracy comparable to the state-of-the-art GGA. Moreover, we developed a novel technique, the sq-decomposition, to analyse the intermolecular interactions for subsystem-DFT in terms of  $s$  and  $q$ . The molecular bonding region is characterized by a well-defined value of  $q$ , see Figure 1B, highlighting the importance of the Laplacian as an ingredient of KE functionals.

ii) We derived a new exact condition for the behaviour of the exact KE density ( $\tau^{\text{KS}}$ ) at the nuclear cusp. Previously, it was believed that  $\tau^{\text{KS}}$  approaches the von Weizsäcker (W) one,

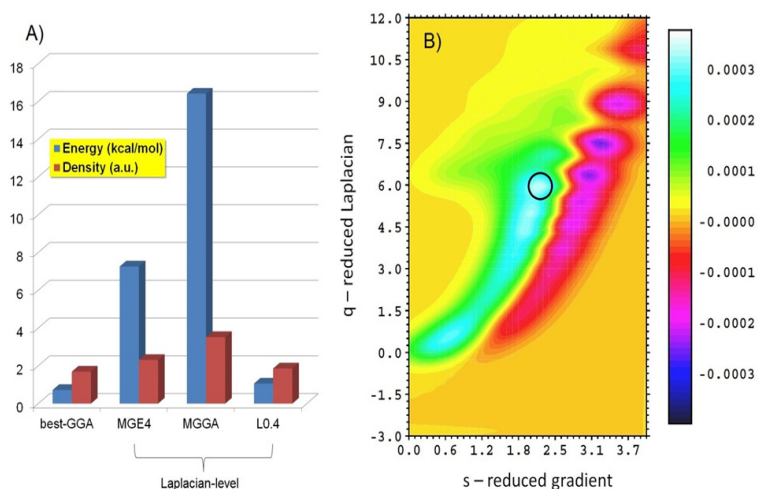


Figure 1. A) Mean absolute errors for the total energy (blue histograms) and the density (red histograms) for a molecular benchmark of weakly interacting complexes, resulting from subsystem-DFT calculations with different kinetic energy functionals. LO.4 is the new functional developed at Cnr Nano. B) sq-decomposition of the Thomas-Fermi non-additive kinetic energy for the Ne-Ar dimer. The circle indicates the most positive region, i.e., the main bonding region in the sq-space.



i.e.,  $\tau^W = |\nabla\rho|^2/(8\rho)$ . Figure 2 reports the relative difference between  $\tau^{KS}$  and  $\tau^W$  at the nuclear cusp, for different atoms: the plot clearly shows that  $\tau^W$  is quite inaccurate at the nuclear cusp, with relative errors up to 12% in the semiclassical limit of an infinite number of electrons. This large difference originates from the density of  $p$ -type orbitals which contribute to  $\tau^{KS}$  but not to  $\tau^W$ : in fact the density of  $p$ -type orbitals vanishes at the nuclear cusp, as well as its gradient.

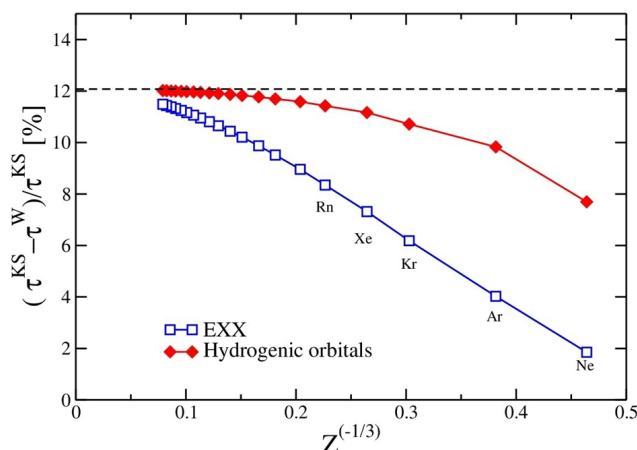


Figure 2. Relative difference between the exact kinetic energy density ( $\tau^{KS}$ ) and the von Weizsäcker ( $\tau^W$ ) one at the nuclear cusp, for all neutral noble atoms up to  $Z=2022$  electrons and considering either exact-exchange (EXX) or hydrogenic orbitals. The horizontal dashed line represents the theoretical semiclassical limit ( $Z \rightarrow \infty$ ).

### Contact person

Fabio Della Sala (fabio.dellasala@nano.cnr.it)

### References

- [1] *Laplacian-Level Kinetic Energy Approximations Based on the Fourth-Order Gradient Expansion: Global Assessment and Application to the Subsystem Formulation of Density Functional Theory*. S. Laricchia, L. A. Constantin, E. Fabiano, and F. Della Sala. *J. Chem. Theory Comput.* 10, 164 (2014).
- [2] *Kohn-Sham kinetic energy density in the nuclear and asymptotic regions: Deviations from the von Weizsäcker behavior and applications to density functional*. F. Della Sala, E. Fabiano, and L. A. Constantin. *Phys. Rev. B* 91, 035126 (2015).

## NOVEL HYBRID DENSITY FUNCTIONALS

Density Functional Theory (DFT) is the most popular first-principles computational method in nanoscience. However, its accuracy depends on the approximation of the exchange-correlation (XC) energy functional, which contains all the electron-electron interaction effects beyond the classical Coulomb repulsion. Thus, the development and testing of XC functionals is an active research field within DFT.

We have developed a new non-empirical XC functional (hAPBE) based on a global hybrid scheme which mixes semilocal and nonlocal exchange contributions. The hAPBE functional shows a very good performance over a large set of tests, generally outperforming other state-of-the-art hybrid functionals.

Hybrid exchange-correlation (XC) functionals are popular tools within density functional theory (DFT). They are based on a wise admixture of non-local exact exchange with a semilocal XC approximation. This leads to high accuracy at a moderate computational cost. However, the performance depends critically on the features of the semilocal part, that must be accurate and well compatible with exact exchange. Hence, the development of non-empirical hybrid XC functionals is still a challenge in DFT. Recently, we have developed a new non-empirical hybrid XC functional, named hAPBE. It is very accurate, being competitive with or better than some of the most popular hybrid functionals (PBE0, B3LYP), and shows broad applicability in chemistry.

The semilocal exchange part of the functional is based on the recovery of the modified second-order gradient expansion (MGE2). The MGE2 has been derived in the context of the semiclassical atom theory and recovers the local-density limit for homogenous densities, resembling the full fourth-order gradient expansion in the slowly-varying density regime. Thus, it is a very powerful tool for the description of the exchange interaction at the semilocal level.

The correlation part of the functional is constructed requiring the respect of the accurate local density approximation (LDA) linear-response behavior with respect to both the exact and the semilocal exchange contributions. For this reason in the hAPBE functional, two different correlation approximations are employed and mixed in a similar fashion as for the exchange part. One approximation, based on the LDA linear response of the MGE2, is used to complement the semilocal exchange. A second correlation term is introduced to complement the non-local exact exchange. Building up on previous studies concerning the compatibility of semilocal correlation with exact exchange, this functional has been constructed using a localization technique for the correlation energy density, which allows

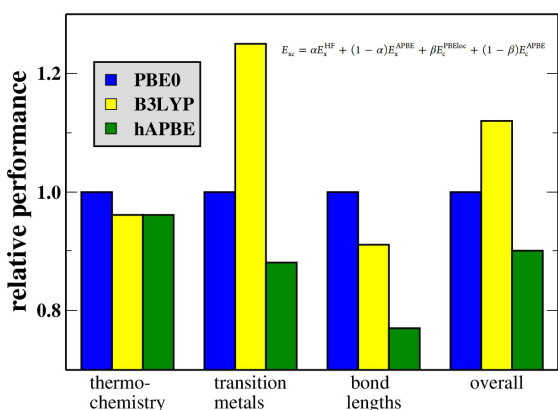
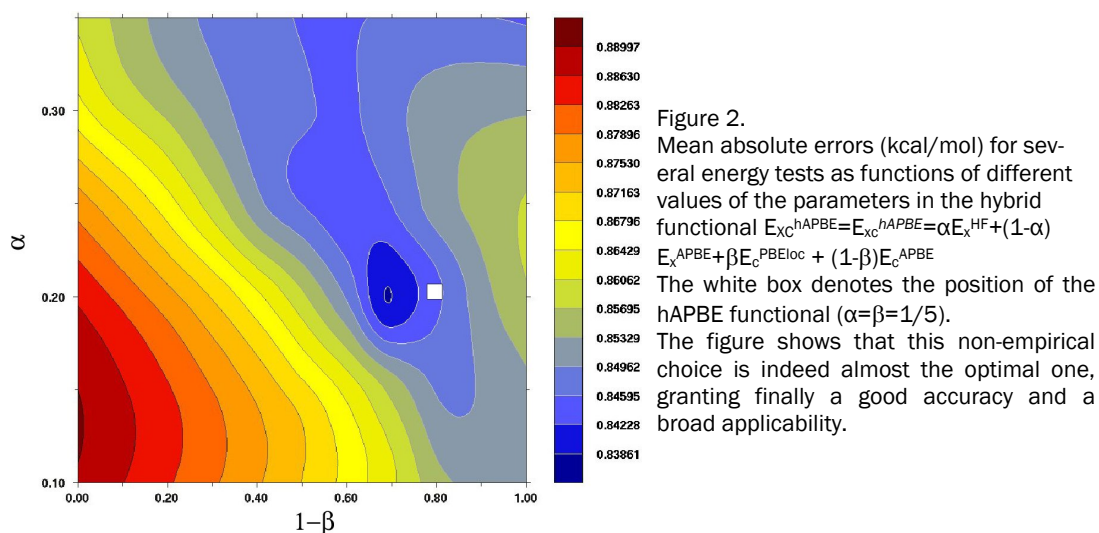


Figure 1.

Overview of the performance of the hAPBE and B3LYP XC hybrid functionals, relative to the PBE0 one, for different areas of computational chemistry. The figure shows that the hAPBE functional performs consistently better than the reference state-of-the-art functionals and finally yields an overall performance about 10% better than PBE0.

to recover the correct LDA second-order behavior without reducing the functional's accuracy.



#### Contact person

Eduardo Fabiano (eduardo.fabiano@nano.cnr.it)

#### Reference

[1] *Global Hybrids from the Semiclassical Atom Theory Satisfying the Local Density Linear Response*. E. Fabiano, L. A. Constantin, P. Cortona, and F. Della Sala. J. Chem. Theory Comput. 11, 122 (2015).

## YBa<sub>2</sub>Cu<sub>3</sub>O<sub>7</sub> MICROWAVE RESONATORS FOR STRONG COLLECTIVE COUPLING WITH SPIN ENSEMBLES

Coplanar microwave resonators made of superconducting YBa<sub>2</sub>Cu<sub>3</sub>O<sub>7</sub> have been realized and characterized in a wide temperature and magnetic field range. The quality factor (Q) exceeds 30000 at low temperature and is magnetic-field resilient, remaining 90% of  $Q(B=0)$  for  $B = 7$  T and  $T = 2$  K. These features allow the coherent coupling of resonant photons with a spin ensemble at finite temperature and magnetic field. To demonstrate this, collective strong coupling was achieved by using a spin ensemble of DPPH organic radical placed at the magnetic antinode of the fundamental mode: the in-plane magnetic field is used to tune the spin frequency gap splitting across the single-mode cavity resonance at 7.75 GHz, where clear anticrossings are observed with a splitting as large as 82 MHz at  $T = 2$  K.

We have shown that coplanar resonators made of high critical temperature YBCO allow expanding temperature and magnetic field ranges with respect to the Nb cavities commonly used in circuit-QED experiments. We fabricated superconducting coplanar resonators upon wet etching of YBCO/sapphire films and characterized their behavior in a low temperature cryomagnetic set-up equipped with 7 T magnetic field applied parallel to the plane of the resonator. At  $T=2$  K, the transmission spectrum shows a well-defined resonance centered at  $f_0 = 7.75$  GHz with typical quality factor exceeding 30000. The measured quality factor remains above 10000 for  $T < 55$  K.

An applied magnetic field (B) generally gives rise both to a decrease of the quality factor and to a hysteretic behavior of the resonant frequency. While this behavior was effectively observed for intermediate temperatures, at low temperature the field dependence of the YBCO coplanar resonator becomes progressively weaker. At 2 K resonant frequency and quality factor are remarkably stable up to 7 T (see Figure 1), being  $Q(0 \text{ T}) \simeq 0.9 \times Q(7 \text{ T})$ . This result is an impressive progress with respect to Nb resonators, where a drop of the quality factor is observed for fields in the mT range.

We exploited these unique properties to perform circuit-QED experiments with a spin ensemble of DPPH organic radical. A layer of DPPH, corresponding approximately to  $6 \times 10^{16}$  spins, was attached to the center of the resonator in correspondence to the magnetic antinode of the microwave field. We measured transmission spectrogram of the resonator

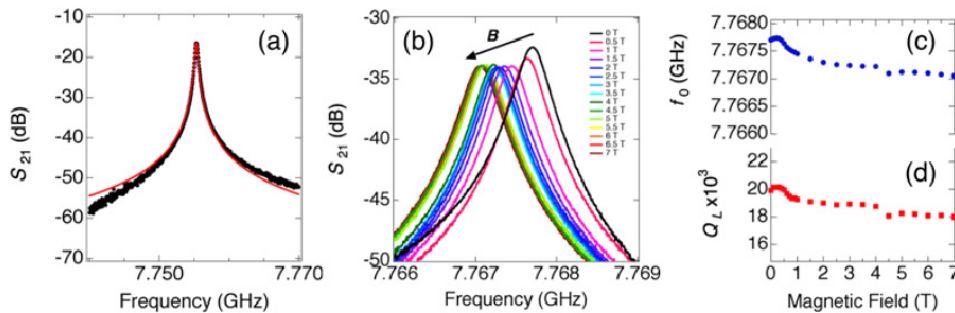


Figure 1.

(a) Transmission spectrum of the bare resonator measured at 2 K. (b) Transmission spectra as a function of frequency measured for applied external magnetic fields up to 7 T. Dependence of (c) the resonant frequency and (d) the loaded quality factor on the external magnetic field.

in the low-excitation limit (photon number  $\ll$  spin number) and observed a large anticrossing between the resonator mode and the spin ensemble. The measured collective coupling strength ( $g_c$ ) is 39 MHz at 2 K. We investigated the temperature dependence of the measured transmission spectra, showing that the collective coupling rate scales as the square root of the number of polarized spins in the ensemble (see Figure 2). Being  $\kappa \simeq 1$  MHz the decay rate of the resonator and  $\gamma \simeq 14$  MHz the linewidth of the spin transition, the condition  $g_c \gg \kappa, \gamma$  is satisfied for  $T < 40$  K, showing that the strong-coupling regime is reached in this temperature range.

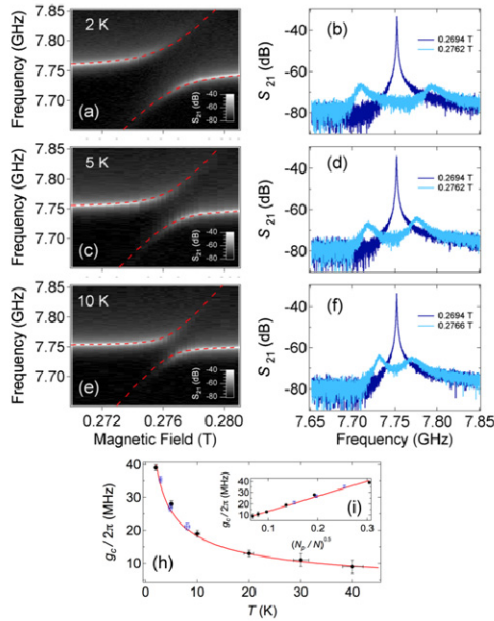


Figure 2.

Transmission spectra of a YBCO microwave resonator loaded with a DPPH spin ensemble. (a, c, e) Series of transmission spectrograms measured at different temperature. (b, d, f) Cross sections related to the corresponding right panel, either on resonance (cyan) or off resonance (blue). The lower panel shows the dependence of the collective coupling strength with respect to (h) temperature and (i) estimated ratio of polarized spins.

### Contact person

Alberto Ghirri (alberto.ghirri@nano.cnr.it)

### Reference

[1] *YBa<sub>2</sub>Cu<sub>3</sub>O<sub>7</sub> microwave resonators for strong collective coupling with spin ensembles*. A. Ghirri, C. Bonizzoni, D. Gerace, S. Sanna, A. Cassinese, and M. Affronte. Appl. Phys. Lett. 106, 184101 (2015).

## STRUCTURED QUANTUM WAVES

The introduction of electron synthetic holograms has opened the way to shape electron beams with specific quantum properties (states) such as a defined angular momentum, apparent self acceleration controlled diffractive properties and so on. This paves the way to innovative electron microscopy techniques for both material science application and basic science exploring the principle of wave equations and quantum mechanics. Our group has introduced the innovative phase hologram and demonstrated some of the most difficult and interesting examples of beam shaping so far.

So far electron microscopists have mainly aimed at improving the resolution and getting more and more information about the sample. However they have given less attention to their main investigation tool: the electron beam.

Since the introduction of electron vortex beams (beam with spiraling wavefront) and electron beam holograms, it has become increasingly clear the possibility to have an unprecedented control over the electron wavefunction and to produce electron beams with specific properties.

Electron microscopy is reaching a control of the beam comparable to that of optic beams. The equations for electrons and photons, in paraxial approximation, are formally the same; however, what really paved the road to holographic electron optics has been the introduction of FIB (Focused Ion Beam) nanofabricated patterns on SiN membranes to induce a controlled phase plate (phase holograms) made by our group.

To demonstrate the flexibility of the new technique we shaped the beam as the CNR logo (see Figure 1a) and demonstrated the first experimental example of Bessel beams (Figure 1b). These beams are invariant upon propagation, they can carry quantized orbital angular momentum, and can be used in interferometry or as a focus invariant probe. We also

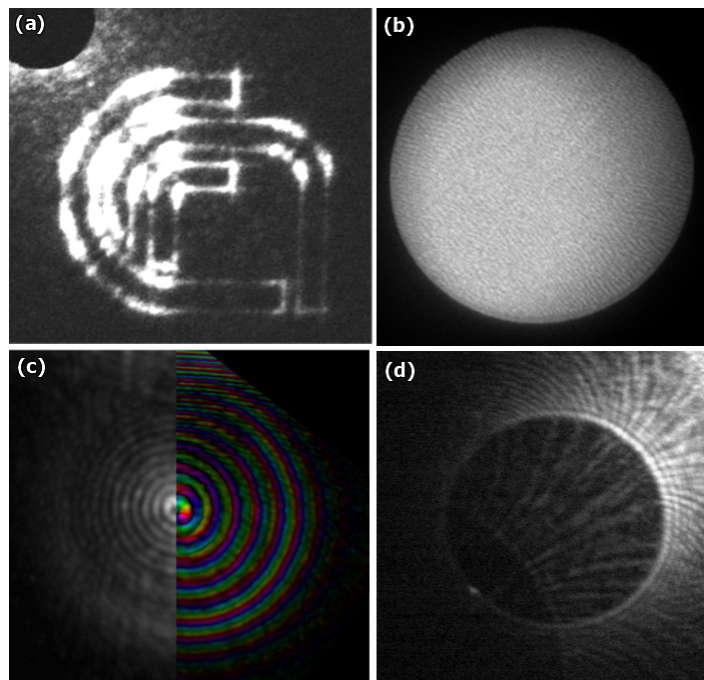


Figure 1.

(a) Example of a beam shaped as the CNR logo. (b) Image of the hologram that generated the logo-beam. (c) Experimental image of a holographically generated Bessel beam, tiled to an experiment-based calculation of the relevant phase (corresponding to different hue colour). This specific beam is endowed with orbital angular momentum 2 as the phase winds up by  $4\pi$  in a turn. The amplitude profile is functionally described by the Bessel function of order two and is largely unaffected by focal changes. (d) Experimental image of the vortex beam with nominal winding number 200. The main beam is ring-shaped with a dark area at the centre. The superimposed intensity arises from the second order of diffraction.

demonstrated the largest vortex beam that carries an orbital angular momentum  $200\hbar$ . This large value implies that a magnetic moment as large as 200 Bohr magnetons is associated to each electron of the beam and makes it the ideal probe for magnetic properties of a material. The image in Figure 1c shows the vortex beam section as a large ring with relatively dark centre (spurious intensity derive from higher diffraction) due to the centrifugal effect of the large orbital angular momentum.

In conclusion, these examples suggest that the additional degree of freedom given by these new holographic optical elements can be used for a completely new paradigm of experiments in material science but also to explore basic physics effects as outlined in our review.

### Contact person

Vincenzo Grillo (vincenzo.grillo@nano.cnr.it)

### References

- [1] *Structured quantum waves*. J. Harris, V. Grillo, E. Mafakheri, G. C. Gazzadi, S. Frabboni, R. W. Boyd, and E. Karimi. Nature Physics 11, 629 (2015).
- [2] *Holographic generation of highly twisted electron beams*. V. Grillo, G. C. Gazzadi, E. Mafakheri, S. Frabboni, E. Karimi, and R. W. Boyd. Phys. Rev. Lett. 114, 034801 (2015).
- [3] *Generation of Nondiffracting Electron Bessel Beams*. V. Grillo, E. Karimi, G. C. Gazzadi, S. Frabboni, M. R. Dennis, and R. W. Boyd. Physical Review X 4, 011013 (2014).



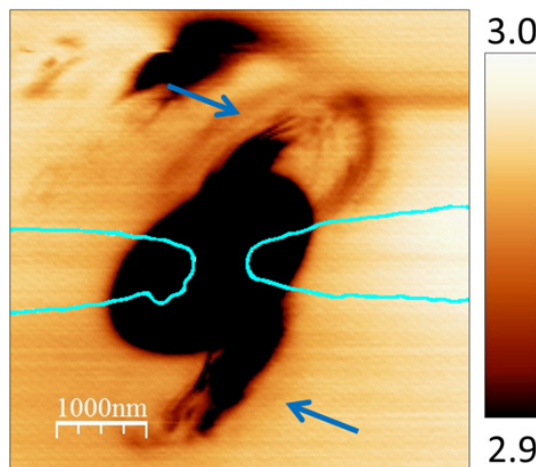
## SCANNING GATE IMAGING OF QUANTUM POINT CONTACTS AND THE ORIGIN OF THE 0.7 ANOMALY

The origin of an anomalous transport feature in quantum point contacts (QPC) –the so-called 0.7 anomaly– represents a long standing puzzle in quantum transport. Several mechanisms have been proposed to explain it, but a general consensus has not been achieved yet. A key open issue is whether point defects are the physical cause behind this conductance anomaly. Here we use scanning gate microscopy (SGM) to map individual impurity positions in several QPCs and correlate these with conductance characteristics. Our data demonstrate that the 0.7 anomaly can be observed irrespective of the presence of localized defects, and we conclude that the 0.7 anomaly is a fundamental property of low-dimensional systems.

The subject of localized defects has been dealt with extensively by channel shifting experiments. If an impurity is present in the QPC, its influence on the conductance can be tuned by laterally shifting the QPC channel. Such a technique is, however, not conclusive since it can detect only defects inside the constriction. Potential variations occurring at the sides of the constriction, or some hundred nanometers outside it, can be invisible to this approach.

In such a configuration, SGM can provide additional information. Indeed, it allows to unequivocally detect localized charged structures and their position with respect to the QPC, as shown in Figure 1. The lower arrow shows an impurity near the QPC entrance that appears in the SGM image as a dark spot and identifies an area where a sharp potential variation occurs. The upper arrow shows concentric ring-like shapes which indicate the formation of a (anti)dot. The results of Figure 1 demonstrate that when impurities are present, their signatures are indeed detected by SGM.

Figure 2a shows an SGM image of the QPC area of another device. No trace of sharp potential fluctuations is detected: we can therefore rule out the presence of localized impurities in the scanned area. On the other hand, the 0.7 anomaly can be observed directly from the SGM map. Figure 2b shows several conductance cross-sections cut along the lines highlighted in Figure 2a. All profiles display a shoulder at  $G \sim 0.7 G_0$ . In each trace, this shoulder appears within a narrow range around the average value, which, consistent with channel shifting measurements, further demonstrates that no impurity is present. Our experiments therefore show that any physical models based on localized defects for the 0.7



structure are not correct, and that the 0.7 anomaly is an intrinsic property of low-dimensional systems. Furthermore, we

Figure 1.  
QPC with localized impurities: SGM scan of the differential conductance  $G$  of the QPC area. The contrast is optimized to highlight the presence of an impurity (lower arrow) and of an additional feature associated with (anti)dot formation (upper arrow).  $G$  is given in units of  $G_0 = 2e^2/h$ . The outline of the split-gates as obtained from an AFM topography image is indicated by the blue lines.



emphasize that by employing the SGM technique, we have performed a 2D channel shifting experiment in an area of the order of  $1\ \mu\text{m}^2$ , against the typical  $\sim 100\ \text{nm}$  1D shift of traditional measurements.

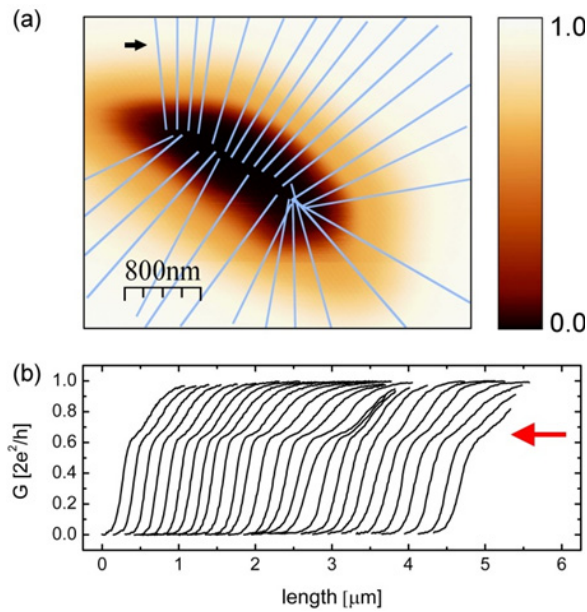


Figure 2.

QPC without localized impurities. (a) SGM scan of the differential conductance  $G$  of the QPC area, showing a QPC constriction without any localized defect. The conductance is given in units of  $G_0 = 2e^2/h$ . (b) Conductance cross-sections obtained from the SGM scan in (a), offset for clarity, displaying a clear 0.7 anomaly (red arrow). The traces, from left to right, are cuts along the lines in (a), starting at the arrow and following the clockwise direction. The 0.7 anomaly is at the same conductance value in all traces.

#### Contact person

Stefan Heun (stefan.heun@nano.cnr.it)

#### Reference

[1] *Scanning gate imaging of quantum point contacts and the origin of the 0.7 anomaly*. A. Iagallo, N. Paradiso, S. Roddaro, C. Reichl, W. Wegscheider, G. Biasiol, L. Sorba, F. Beltram, and S. Heun. *Nano Research* 8, 948 (2015).

## FRICTIONAL TRANSITION FROM SUPERLUBRIC ISLANDS TO PINNED MONOLAYERS

Inertial movements of physisorbed Xe islands on Cu(111) crystal surface at low temperature (47 K) reveal unexpected information on the ultra smooth, frictionless sliding associated with incommensurate superlubricity and on the mechanisms of its disappearance. Thanks to a joint experimental and computational effort, we shown how superlubricity emerges in the large size limit of naturally incommensurate Xe islands. Then, approaching full monolayer coverage, an abrupt adhesion-driven two-dimensional density compression transforms Xe into a commensurate immobile monolayer. This scenario is predicted by frictional molecular dynamics simulations and fully supported by Quartz Crystal Microbalance data.

Superlubricity, i.e., the vanishing of static friction and the consequent ultra-low dynamic friction, is a critical effect expected when surfaces in sliding contact are mutually incommensurate and sufficiently hard.

Here we measured the sliding friction of Xe island adsorbed on Cu(111), a system that meets these characteristics, by Quartz Crystal Microbalance (QCM). Monitoring the QCM resonance as a function of Xe deposition at 47 K, we evaluated the islands inertial sliding friction by the inverse of slip time  $\tau_s = (1/4\pi)[\delta(Q^{-1})/\delta f]$ , defined as the ratio of the adsorbate-induced change of the inverse quality factor (Q) over the respective change in the substrate oscillation frequency (f) (Figure 1).

Actually the peak of the inertial force acting on an island is expressed as  $F_{in} = \rho_{isl} SA(2\pi f)^2$  (where  $\rho_{isl}$  is the 2D density of an island of area S, and A and f are the QCM oscillation amplitude and frequency, respectively), and it equals the viscous frictional force  $F_{visc} = M\sqrt{\tau_s}$  (where M is the mass of the island, v its speed). This means that superlubricity should indirectly show up as an unusually large slip time  $\tau_s$ .

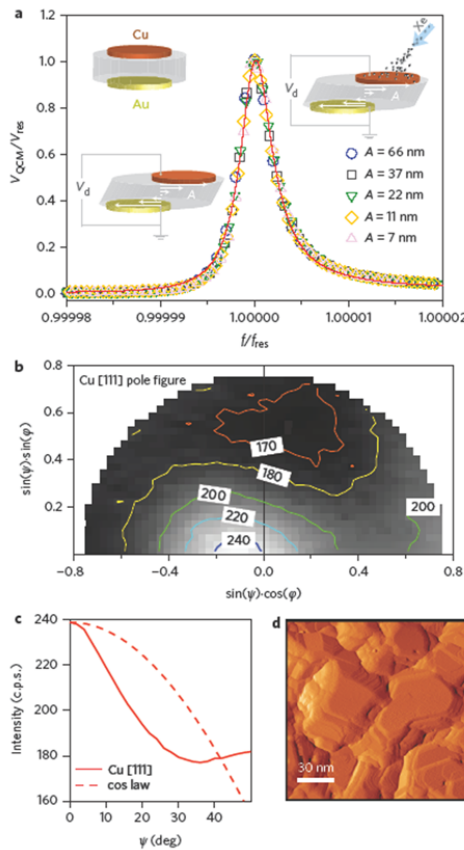


Figure 1.

The quartz crystal microbalance and characterization of the Cu(111) electrode. a) Normalized resonance curves of the QCM measured in vacuum and at  $T = 48$  K for different oscillating amplitudes A. The red line is a fit to the data for  $A = 7$  nm, and  $f_{res} \approx 5$  MHz represents the series resonance of the quartz crystal. Top left inset: sketch of the QCM with Cu and Au electrodes. Bottom left inset: the shear motion of the QCM at resonance. Arrows represent lateral displacements. Top right inset: Xe gas dosing on the QCM. b) Pole figure (stereographic plot) of the Cu [111] peak. The units of the contour plot labels are counts per second (c.p.s.).  $\psi$  (sample tilt angle) is varied between 0 and 50° and  $\phi$  (sample rotation angle) between 0 and 180°. c) Continuous line:  $\phi$ -averaged Cu [111] intensity as a function of  $\psi$ . Dashed line:  $\cos(\psi)$  law normalized to Cu [111] intensity at  $\psi=0^\circ$ . d) STM derivative image of the Cu film. Image size: 150 × 150 nm.

Data presented on Figure 2 show depinning and a rapid increase of  $\tau_s$  for increasing Xe coverage, reaching peak values of up to 4 ns, nearly an order of magnitude larger than  $\tau_s$  measured with Xe on gold and on graphene at the same temperature. Moreover, by further increasing coverage, we also found an unusual and sudden slip time collapse near monolayer completion.

All these features have been reproduced by frictional molecular dynamics (MD) simulations of a hard crystalline Xe island, by taking into account an intrinsic term (friction of an area  $S$  of infinite adsorbate) and defect terms, representing corrections for the island finite size and substrate defects. The increase of  $\tau_s$  with coverage, shown in Figure 3, can be attributed to the progressively decreasing role of edge pinning. The intrinsic, defect-free slip time, asymptotically reached in the large size limit, is dictated by the ideal Xe lattice, which is incommensurate and hard. We concluded that the unusually large  $\tau_s$  at submonolayer coverage signifies precisely that Xe islands sliding on Cu(111) are asymptotically superlubric. A sudden spontaneous compression at monolayer completion, caused by strong adhesion to the substrate, is predicted and, specific to Xe/Cu(111), is the ensuing of a  $\sqrt{3} \times \sqrt{3}$  commensuration during compression, causing a sudden transition from superlubric sliding to a pinned dense state.

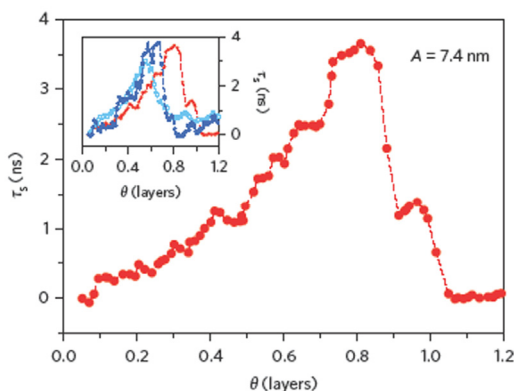
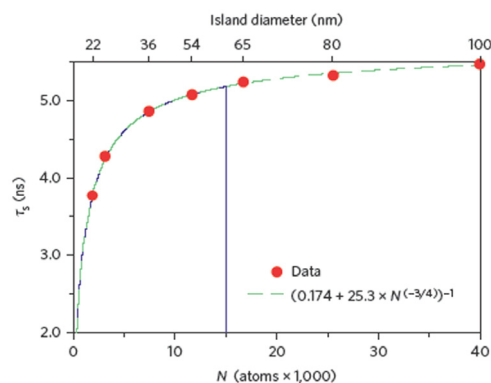


Figure 3.

Theoretical slip time from sliding simulations for incommensurate Xe islands of growing size, on a perfectly periodic potential representing Cu(111). The fit (dashed green line) shows that the size-controlled defect friction (here due to the island edge) gives way to very long slip times arising from bulk superlubricity in the large size limit ( $\tau_s$  bulk  $\approx 5.75$  ns). The vertical line marks full monolayer coverage for an estimated experimental Cu(111) terrace size of 60 nm. When islands reach this size, we expect a spontaneous density increase with sudden slip time collapse due to  $\sqrt{3} \times \sqrt{3}$  commensurability.

Figure 2.

Slip time of Xe on Cu(111) as a function of film coverage. The scan was taken at  $T = 47$  K with  $f_{res} \approx 5$  MHz and at an oscillating amplitude of the Cu electrode of  $A = 7.4$  nm. Inset: scans of Xe on Cu(111) taken for different Xe depositions on the same substrate at the same  $A$  and temperatures between 47 and 49 K. Note the sharp drop occurring near a full monolayer coverage, albeit with large fluctuations.



### Contact person

Guido Paolicelli (guido.paolicelli@nano.cnr.it)

### Reference

[1] *Frictional transition from superlubric islands to pinned monolayers*. M. Pierno, I. Bruschi, G. Mistura, G. Paolicelli, A. di Bona, S. Valeri, R. Guerra, A. Vanossi, and E. Tosatti. *Nature Nanotechnology* 10, 714-718 (2015).

## AB INITIO THEORY OF SPIN ENTANGLEMENT IN ATOMS AND MOLECULES

Entangled states are at the basis of quantum information, quantum computation, and other emerging quantum technologies. These states may be realized in different many-body systems and the interactions among the elementary constituents may enhance or suppress the degree of entanglement. The understanding and estimation of these many-body effects are desirable both theoretically and experimentally. Here, we introduce a first-principles atomistic approach for the estimation of spin entanglement in weakly correlated many-electron systems. We also provide fundamental insights for the construction of modern density functional approximations.

The Pauli exclusion principle implies that the state of two coalescent electrons is necessarily a spin singlet, i.e., a maximally entangled two-qubit state. Simple theoretical considerations that apply to an ideal Fermi gas, however, suggest that this kind of entanglement could be remarkably short ranged in many-electron systems. In this work, we show that for realistic inhomogeneous systems the situation is far more rich and interesting.

We show that Density Functional Theory (DFT) enables a practical and effective ab initio estimation of the concurrence function, which quantifies the entanglement between two electron spins. We derive the concurrence from the Kohn-Sham (KS) state, therefore the approach provides particularly useful information for weakly correlated systems.

Calculations performed for two representative systems, namely the Ar atom and the C<sub>2</sub>H<sub>2</sub> molecule, show that spin entanglement is remarkably long ranged within atomic shells (Figure 1) and molecular bonds (Figure 2). We also elucidate that the local entanglement length (IE) extracted in this way is a fundamental ingredient of the Electron-Localization Function (ELF) – often invoked in quantum chemistry as a useful tool for the visualization of atomic shells and molecular bonds – and of modern exchange-correlation approximations with improved performance for different kinds of bonds. We conclude that progress in DFT may greatly benefit from entanglement-based methods.

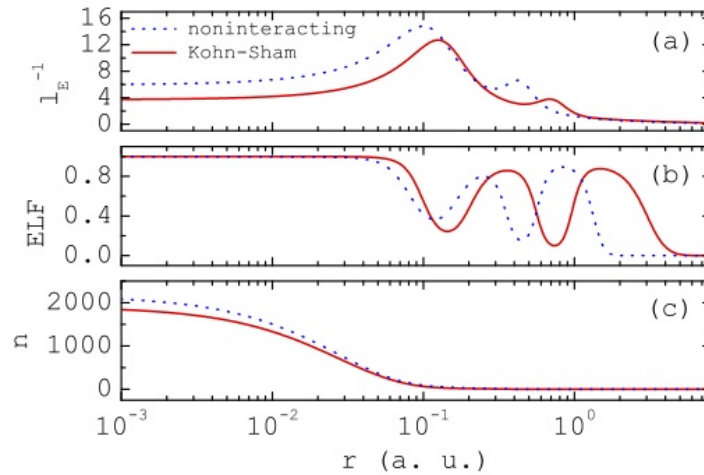


Figure 1.

Panel (a) shows the inverse of the local entanglement length (IE) for Argon atom; a comparison with the ELF in panel (b) confirms that the extension of the entanglement is enhanced within atomic shells; this information cannot be extracted solely from the electron density which, as shown in panel (c), decreases monotonically. The dashed blue lines are for truly non-interacting electrons, whereas the solid red lines are for KS electrons.

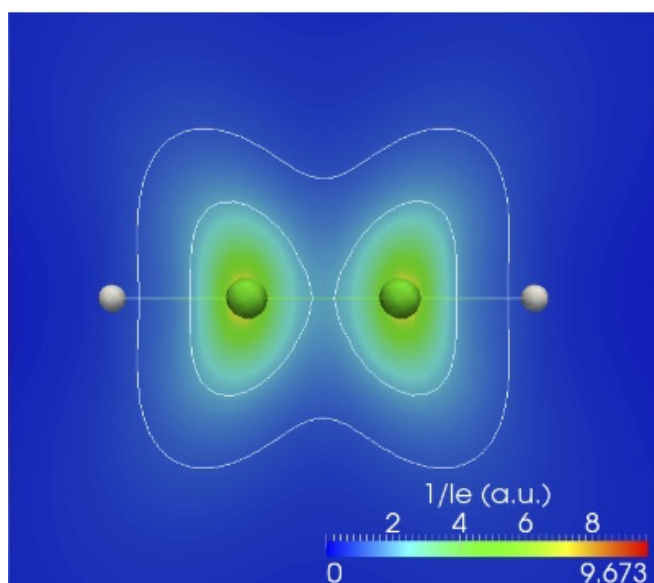


Figure 2.

The plot shows the inverse of the local entanglement length ( $l_e$ ) for the valence electrons in Acetylene in a molecular plane containing the main axis. While the electron density has minima within bonds and vanishes in the asymptotic region, the spin entanglement gets long ranged in the same regions.

#### Contact person

Stefano Pittalis (stefano.pittalis@nano.cnr.it)

#### Reference

[1] *Ab initio theory of spin entanglement in atoms and molecules*. S. Pittalis, F. Troiani, C. A. Rozzi, and G. Vignale. Phys. Rev. B 91, 075109 (2015).

## EXCITON-DOMINATED OPTICAL RESPONSE OF ULTRA-NARROW GRAPHENE NANORIBBONS

Narrow graphene nanoribbons (GNRs) exhibit substantial electronic bandgaps and optical properties fundamentally different from those of graphene. Unlike graphene—which shows a wavelength-independent absorbance for visible light—the electronic bandgap, and therefore the optical response, of GNRs changes with ribbon width. Reflectance difference spectroscopy in combination with ab initio calculations show that ultranarrow GNRs grown on metal substrate have fully anisotropic optical properties dominated by excitonic effects that sensitively depend on the exact atomic structure. Ab-initio calculations also reveal an absorbance of more than twice the one of graphene for visible linearly polarized light.

Prototypical GNRs with atomically precise edges have been achieved using a bottom-up approach, based on the covalent assembly of suitably designed molecular precursors, and they have revealed substantial band gaps. They are also predicted to exhibit characteristic absorption bands related to band gap openings as well as to pronounced excitonic effects that become dominant for quasi one-dimensional (1D) systems [1]. In this work, reflectance difference spectroscopy is used to detect optical excitations of uniaxially oriented GNRs on gold, which are caught in the act of their formation. We find sensitive changes of the optical properties during the on-surface synthesis of N=7 armchair GNRs (7-AGNRs). The optical spectra of both GNRs and the intermediate PA (polyanthrylene) oligomers are found to be dominated by strongly anisotropic features in the visible range that are of excitonic nature, as elucidated by ab-initio calculations, based on many-body perturbation theory. Experimentally, the GNR optical gap turns out to be very similar to the transport gap as determined by scanning tunnelling spectroscopy (STS). Far from indicating negligible

excitonic effects, this results from an incidental compensation between substrate-induced polarization effects and

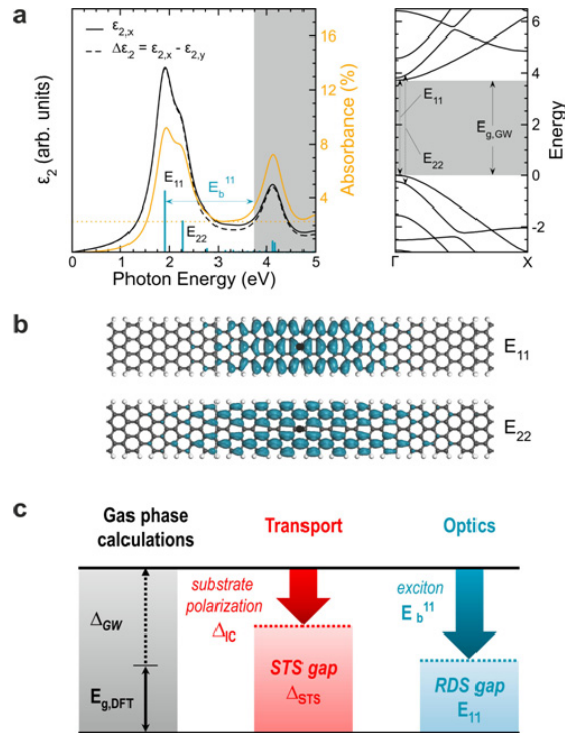
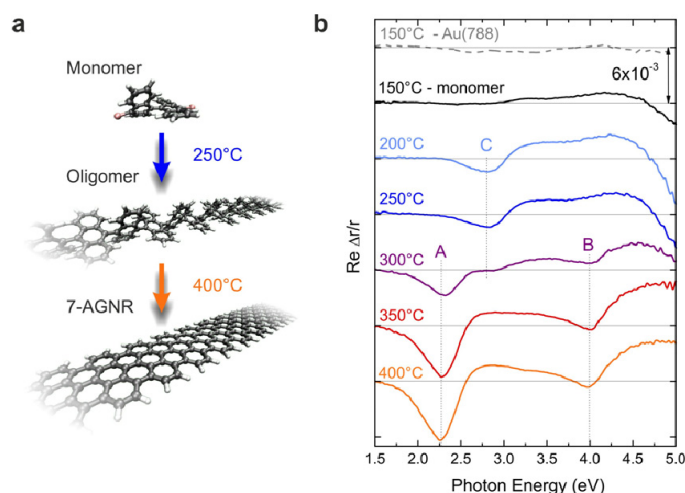


Figure 1. Calculated optical response of 7-AGNRs. a, Optical absorption spectrum and electronic band structure of 7-AGNRs calculated from first principles within the GW-BSE approach. The blue bars indicate the energy position and oscillator strength of the calculated optical excitations. The spectrum was obtained with a broadening of 0.5 eV and the same spectral lineshape used for fitting the reflectance difference spectroscopy (RDS) data. The absolute absorbance for full coverage and light polarized along the longitudinal (x) direction is also shown (orange curve), as compared to the reference value of 2.3% for monolayer graphene (dotted orange line). b, Exciton wavefunctions of the first and second excitons for 7-AGNRs. The calculated electron distribution is shown at fixed hole position (black dot). c, Schematics of the relations between transport and optical gaps determined by STS and RDS, as compared to ab-initio calculations in vacuum.



large lowest exciton binding energy, which is not the case for the PA oligomers. Our results demonstrate that achieving the limit of atomically precise GNRs allows engineering of specific optical features in the visible range, and predict an enhancement of the optical absorbance by a factor of about 2.4 as compared with ML (monolayer) graphene for visible linearly polarized light. This opens the field for optical and optoelectronic applications that build on tailor-made optical properties of GNRs.



**Figure 2.** In-situ RDS monitoring of the bottom-up formation of GNRs. a, Reaction scheme showing the evolution from the precursor monomer to atomically precise 7-AGNRs. b, RDS spectra recorded during 7-AGNR synthesis on Au(788). The black curve is obtained after deposition of  $\sim 0.8$  ML of precursor monomers on Au(788). Coloured curves correspond to successively higher annealing temperatures to induce polymerization and finally cyclodehydrogenation into planar, straight 7-AGNRs.

### Contact person

Deborah Prezzi (deborah.prezzi@nano.cnr.it)

### Reference

[1] *Exciton-dominated optical response of ultra-narrow graphene nanoribbons*. R. Denk, M. Hohage, P. Zeppenfeld, J. Cai, C. A. Pignedoli, H. Söde, R. Fasel, X. Feng, K. Müllen, S. Wang, D. Prezzi, A. Ferretti, A. Ruini, E. Molinari, and P. Ruffieux. Nat Commun 5, 4253 (2014).

## ULTRAFAST CHARGE TRANSFER IN PHOTOVOLTAIC MATERIALS

Blends of conjugated polymers and fullerene derivatives are prototype systems for organic photovoltaic devices. Here, we elucidate the ultrafast quantum dynamics of light-induced electron transfer in these materials. We observe coherent vibrational motion of the fullerene moiety after optical excitation of the polymer. Comparison with first-principle simulations evidences coherent electron transfer between donor and acceptor and oscillations of the transferred charge with a 25-femtosecond period matching that of the observed vibrational modes. Our results show that coherent coupling between electronic and nuclear degrees of freedom is of key importance in triggering charge delocalization.

The currently accepted model for the basic working principle of a bulk-heterojunction organic solar cell, comprising a conjugated polymer donor and an electron acceptor material, relies on four elementary steps: (i) photon absorption, creating a spatially localized, Coulomb-bound electron-hole pair (exciton) in the donor phase; (ii) exciton diffusion to the donor/acceptor interface; (iii) exciton dissociation at the interface leading to the formation of a charge-separated state, often called charge transfer exciton or polaron-pair; (iv) dissociation of the polaron pair into free charges and their transport to the electrodes.

In this work, we focus on the dynamics of the primary light-induced steps, (i) and (iii). So far all charge photogeneration in organic photovoltaic materials has been described within the framework of an incoherent transfer model. Here we investigate the role of quantum coherence at room temperature in the earliest stage of the photovoltaic conversion process.

Our experiments, performed with sub-10 fs resolution, show that the ultrafast electron transfer from the polymer triggers coherent vibrational motion of the fullerene (Figure 1). First-principle calculations (Figure 2) complete a consistent and general picture of the photo-induced charge separation: optical excitation locally creates an electron-hole pair on the polymer moiety; the strong coupling between electronic and nuclear degrees of freedom

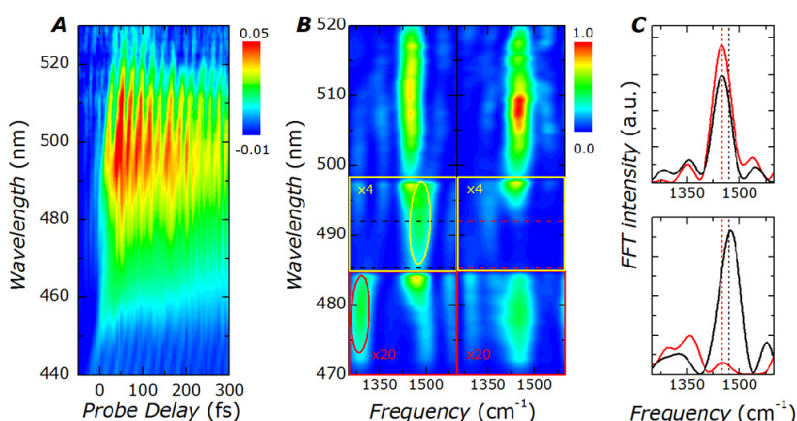


Figure 1. (A) Experimental differential transmission (DT=T) map of the P3HT:PCBM blend as a function of probe delay and probe wavelength. The pronounced oscillations in the DT/T signal reflect coherent vibrational wave-packet motion initiated by the short pump pulse. (B) Fourier transform spectra of the DT/T dynamics of the blend (left) and pristine P3HT (right). The spectral intensity is amplified by a factor of 4

for  $\lambda = 498$  to  $485$  nm and by a factor of 20 for  $\lambda = 485$  to  $470$  nm. (C) Integrated Fourier transform spectra for  $\lambda = 520$  to  $498$  nm (top) and  $\lambda = 492$  to  $485$  nm [bottom, dashed lines in (B)] of the blend (black) and pristine P3HT (red). The dashed vertical lines indicate the frequency of the P3HT C=C stretch mode (red) at  $1450\text{ cm}^{-1}$  and pentagonal pinchmode of the fullerene (black) at  $1470\text{ cm}^{-1}$ .



promotes a delocalization of the optically excited electronic wavepacket across the interface. Both the electronic density and the nuclei display oscillations on the same time scales, that are essential for an ultrafast charge transfer from the donor to the acceptor.

Observing coherent electron-nuclear motion in a non-covalently bonded complex, averaging over a macroscopic ensemble of P3HT:PCBM moieties with variable environment and interfaces, there is strong evidence for the dominant role of quantum coherences in the early stages of the charge transfer dynamics in this class of organic photovoltaic materials.

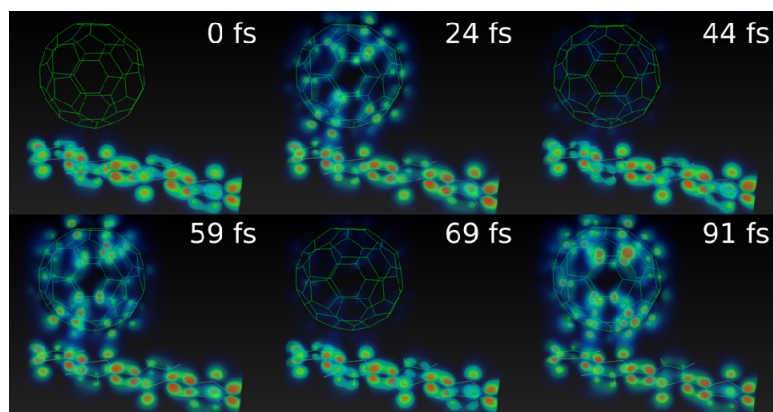


Figure 2.

This film strip contains frames taken from the quantum simulation of a portion of an organic solar cell composed by a polymer chain, and a Fullerene buckyball. The quantity depicted illustrates the wavelike oscillations of an electron after sun light is absorbed at time 0. The time scale is in femtoseconds (fs). The two parts of the system separated by a small space act as the poles of a microscopic sun-operated battery. Each frame depicts a scene about 2 nanometers wide.

#### Contact person

Carlo Andrea Rozzi (carloandrea.rozzi@nano.cnr.it)

#### References

- [1] *Coherent ultrafast charge transfer in an organic photovoltaic blend*. S. M. Falke, C. A. Rozzi, D. Brida, M. Maiuri, M. Amato, E. Sommer, A. De Sio, A. Rubio, G. Cerullo, E. Molinari, and C. Lienau. *Science* 344, 1001 (2014).
- [2] *Charge separation dynamics and opto-electronic properties of a diaminoterephthalate-C60 diad*. S. Pittalis, A. Delgado, J. Robin, L. Freimuth, J. Christoffers, C. Lienau, and C. A. Rozzi. *Adv. Func. Mat.* 25, 2047 (2015).

## THERMOELECTRIC EFFICIENCY OF THREE-TERMINAL QUANTUM THERMAL MACHINES: SEPARATION OF HEAT AND CHARGE CURRENTS FOR BOOSTED THERMOELECTRIC CONVERSION

The efficiency of a linear-response thermal engine in multi-terminal configurations is discussed. For the generic three-terminal case we provide a general definition of local and non-local transport coefficients, and we derive analytical expressions for the efficiency at maximum power, which can be written in terms of generalized figures of merit. Using two examples, we investigate numerically how a third terminal could improve the performance of a quantum system. Moreover, we show that charge and heat currents can be controlled independently in a three-terminal system containing a superconducting lead, thus leading to a great enhancement of thermoelectric performances at low temperatures.

Thermoelectricity has recently received enormous attention due to the constant demand for new and powerful ways of energy conversion. Increasing the efficiency of thermoelectric materials, heat engines and refrigerators at the nano-scale is one of the main challenges for several different technological applications. One of the keys to success in this field is the ability to modulate, control, and route heat and charge currents, ideally achieving their separate control. This is however by no means obvious as the charge and (the electronic contribution to) the heat are transported by the same carriers. In two-terminal systems, for example, within the linear response regime, electrical and thermal currents are strictly interrelated, as manifested by the emergence at low enough temperatures of the Wiedemann-Franz (WF) law. In this respect, multi-terminal devices, so far poorly investigated, offer the possibility to ‘decouple’ energy and charge flows, and improve thermoelectric efficiency.

In this context we have developed a general formalism for linear-response multi-terminal thermoelectric transport. In particular, we have worked out analytical expressions for the efficiency at maximum power in the three-terminal case. By means of two simple quantum-dot-based non-interacting models, we have shown that a third terminal can be useful to improve the thermoelectric performance of a system with respect to the two-terminal case. Furthermore, we have analysed the performance of a thermal machine that allows for the spatial separation between heat and charge currents. It is realized by connecting a conductor to a superconducting lead, a voltage probe, and a normal lead. We have shown that in the low temperature limit such system violates the WF law and allows, to some extent, an independent control of electrical conductance, thermal conductance, and

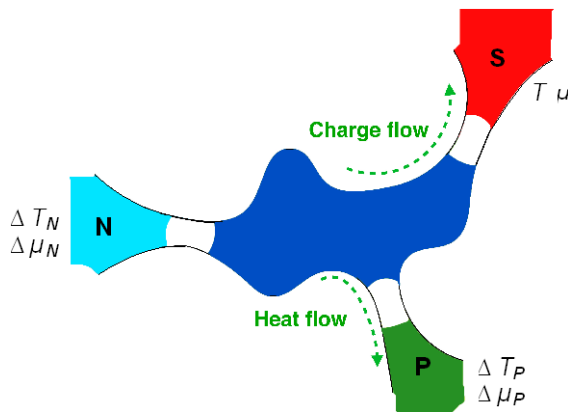


Figure 1.

The heat-charge current separation scheme (SPN setup). A generic conductor is connected to three reservoirs labelled by the letters S (superconducting lead), P (voltage probe), and N (normal metal lead). The reservoir S is the reference for the temperature  $T$  and the chemical potential  $\mu$ . A temperature (chemical potential) difference  $\Delta T_N$  and  $\Delta T_P$  ( $\Delta \mu_N$  and  $\Delta \mu_P$ ) is present in reservoir N and P, respectively. As indicated by the arrows, only charge flows inside lead S whereas only heat flows inside lead P.

thermopower. We have thus shown, on statistical grounds, that the system exhibits much larger values of the power factor  $Q$  and of the figure of merit  $ZT$  (one order of magnitude), with respect to the two-terminal counterpart.

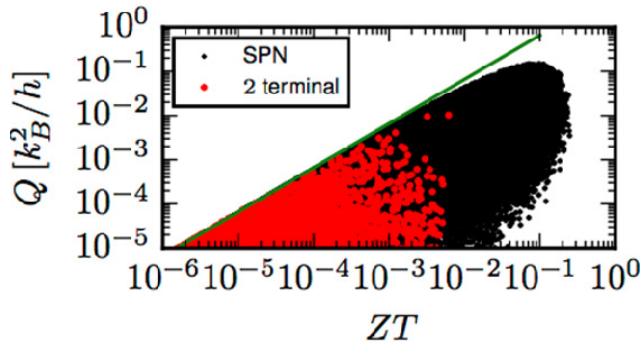


Figure 2.

Correlation between the power factor  $Q$  and the figure of merit  $ZT$  relative to systems consisting of three quantum dots for the SPN setup (black points) and the two-terminal setup (red points). The green curve corresponds to the bound given by the unitarity of the scattering matrix, and sets a maximum value for  $Q$  as a function of  $ZT$ . The plot shows that for the SPN setup both  $Q$  and  $ZT$  are one order of magnitude larger with respect to the corresponding values for the two-terminal system. The plot

refers to  $10^5$  Hamiltonian realizations, taking the couplings with the reservoirs P and N equal to  $10^3$   $k_B T$ .

#### Contact person

Fabio Taddei (fabio.taddei@nano.cnr.it)

#### References

- [1] *Thermoelectric efficiency of three-terminal quantum thermal machines*. F. Mazza, R. Bosisio, G. Benenti, V. Giovannetti, R. Fazio, and F. Taddei. *New J Phys* 16, 085001 (2014).
- [2] *Separation of heat and charge currents for boosted thermoelectric conversion*. F. Mazza, S. Valentini, R. Bosisio, G. Benenti, V. Giovannetti, R. Fazio, and F. Taddei. *Phys Rev B* 91, 245435 (2015).
- [3] *Magnetic thermal switch for heat management at the nanoscale*. R. Bosisio, S. Valentini, F. Mazza, G. Benenti, R. Fazio, V. Giovannetti, and F. Taddei. *Phys Rev B* 91, 205420 (2015).

## STATIC AND DYNAMICAL GRAPHENE RIPPLING FOR HYDROGEN STORAGE AND TRANSPORT

Due to its large surface to mass ratio, graphene is a candidate for gas (e.g.,  $H_2$ ) storage. However,  $H_2$  is weakly physisorbed by graphene, which allows useful storage densities only at low temperature/high pressure. Conversely, chemisorption leads to stable loading at room temperature, but with slow kinetics. Considering that the sheet local curvature alters its physics-chemical properties, we showed by computer simulations that static rippling can be used to aid chemisorption, while curvature inversion or travelling ripples such as those generated by flexural phonons allow  $H_2$  desorption and transport through graphene multilayers. Our results could be used to aid H-storage devices design.

In spite of its exceptional properties, bare graphene is not optimal for many applications [1]. It is a high-mobility conductor with null density of carriers. Thus, for electronics, it requires doping or gap opening. Its weight and mechanical properties make it a candidate as a medium for H-storage. However, it is rather inert, implying either too slow kinetics of loading/release for chemisorption, or low gravimetric density for physisorption. In addition, storage applications require building 3D frameworks. Therefore one needs to control graphene structure at the nano-metric level, creating loci for (either chemical or physical) adhesion, e.g., by (substitutional) defects, adhesion of atoms or chemical groups, deposition of molecular clusters, or corrugation.

We address the nano-scale graphene morphing issues with computer simulations, combining Density Functional Theory and classical Molecular Dynamics. Following the idea that graphene reactivity is enhanced over ripples, we performed an analysis of the structural and electronic properties of graphene with different levels of corrugation [2]. After confirming the enhanced stability of adatoms on convexities, we examined increasingly

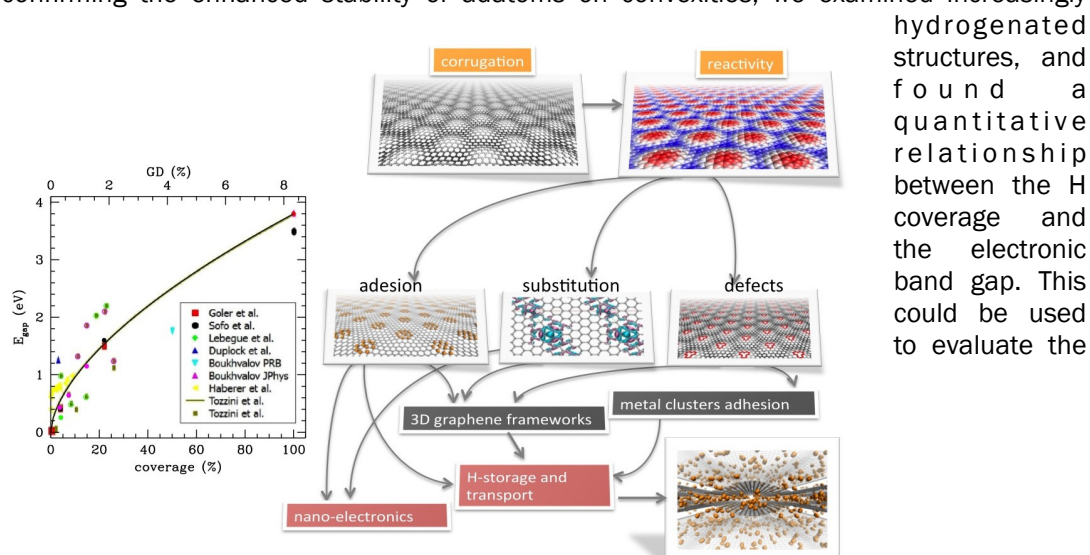


Figure 1.

Corrugation and related properties in graphene. Corrugation produces reactive hot-spots (right, in red) and can drive chemical adhesion, substitutions and structural defects. Applications to H-storage are direct (by chemical adhesion) or mediated by 3D framework creation and metal clusters deposition. Substitutions produces electronic doping, while hydrogenation induces gap opening as quantified in the plot on the left, reporting the gap vs H coverage (line and green magenta dots are our work, other dots are literature data).

H loading by means of STS (Scanning Tunnelling Spectroscopy) measurements or to tune the band gap by means of hydrogenation, with applications in H-storage and nano-electronics (Figure 1).

As the stability of adatoms is enhanced on convexities, it is decreased in concavities, and curvature inversion can induce desorption of H<sub>2</sub>. Conversely, physisorbed H<sub>2</sub> has larger affinity for concavities. We then studied the possibility of transporting H<sub>2</sub> by means of travelling cavities generated by coherent flexural phonons in multilayers. We showed that as far as the coherency is maintained, H<sub>2</sub> can be moved over macroscopic distances, or pumped through multilayers, to enhance storage capacity [3] (Figure 2).

This work is supported by EU (Graphene Flagship, MCSA, and PRACE) and by CINECA-ISCRA.

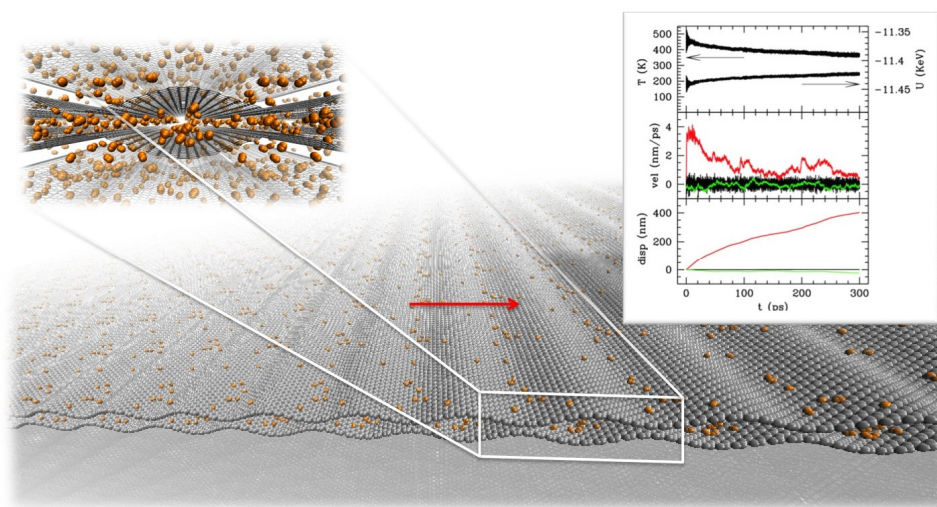


Figure 2.

Hydrogen transportation within graphene multilayers with ZA phonons travelling along the x direction (the red arrow in the graphical representation in the bottom, with graphene in grey and hydrogen in orange). The plot on the right reports temperatures and energies, average H<sub>2</sub> velocities and average travelled distances along the three directions in a 300 ps simulation run. Red lines are relative to the wave propagation direction. The plot shows that hydrogen travels at about 400 nm before spontaneous damping of phonons, due to absence of external powering. Macroscopic distances are expected to be travelled if a mechanism for phonons coherency maintenance is included.

### Contact person

Valentina Tozzini (valentina.tozzini@nano.cnr.it)

### References

- [1] *Graphene, related two-dimensional crystals, and hybrid systems for energy conversion and storage*. F. Bonaccorso, L. Colombo, G. Yu, M. Stoller, V. Tozzini, A. C. Ferrari, R. S. Ruoff, and V. Pellegrini. *Science* 347, 1246501 (2015).
- [2] *Nano-Scale Corrugations in Graphene: a Density Functional Theory Study of Structure, Electronic Properties and Hydrogenation*. A. Rossi, S. Piccinin, V. Pellegrini, S. de Gironcoli, and V. Tozzini. *J Phys Chem C* 119, 7900–7910 (2015).
- [3] *Hydrogen transport within graphene multilayers by means of flexural phonons*. V. D. Camiola, R. Farchioni, V. Pellegrini, and V. Tozzini. *2D Mater* 2, 014009 (2015).



## COHERENT PERFECT ABSORPTION IN STRONGLY-COUPLED SYSTEMS

The ability to drive a system with an external input is a fundamental aspect of light-matter interaction. The coherent perfect absorption (CPA) phenomenon extends to the general multibeam interference phenomenology the well-known critical coupling concepts. The latter defines the conditions under which the energy of the input field is fed in full to the absorbing element. Here we have studied CPA in reference to photonic structures which can resonantly couple to a material transition and have demonstrated that the strong coupling regime and the critical coupling condition can indeed coexist. In this situation, termed strong critical coupling, all the incoming energy is converted into polaritons.

The light absorption properties of a system are typically considered an intrinsic material feature, mostly determined by its dielectric constant, thickness, etc. It has recently been shown, however, that full interferometric control of absorption can instead be accomplished by varying the relative phase of two coherent optical fields. Depending on the phase relation, the system can become totally opaque (coherent perfect absorption – CPA) or tune to complete transparency (coherent perfect transparency – CPT).

These phenomena are now starting to be widely investigated at a fundamental level (CPA is actually considered the time-reversed process of lasing) and in view of innovative applications in diagnostics and imaging techniques.

Surprisingly, up to now CPA and CPT have never been considered in the presence of material resonances. Here it is of course the non-perturbative regime, in which the interaction of the resonance with the electromagnetic field is stronger than all dephasing and damping rates, that is particularly interesting. In this so-called strong coupling regime, the matter and light degrees of freedom are in fact mixed into dressed states, leading to new eigenstates called polaritons.

We have shown that the strong coupling regime and the critical coupling condition can indeed coexist; in this situation, which we term strong critical coupling, all the incoming energy is converted into polaritons. A semiclassical theory reveals that the strong critical coupling corresponds to a special curve in the phase diagram of the coupled light-matter oscillators. Polaritonic CPA has been verified in a semiconductor-based photonic-crystal membrane resonator, by exploiting the interaction with intersubband transitions in an embedded multi-quantum-well structure.

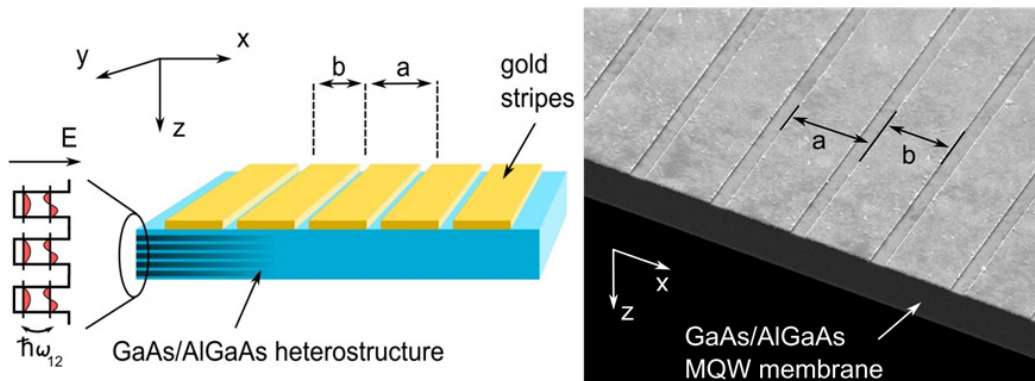


Figure 1.  
Scheme (left) and actual picture (right) of the membrane sample with metallic grating and embedded quantum wells used for the polariton CPA experiments.

These concepts open new avenues in the exploration of polariton physics, making it possible to control the pumping efficiency of a system almost independently of its Rabi energy, i.e., of the energy exchange rate between the electromagnetic field and the material transition.

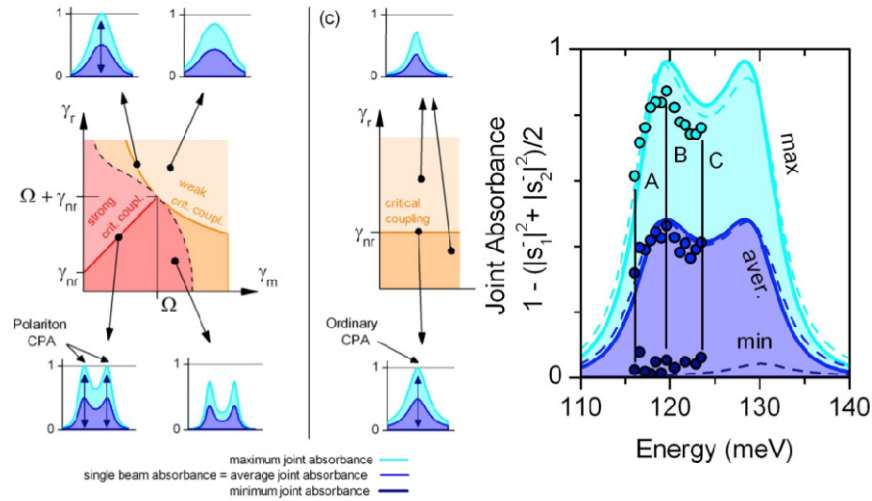


Figure 2.

Left: Phase space of resonator radiative linewidth  $\gamma_r$  and the corresponding absorption regimes: orange - weak coupling (one absorption peak), red - strong coupling (two polaritonic peaks), orange line - weak critical coupling (one peak CPA), red line - strong critical coupling (two peak, polaritonic CPA).  $\Omega$  is the vacuum Rabi energy and  $\gamma_{nr}$  the non-radiative resonator linewidth. Center: the same for  $\Omega=0$ , i.e., no material resonances (conventional CPA). Right: experimental points for different dephasing conditions showing full modulation from CPT to nearly complete CPA.

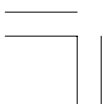
### Contact person

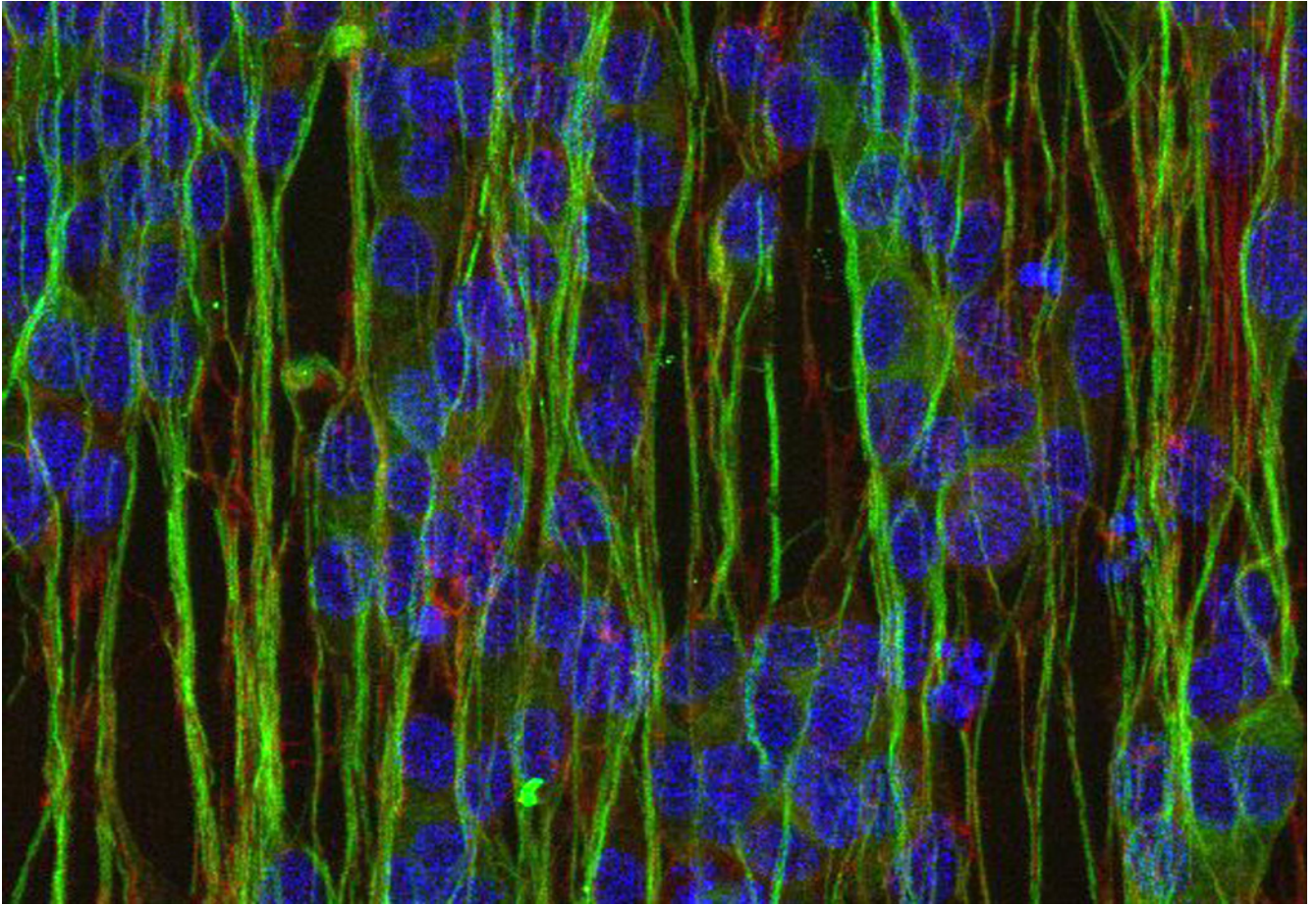
Alessandro Tredicucci (alessandro.tredicucci@unipi.it)

### References

- [1] *Perfect energy-feeding into strongly coupled systems and interferometric control of polariton absorption.* S. Zanotto, F. Mezzapesa, F. Bianco, G. Biasiol, L. Baldacci, M. S. Vitiello, L. Sorba, R. Colombelli, and A. Tredicucci. *Nature Phys.* 10, 830 (2014).
- [2] *Interferometric control of absorption in thin plasmonic metamaterials: general two port theory and broadband operation.* L. Baldacci, S. Zanotto, G. Biasiol, L. Sorba, and A. Tredicucci. *Opt. Express* 23, 9202 (2015).

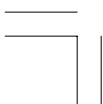






# **Highlights**

## **Nanobiotechnology**



## Introduction to Nanobiotechnology

A paradigmatic example of the multidisciplinary approach of the Institute is the strong connection of **nanotechnology** with **bio-inspired** activities. The application of nanotechnology-based techniques to biophysics and to biomedical applications is a strongly growing sector whose economic value has a projected compound growth rate of 12% and this data suggests the strategic importance of fostering this convergence.

The full spectra of biotechnology activities of the Institute can be broadly divided into three general themes:

**Computational simulations of biomolecules and their interaction with nanosystems:** Simulations at multiple levels of theory (from atomistic *ab initio* to classical coarse-grained) are performed to investigate biophysical processes in biomolecules, the effects of nanomaterials on biomolecular properties and biofunctionalized nanomaterials for biotechnological applications. Molecular dynamics and computational analysis of biomolecules.

**Interactions between biomolecules and matter at the nanoscale:** Here we group activities that explore the world of molecular interactions by means of tools characteristic of nanoscience such as the atomic force microscope, or that use micro- and nano-fabrication techniques for the control of matter and for the development of new nano/bio-electronic devices and systems, and of novel tools and concepts for nanomedicine. In this area, activities focused on the development of lab-on-chip devices use microfluidic and electro-optical techniques for the control of fluids and for the detection of solutes and the use of polymer and composite nanostructures, on areas of many  $\mu\text{m}^2$ , to study and control the adhesion, growth, apoptosis, and differentiation of cells.

**Fluorescent molecules as tools for the multiscale study of living cells and systems:** Fluorescence is a powerful tool to investigate the intracellular environment in a relatively non-invasive way: the fluorescent sensors can be designed in such a way that their optical properties depend on the nanoscopic environment surrounding the fluorophore. The groups operating in this sector are investigating a wide variety of cell systems at different spatial scales, ranging from super-resolution studies of the sub-cellular environment to the *in vivo* studies of brain function by means of non-linear microscopy and spectroscopy.

In perspective, a clear goal for the Institute development is the cross-contamination among these large thematic areas. A step in this direction was undertaken three years ago with the participation of the Institute to the Cnr project “Nanomax”. Here, Cnr Nano coordinates a sub-project that aims to develop new tools for the early diagnosis of glioblastoma multiform (GBM), an extremely aggressive tumor with a life expectancy of about 18 months.

## EFFECTS OF NEUROSTEROIDS ON MODEL LIPID BILAYERS: A POSSIBLE ROLE OF THE LIPID BILAYER IN DETERMINING THEIR MECHANISM OF ACTION

Amphiphilic molecules which have a biological effect on specific membrane receptors, could also affect lipid bilayer properties resulting in a modulation of the overall membrane behaviour. In light of this consideration, it is important to study the possible effects of amphiphilic molecule on model systems which recapitulate some of the main properties of the plasma membranes. We studied the effect of different neurosteroids on model bilayers composed by ternary lipid mixtures and we found that different physiological effects of the molecules are related to dissimilar effects on pure lipid bilayers, pointing to a possible role of the lipids in determining the effects on membrane receptors.

Amphiphilic molecules which affect membrane protein activity could exert lipid-mediated effects on the same proteins. Neurosteroids are molecules that bind to membrane receptors of the nervous system and their action mechanisms are still under debate. In fact, due to their mainly amphiphilic nature and to the fact that their recognition site with the receptor is intramembranous, the lipid bilayer could exert non-specific effects which add up to the allosteric regulation. The non-specific roles include both the modulation of lipid bilayer mechanical properties, that are relevant in the conformational transitions of membrane proteins, and the membrane lateral heterogeneity. We used the Micropipette Aspiration Technique (MAT) and AFM to study the effects on model lipid bilayers (Giant Unilamellar Vesicles, GUVs, and Supported Lipid Bilayers, SLBs) of two neurosteroids: allopregnanolone (Allo), an endogenous highly lipophilic molecule known to potentiate GABA<sub>A</sub>-evoked currents through GABA<sub>A</sub> receptors at low nanomolar concentrations, and its diastereomer isallopregnanolone (isoAllo), a non-competitive antagonist of Allo of GABA<sub>A</sub> receptors. By MAT we measured the interaction kinetics of both neurosteroids with GUVs composed by ternary lipid mixture which recapitulates the properties of more complex lipid bilayers. We found that Allo induced a strong increase (up to 13%) of the bilayer area (Fig. 1) and decreased the bilayer stretching constant, whereas isoAllo induced a small decrease (about 2%) of the bilayer area while leaving unaltered the mechanical properties. By using AFM we studied the effect of both molecules on the distribution of Liquid disordered (L<sub>d</sub>) and Liquid ordered (L<sub>o</sub>) domains. Allo promotes phase separation inducing also an increase of the L<sub>d</sub> fraction, whereas isoAllo has opposite effects (Figure 2). The results show that two molecules acting with almost opposite effects on the same membrane receptor have an

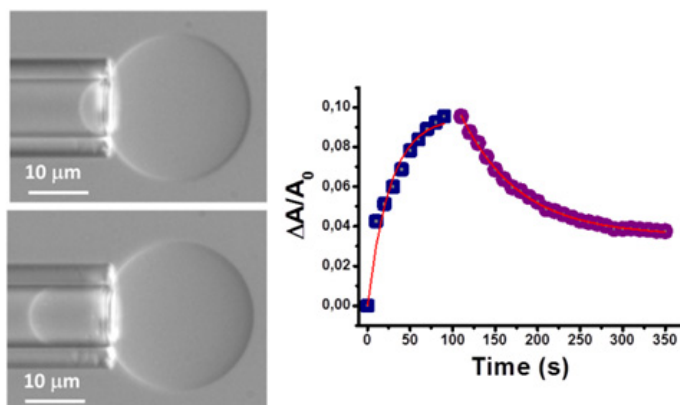
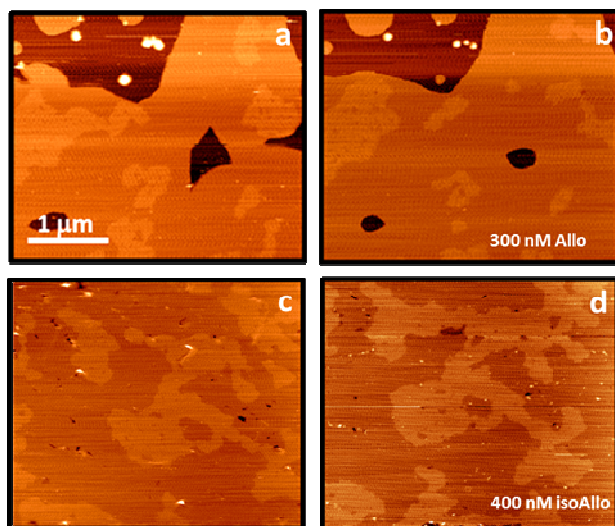


Figure 1. Interaction kinetic between Allo and a DOPC/bSM/cholesterol GUV as measured by MAT; a) The GUV at the beginning of the experiment; b) The GUV after 100 s of exposure to Allo 100 nM. The increase of the surface area is evident; c) Kinetics of the Allo adsorption process as measured from the relative area increase. After 100 s the GUV was moved to a solution without Allo and the Allo release from the bilayer was monitored.

opposite effect also on lipid bilayers, pointing to a probable relevant effect of the membrane in determining their physiological action mechanism.



**Figure 2.** Effect of Allo and isoAllo on the nanoscopic structure of DOPC/bSM/choI supported lipid bilayers on mica as studied by AFM. a) AFM image of a lipid bilayer presenting L<sub>o</sub> and L<sub>d</sub> domains; b) the same region of the lipid bilayer as in a) after exposing it to 300 nM Allo. The lipid bilayer area increases and the L<sub>o</sub> fraction decreases. c) AFM image of a lipid bilayer presenting L<sub>o</sub> and L<sub>d</sub> domains. d) the same region of the lipid bilayer as in a) after exposing it to 400 nM isoAllo. An opposite effect with respect to Allo is obtained.

#### Contact person

Andrea Alessandrini (andrea.alessandrini@unimore.it)

#### References

- [1] *Effects of neurosteroids on a model membrane including cholesterol: A micropipette aspiration study.* D. Balleza, M. Sacchi, G. Vena, D. Galloni, G. Puia, P. Facci, and A. Alessandrini. *Biochim Biophys Acta* 1848, 1268-1276 (2015).
- [2] *Effect of neurosteroids on a model lipid bilayer including cholesterol: An Atomic Force Microscopy study.* M. Sacchi, D. Balleza, G. Vena, G. Puia, P. Facci, and A. Alessandrini. *Biochim Biophys Acta* 1848, 1258-1267 (2015).



## PROTEIN DIFFUSION AT NANOSCALE

Many biochemical processes occurring in living cells are modulated by protein dynamics at nanoscale. To address this general issue, we set out to combine a technique inherently sensitive to the spatial features (e.g., barriers, corrals) that influence single molecule dynamics (spatiotemporal fluorescence correlation spectroscopy) with optical imaging methods reporting on phenomena at sub-diffraction scale ( $<200$  nm). Our novel approach was applied to highlight the subtle dynamics of nuclear protein import in close proximity of the nuclear envelope, as well as the complex network of diffusion-binding interaction of the membrane nociceptor TRPV1.

Fluorescence Correlation Spectroscopy (FCS) represents an established technique to recover protein dynamics in cells. Yet, many biochemical processes in the living cell can not be fully studied by purely temporal FCS, since the spatial (nano)scale is a powerful modulator of protein dynamics through barriers, corrals, or supramolecular assemblies. To integrate the spatial dimension, FCS can be combined with scanning microscopy imaging, an approach named spatiotemporal fluorescence correlation spectroscopy (stFCS).

Fluorescence cross-pair correlation spectroscopy (pCF) is an efficient stFCS strategy that provides details about the routes followed by the proteins in the specimen. For the first time, we combined pCF and continuous-wave stimulated emission depletion (CW-STED) to monitor intracellular protein dynamics at spatial resolution below the optical diffraction limit (super-resolution) [1]. We focused on Nuclear Localization Signal (NLS) fused to the Green Fluorescent Protein (NLS-GFP), since NLS-GFP is a well-known model of actively nuclear-imported protein [2]. Remarkably, we discovered the persistence of complexes between nucleocytoplasmic transporters and NLS-GFP at distances  $>200$  nm from the nuclear envelope (Figure 1), a phenomenon otherwise invisible at the best resolution of conventional confocal imaging mode.

The Transient Potential Vanilloid 1 (TRPV1) is a fascinating polymodal membrane receptor implied in nociception and target of pain therapy. We targeted the spatiotemporal dynamics of TRPV1 by combining for the first time the nanoscale resolution of Fluorescence Resonance Energy Transfer (FRET) with a stFCS method based on the extraction of the molecular mean square displacement directly from imaging data (FRET-iMSD) [3]. We found

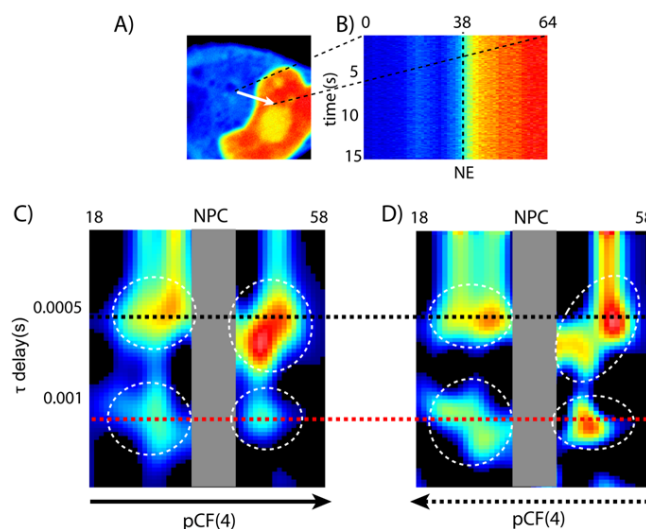


**Figure 1.** STED-pCF analysis of NLS-GFP in cells [1]. (A) Fluorescence intensity image of a cell expressing NLS-GFP: the nuclear accumulation is clearly visible. (B) Fluorescence intensity carpet in which the x-coordinate corresponds to the pixels along the scanned line (denoted as an arrow in A) and the y-coordinate corresponds to the time of acquisition (seconds). pCF(4) carpets obtained along the N->C (C) and C->N (D) directions. For further reference see ref. [1]



that TRPV1 is split in three pools with distinct functional roles: 1) TRPV1-C, binding to caveolin-1, trapped in caveolae, and implied in long-term receptor desensitization; 2) TRPV1-T, binding to and stabilized by microtubules, and organized in large supramolecular assemblies, and 3) TRPV1-I, a freely diffusing reservoir of the receptor.

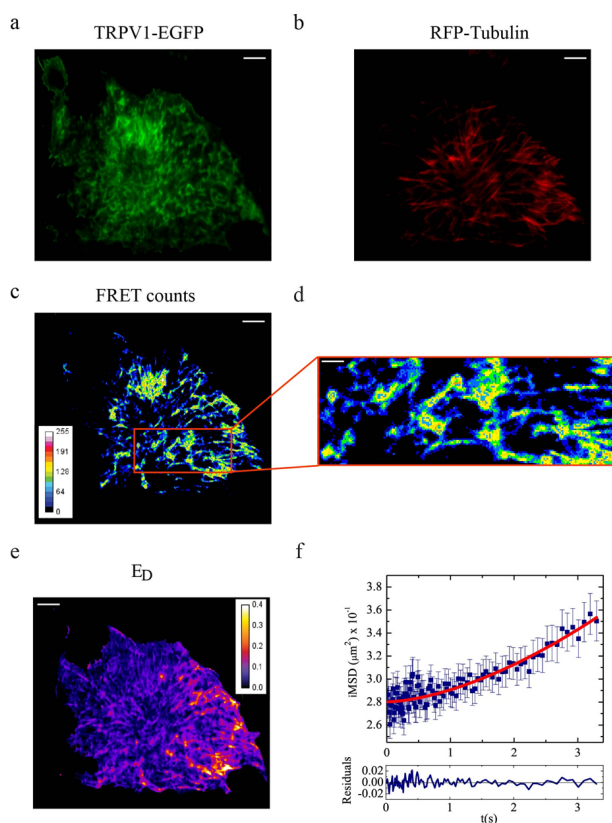


**Figure 2.** Steady-state and dynamic FRET analysis of TRPV1-microtubules interaction. Panels a-e refer to FRET analysis, whereas panel f refers to FRET-iMSD analysis. (a) Donor (TRPV1-EGFP) emission image; (b) acceptor (tubulin-RFP) emission image; (c) FRET intensity image (scale bar: 5  $\mu\text{m}$ ); (d) zoom of a cellular region where FRET-iMSD analysis is later performed (scale bar: 1  $\mu\text{m}$ ); (e) donor-normalized apparent FRET efficiency  $E_D$ . (f) iMSD vs. time plot for FRET signal between TRPV1-EGFP and RFP-tubulin in physiological condition. For further reference see [2].

### Contact person

Ranieri Bizzarri (ranieri.bizzarri@nano.cnr.it)

### References

- [1] *Nanoscale Protein Diffusion by STED-Based Pair Correlation Analysis*. P. Bianchini, F. Cardarelli, M. Di Luca, A. Diaspro, and R. Bizzarri. PLoS ONE 9, e99619 (2014).
- [2] *Unveiling TRPV1 Spatio-Temporal Organization in Live Cell Membranes*. B. Storti, C. Di Rienzo, F. Cardarelli, R. Bizzarri, and F. Beltram. PLoS ONE 10, e0116900 (2015).

## PROBING THE INFLUENCE OF CITRATE-CAPPED GOLD NANOPARTICLES ON AN AMYLOIDOGENIC PROTEIN

We present the first structural characterization and molecular mechanics model of the interaction between a fibrillogenic protein,  $\beta$ 2-microglobulin ( $\beta$ 2m), and 5 nm hydrophilic citrate-capped gold nanoparticles (NP).

NMR measurements and simulations at multiple levels explain the origin of the observed protein perturbations mostly localized at the amino-terminal region. Experiments show that the protein-NP interaction is weak and does not induce protein fibrillation. Simulations reproduce these findings and reveal the role of the citrate in destabilizing  $\beta$ 2m at the lower pH. The results offer possible strategies for controlling the desired effect of NPs on the fibrillation process.

A systematic investigation is carried out on the interaction of an amyloidogenic system and citrate-coated gold nanoparticles (cit-AuNPs). Selection of  $\beta$ 2m is due to the crucial relevance of protein misfolding in pathology and degenerative processes and the interference that NPs could exhibit with the protein along the pathway leading to fibrillogenesis. In particular,  $\beta$ 2m is the protein responsible for a tissue-specific amyloidosis in long-term hemodialysis patients. The interaction is modelled at multiple levels (enhanced sampling molecular dynamics, Brownian dynamics and Poisson-Boltzmann electrostatics). The results are in excellent agreement with experimental NMR data and explain the origin of the observed protein signal perturbations in terms of electrostatic interaction mostly. Both experiments and simulations suggest that the internal rearrangements of the protein induced by the interaction with the charged surface of cit-AuNPs are not able to disrupt the secondary structure of the native protein thus do not lead to unfolded amyloidogenic intermediates. Contrary to the expectations based on previously reported results for the same  $\beta$ 2m species at acidic pH, the protein solutions with AuNPs were stable for over 2

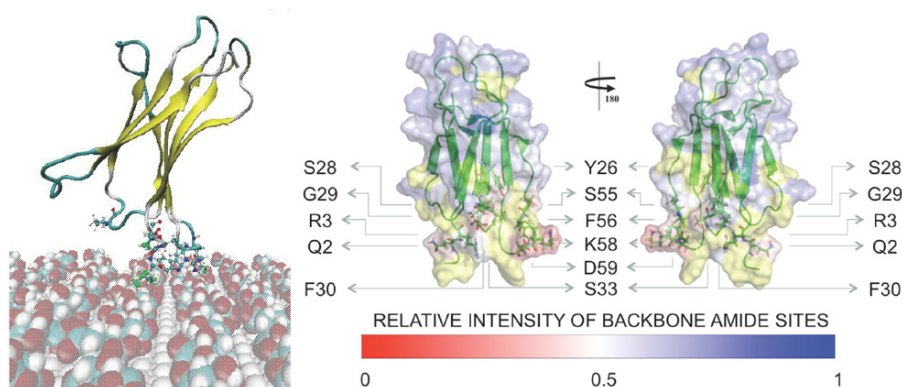


Figure 1.

Orientation of the protonated protein on cit-AuNPs (on the left) obtained after rigid body docking with Brownian Dynamics (BD) followed by 20 ns of T-REMD simulations. The binding orientation is in agreement with the experimental results from NMR spectroscopy. On the right: the normalised intensities are highlighted on the  $\beta$ 2m molecular structure (pdb code: 1JNJ) through appropriate colour coding. The residues whose backbone amide sites have less than 0.5 relative intensities are highlighted. In yellow the amide residues not measured in the analysis.

months in physiologic-like conditions and no evidence of increased aggregation or partial unfolding was observed.

The obtained results suggest that, by properly balancing the extent of electrostatic and hydrophobic interactions, the NP surface may provide stabilization/destabilization to amyloidogenic proteins. Therefore, NP-based approaches to treat amyloid pathologies may be definitely conceived due to the interest in possible therapeutic approaches for a class of pathologies with poor treatment, if any. In the specific instance of  $\beta 2m$  the availability of an efficient NP-based chemical surface for uptake of the protein can be profitably applied to haemodialysis systems, whereby extracorporeal blood circulation is forced to remove urea, creatinine, and other waste accumulations due to renal failure.

### Contact person

Giorgia Brancolini (giorgia.brancolini@nano.cnr.it)

### References

- [1] *Can small hydrophobic gold nanoparticles inhibit Beta2-Microglobulin fibrillation?* G. Brancolini, D. Toroz, and S. Corni. *Nanoscale* 6, 7903-7911 (2014).
- [2] *Computational Strategies for Protein-Surface and Protein-Nanoparticle Interactions.* G. Brancolini, L. Zanetti-Polzi, and S. Corni. *Journal of SAME* 2, 1-26 (2015).

## NANOLITER-DROPLET ACOUSTIC STREAMING VIA ULTRA HIGH FREQUENCY SURFACE ACOUSTIC WAVES

A fundamental limitation within the field of digital microfluidics is the minimum droplet volume that can be internally-controlled and exploited. Surface acoustic waves (SAWs) have been shown to be a fast and efficient method for generating internal flows in microfluidic droplets, but no improvements in droplet miniaturization have been reported since its introduction. Here we demonstrate the relevant length scales in sub-nanometer amplitude SAW-driven acoustic streaming. We illustrate the absence of any physical limitations beyond fabrication capabilities preventing the downscaling of SAW-driven internal streaming to nanoliter microreactors and beyond. The scaling is applied to demonstrate ultrafast fluid mixing in nanoliter order droplets by exploiting 1.1 GHz SAW.

The outstanding performance of SAW-driven micro-fluidic devices arises from SAW-driven acoustic streaming. SAWs radiate acoustic energy into fluids owing to the sound velocity mismatch between the fluid and the substrate. The induced pressure wave in turn drives a steady state flow, namely acoustic streaming. In order to downscale SAW microfluidics, we have studied for the first time here acoustic streaming and particle patterning as a function of the operating SAW frequency from 47.8 – 1107 MHz while varying the droplet mixing in nanoliter order droplets is investigated by exploiting SAWs volumes from microliters down to  $< \sim 1$  nanoliter. For the first time acoustic streaming and ultrafast in the ultra high frequency range (UHF).

SAW microfluidic devices (Figure 1), were fabricated at nominal frequencies of 50, 100, 200, 400, 833, and 1250 MHz. Each SAW device consisted of straight-fingered interdigital transducers (IDT) patterned on  $128^\circ$  Y-cut, X-propagating lithium niobate substrates.

Figure 2 demonstrates downscaling of the SAW microfluidic technology. Flow patterns inside three significantly smaller nanoliter order droplets actuated by four frequencies are shown: (a) 47.8 MHz, (b) 94.9 MHz, (c) 191 MHz and (d) 1107 MHz.

This UHF-SAW driven streaming was exploited to demonstrate one of the most important, difficult and limiting aspects of microfluidics-efficient and fast fluid mixing in microdroplets. Figure 3 (a) shows the mixing half-lives for 1  $\mu$ L droplets over the investigated range of frequencies. We find that fast mixing is obtained for all the tested frequencies. Mixing times are reduced by increasing the SAW frequency while keeping the SAW amplitude constant.

The truly impacting application, is shown in Figure 3 (b)–(d), where we apply the 1.1 GHz generated streaming to drive mixing in nanoliter order droplets. Standing wave patterns and particle accumulations are generated in nanoliter scale droplets at typical SAW frequencies, which are not beneficial for mixing. The UHF regime of acoustic streaming is instead effective in generating mixing flows in these very small droplets. Figure 3 (b) and (c) shows

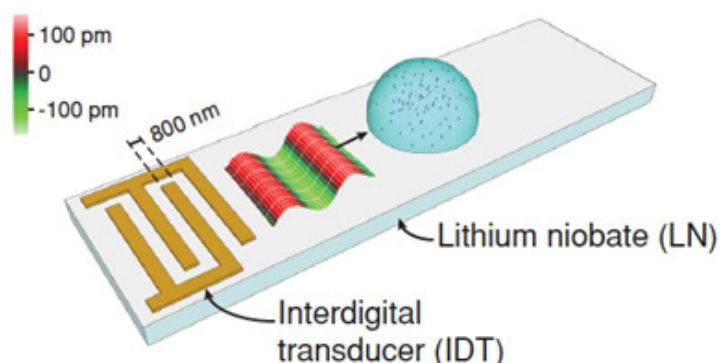


Figure 1. Schematic of the 1.1 GHz surface-acoustic-wave microfluidic device (not to scale). An overlaid section of a representative LDV (laser Doppler vibrometer) measurement shows a 100 pm amplitude SAW travelling from the IDT to the fluid droplet.

typical comparison images over time between mixing in a  $\sim 6$  nL droplet via (b) diffusion alone, and (c) 1.1 GHz SAW driven acoustic streaming. We see a dramatic decrease in mixing time of over two orders of magnitude.

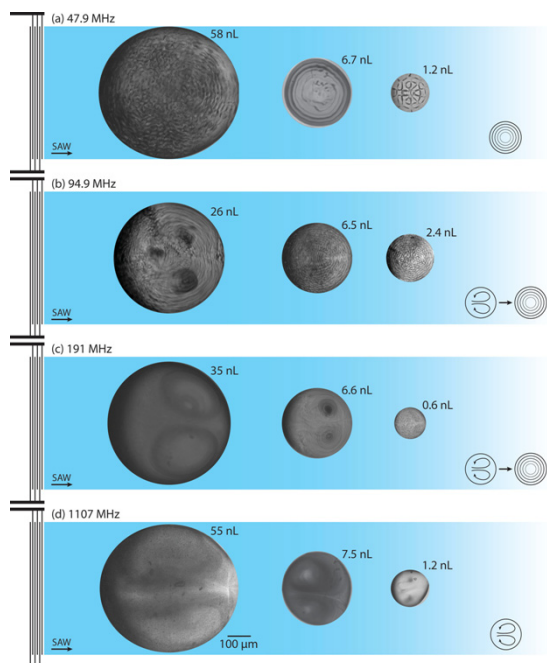


Figure 2.

Acoustic streaming within nanoliter order free droplets actuated by (a) 47.8 MHz, (b) 94.9 MHz, (c) 191 MHz, and (d) 1107 MHz SAW. In the (a) 47.8 MHz case we see particles accumulating in patterns and rings as standing waves are formed in the droplets. The (b) 94.9 MHz, and (c) 191 MHz cases show transitional regions where the larger droplet exhibits streaming, with particle aggregations beginning to dominate as the drop volume decreases. For the (d) 1107 MHz case, however, we see the standard vortical streaming pairs forming in each droplet size.

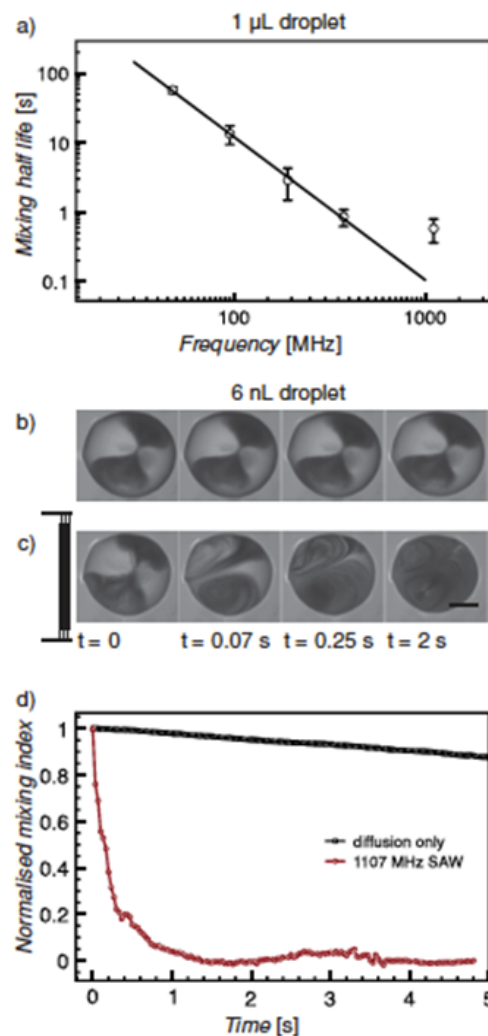


Figure 3.

Active digital microfluidic mixing driven by ultra high frequency acoustic streaming. For typical  $1 \mu\text{L}$  droplets (a) mixing half-lives are shown over the range of frequencies, and scale as  $M\tau \sim f^{-2}$  (black line). Mixing is shown for a  $\sim 6$  nL droplet via (b) diffusion only, and actuated via a (c) 1107 MHz SAW. For nanoliter order droplets a shift to the UHF region is necessary to induce streaming. The normalized mixing of (b) and (c) are shown over time in (d), and shows a dramatic decrease in mixing time of over 100 times when the SAW is applied. Scale bar is  $100 \mu\text{m}$ .

### Contact person

Marco Cecchini (marco.cecchini@nano.cnr.it)

### Reference

[1] *Nanoliter-Droplet Acoustic Streaming via Ultra High Frequency Surface Acoustic Waves*. R. J. Shilton, M. Travaglini, F. Beltram, and M. Cecchini. *Adv Mater* 26, 4941-4946 (2014).



## SCHWANN CELL CONTACT GUIDANCE VERSUS BOUNDARY INTERACTION IN FUNCTIONAL WOUND HEALING ALONG NANO AND MICRO-STRUCTURED MEMBRANES

Peripheral nerve transection is often encountered after trauma and can lead to long-term/permanent loss of sensor/motor functionality. The effect of pure contact interaction of nano/micro-grooved substrates on glial Schwann cells (SCs) was studied in view of their possible use for nerve-repair applications. Elastomeric gratings were developed with different micro/sub-micron dimensionality leading to two distinct cell-material interaction regimes: contact guidance (grating period < cell body diameter) and boundary guidance (grating period  $\geq$  cell body diameter). We showed that the contact guidance regime offers the best performance in improving wound healing and cell-cell interactions.

We tested the ability of grating (GR)-patterned elastomeric membranes to control and direct Schwann cell (SC) shaping and migration, with the aim to evaluate these geometries for nerve-regeneration applications. Poly(dimethylsiloxane) (PDMS) GRs were developed with different lateral periods (ranging from 1 to 20  $\mu\text{m}$ ) and depths (from 0.35 to 2.5  $\mu\text{m}$ ) (Figure 1 left), leading to two distinct cell-substrate interaction regimes: contact guidance (GR period < cell body diameter, obtained for T1 and T4) and boundary guidance (GR period  $\geq$  cell body diameter, obtained for T20). We examined the response of primary rat SCs to GRs in terms of cell morphology, actin cytoskeleton organization, single and collective migration, and cell-cell interaction.

The analysis of single SCs revealed important variations following GRs contact-interaction, regardless the interaction regime. Specifically, T20 performed best among all tested GRs, showing the best SC aspect ratio and alignment, nuclear alignment, actin organization and single-cell directional migration. Conversely, wound-healing experiments demonstrated that contact-guidance can be more effective in driving collective SC migration than boundary guidance and indeed only T4 could significantly improve wound-closure speed (Figure 1 centre). We linked this behaviour to the properties of the SC monolayers generated on the different GRs by studying the

expression of the neural calcium-dependent cell-adhesion molecule cadherin (N-cadherin), a protein that mediates cell-cell

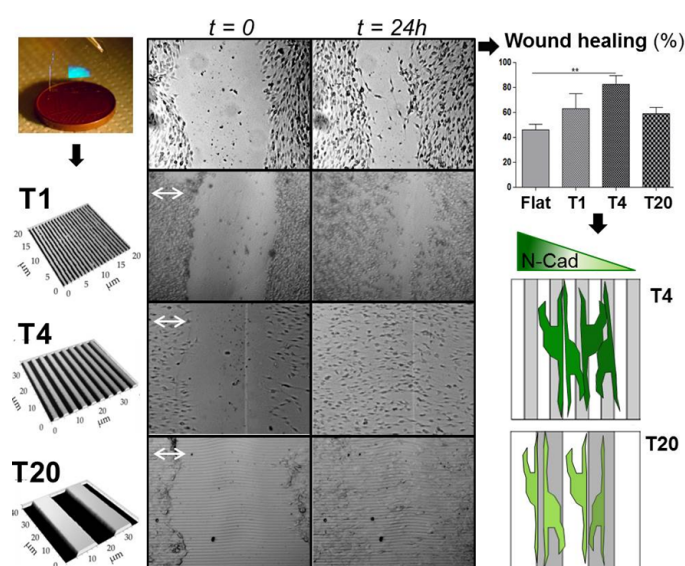


Figure 1. Left) PDMS nano/micro-grooved membranes were developed with lateral period of 1 (T1), 4 (T4) and 20 (T20)  $\mu\text{m}$ ; z -scales are 350 nm, 850 nm, and 2.5  $\mu\text{m}$  for T1, T4, and T20, respectively.

Center) Representative bright-field images of SC collective migration on FLAT, T1, T4, and T20 substrates (from top to the bottom), immediately after the scratch ( $t = 0$ ) and at  $t = 24\text{h}$ ; white arrows = GR direction, 200  $\mu\text{m}$ .

Right) Wound closure (%) at  $t = 24\text{h}$ :

\*\*  $P < 0.01$  T4 vs. FLAT, Dunnett's test. The collective migration performances are linked to the properties of the SC monolayers generated on the different GRs: SCs on large-period GRs (T20) are characterized by the downregulation of N-Cadherin, a protein that mediates cell-cell and cell-extracellular matrix adhesion.

and cell-extracellular matrix adhesion, and triggers intracellular signalling cascades to promote migration. SCs on large-period GRs are characterized by N-cadherin downregulation and enhanced single-cell scattering with respect to SCs on small-period GRs, indicating a less compact monolayer in the boundary guidance regime (Figure 1 right). Overall T4 (4  $\mu\text{m}$  period and 0.85  $\mu\text{m}$  depth) emerged as the most effective topography in tuning SC directional orientation and migration.

Our results provide information of the impact of specific topographical elements that can be exploited for tissue engineering applications and for the production of new devices enhancing peripheral-nerve regeneration.

### Contact person

Marco Cecchini (marco.cecchini@nano.cnr.it)

### Reference

[1] *Schwann Cell Contact Guidance versus Boundary Interaction in Functional Wound Healing along Nano and Microstructured Membranes*. I. Tonazzini, E. Jacchetti, S. Meucci, F. Beltram, and M. Cecchini. *Adv Healthc Mater* 4, 1849-1860 (2015).



## MODELLING PROPERTIES OF REDOX PROTEINS AT SURFACES BY MULTISCALE METHODS

The investigation of redox-active proteins immobilized on solid surfaces is receiving an increasing interest for its importance in fields such as biofuel cells and sensing. However, it is difficult to predict how the properties of the protein are modified upon surface immobilization. Here, we investigated the prototypical cytochrome c redox protein covalently bound to a gold surface by large scale atomistic simulations and multiscale (QM/MM) calculations. Thanks to such simulations, we clarified at the molecular level how the immobilization affects the redox thermodynamics of the protein.

The electrochemical investigation of redox-active proteins at electrodes is a challenging but highly rewarding area of research, since these systems can be exploited for applications ranging from biofuel cells to biosensors and bioelectronics. Currently, the behaviour of proteins immobilized on electrodes is still poorly understood. In particular, it is difficult to predict how the redox potential (the fundamental thermodynamics quantity that characterizes a redox protein) is affected by surface immobilization, as it depends on many features (e.g., the protein conformation and dynamics or the local protein environment).

Here, by means of classical molecular dynamics simulations and a hybrid multiscale quantum mechanics/molecular mechanics (QM/MM) methodology, the perturbed matrix method (PMM), we calculated the redox potential of cytochrome c adsorbed on a bare gold surface. After validation by comparison with experimental results, we gained insights into the structural and dynamic determinants to the redox thermodynamics of the adsorbed molecule.

The chosen approach gives redox potentials of immobilized proteins in quantitative agreement with the experimental data. In particular, we found a surface concentration dependence of the redox potential shift that reconciles two different experimental estimates reported in the literature. We demonstrated that the dependence of the reduction potential on the surface concentration stems from the changing of polarizability of the environment surrounding the protein.

In addition, we investigated the structural and dynamic changes in the protein as a consequence of the adsorption on the surface. In particular, we revealed that a reversible

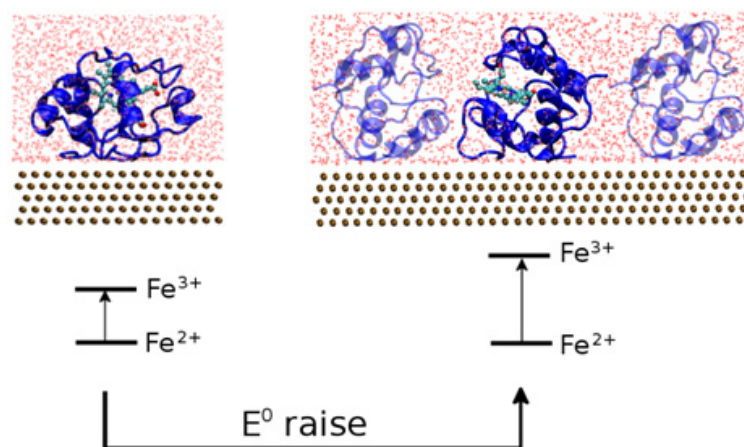


Figure 1.

Representative sketch of the mechanism at the basis of the redox potential dependence on the concentration of the Fe-containing protein cytochrome c on the surface. In the low concentration system the protein is surrounded by water. Upon oxidation, the solvent efficiently interacts with the oxidized protein, i.e., it is polarized. In the high concentration system, the protein is mainly surrounded by other proteins, which have a lower polarizability (dielectric constant). The inability of the

environment that surrounds the active site to polarize upon oxidation destabilizes the oxidized state in the high concentration system and thus is at the origin of the change in the redox potential.

conformational change, taking place dynamically in cytochrome c, is found to be disrupted when the protein is adsorbed on gold. This modification exemplifies a mechanism that potentially leads to changes in the protein properties by surface-induced modification of its dynamical behaviour, rather than its structure.

**Contact person**

Stefano Corni (stefano.corni@nano.cnr.it)

**Reference**

[1] *Surface Packing Determines the Redox Potential Shift of Cytochrome c Adsorbed on Gold*. L. Zanetti-Polzi, I. Daidone, C. A. Bortolotti, and S. Corni. J. Am. Chem. Soc. 136, 12929 (2014).

## CATALYTIC SELF-PROPULSION OF SUPRAMOLECULAR CAPSULES POWERED BY POLYOXOMETALATE CARGOS

Multi-compartment, spherical micro-containers were engineered through a layer-by-layer (lbl) polyelectrolyte deposition around a fluorescent core while integrating a ruthenium polyoxometalate ( $\text{Ru}_4\text{POM}$ ). The obtained multicomponent colloid works as molecular motor, due to its catalytic activity, fuelled upon  $\text{H}_2\text{O}_2$  decomposition. The resulting chemo-mechanical system, with average speeds of up to  $25 \mu\text{m s}^{-1}$ , is amenable for integration into a microfluidic set-up for mixing and displacement of liquids, whereby the propulsion force and the resulting velocity regime can be modulated upon  $\text{H}_2\text{O}_2$ -controlled addition.

Micro- and nano-motors are a class of miniaturized manmade machines that are able to convert chemical or external energy into mechanical motion. The self-propelled micro-machine holds tremendous promise for diverse fields, from drug delivery to electronic sensing. Polyelectrolyte multilayer capsules can be engineered with catalase enzymes or other catalysts (Pt, Mn, Ag) to create multifunctional spherical catalytic micromotors. Encapsulation provides the distinct advantages of concentrating and protecting the catalytic effectors in a defined volume, creating a partitioned microenvironment with tunable properties, which could therefore be used to balance the diffusion and reaction as needed for the desired function.

Within this framework we have recently entrapped a ruthenium polyoxometalate ( $\text{Ru}_4\text{POM}$ ) cargo, having a catalase-like activity and propeller function, within the multilayer shell of lbl-assembled capsules. The selective shell permeability of capsules allows the free diffusion of substrate ( $\text{H}_2\text{O}_2$ ) and reaction products ( $\text{H}_2\text{O}$  and  $\text{O}_2$ ) through the shells, whereas the catalytic effector is stably confined within the carrier (Figure 1). Upon addition of  $\text{H}_2\text{O}_2$  (1.23M), the release of oxygen bubbles from the capsule surface occurs as a continuous phenomenon. Time-lapse images show the formation of a long tail of oxygen bubbles [dark circles in Figure 2 a) and b)], with average diameter  $<10 \mu\text{m}$ , that coalesce into macrobubbles with diameter  $>500 \mu\text{m}$ . The behaviour of the catalytic micro-motors, and their  $\text{H}_2\text{O}_2$  fuelled propulsion effect have been studied under capillary-driven fluidodynamic conditions, in a microfluidic device. The flow dynamics under catalytic oxygen

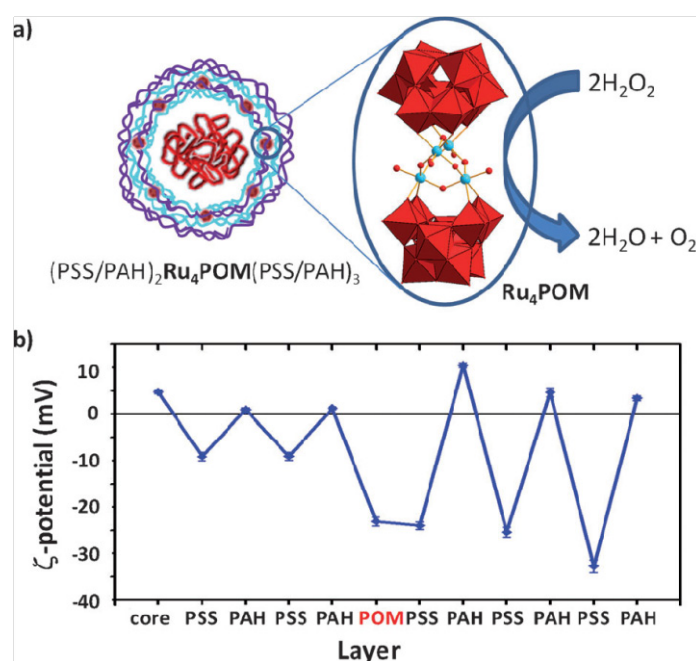
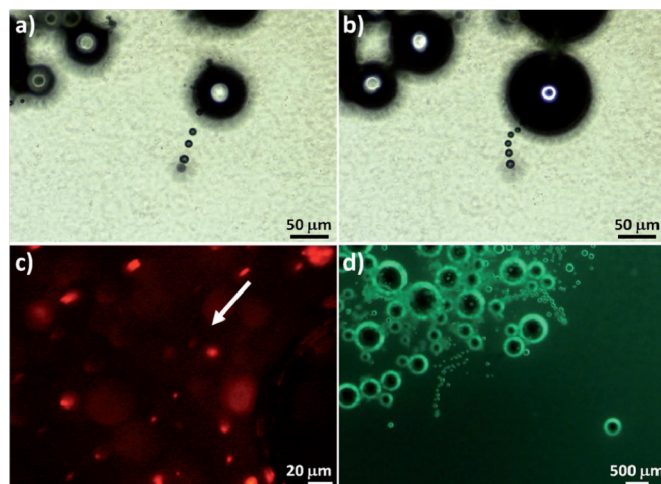


Figure 1. a) Illustration of the composition of a polyelectrolyte multilayer capsule carrying dextran-RITC into the cavity (red bundle) and  $\text{Ru}_4\text{POM}$  complexes (red spots) into the multilayer shell (left);  $\text{Ru}_4\text{POM}$  structure and its catalase-like reactivity (right); b) z-potentials variations during  $\text{CaCO}_3$  particles coating with PSS, PAH and  $\text{Ru}_4\text{POM}$  layers.

evolution were measured in real time within a micro-channel, at different  $\text{H}_2\text{O}_2$  concentrations, in the range 0-1.23 M.

When observed in 1.23M  $\text{H}_2\text{O}_2$ , the capsule displacement occurs along linear or circular trajectories with speeds of up to  $25 \mu\text{m s}^{-1}$ . This corresponds to a calculated driving force of at least 0.94 pN per particle.



**Figure 2.** Optical microscopy images, showing oxygen evolution and motion of the  $\text{Ru}_4\text{POM}$ -loaded capsules upon addition of  $\text{H}_2\text{O}_2$  (1.23M): a), b) continuous release and coalescence of oxygen bubbles, c) fluorescence tracking of capsule motion observed as red spheres, d) fluorescein isothiocyanate (FITC) staining of the water suspension mixed and displaced by the turbulence-seeded phenomena due to oxygen release.

### Contact person

Rosaria Rinaldi (ross.rinaldi@unisalento.it)

### References

- [1] *Catalytic Self-Propulsion of Supramolecular Capsules Powered by Polyoxometalate Cargos*. L. L. del Mercato, M. Carraro, A. Zizzari, M. Bianco, R. Miglietta, V. Arima, I. Viola, C. Nobile, A. Sorarù, D. Vilona, G. Gigli, M. Bonchio, and R. Rinaldi. *Chem-Eur J* 20, 1-6 (2014).
- [2] *Biological Applications of LbL Multilayer Capsules: From Drug Delivery to Sensing*. L. L. del Mercato, M. M. Ferraro, F. Baldassarre, S. Mancarella, V. Greco, R. Rinaldi, and S. Leporatti. *Adv Colloid Interface Sci* 207, 139–154 (2014).

## MICROFLUIDIC THz SENSORS

Terahertz (THz) spectroscopy and imaging have been heralded for some time as potentially revolutionary techniques for biomedical applications. A crucial practical goal is the ability to perform such measurements on tiny amounts of biological fluids or even on individual organic structures. Furthermore, all analysis relevant from a biological perspective must be performed in a water environment, which presents a strong absorption across the whole THz spectral range.

Here one shows how both issues can be overcome with a lab-on-a-chip approach based on a microfluidic platform coupled to a plasmonic antenna. Using a quantum cascade laser as THz illumination source, liquid volumes down to the picoliter range are probed and direct operation on individual 10- $\mu\text{m}$  diameter microparticles flowing in water is shown.

In this work we present a new portable microfluidic platform for on-chip THz transmission analysis that effectively meets all operational requirements of bio-compatible materials, high-signal-to-noise ratios in water, deeply sub-wavelength sensitivity, and real-time response speed. The system is realized using conventional microfluidic materials and exploits a compact THz Quantum Cascade Laser (QCL) as source. Deep-subwavelength resolution is obtained by integrating a metallic plasmonic antenna on-chip in the form of an elongated X-shaped aperture, according to the concept sketched in Figure 1. The antenna consists of a metallic pattern whose geometry is chosen in order to concentrate the electric field of the impinging radiation into a specific region of space. The slot is aligned and in close contact with the microfluidic channel ensuring that most of the transmitted THz light is funneled through the channel.

This microfluidic platform is then used to demonstrate the fast detection and characterization of subwavelength ( $<\lambda/10$ ) objects flowing in a water suspension as shown in Fig. 2, and to show the ability to perform a chemical analysis over volumes of the order of a picoliter.

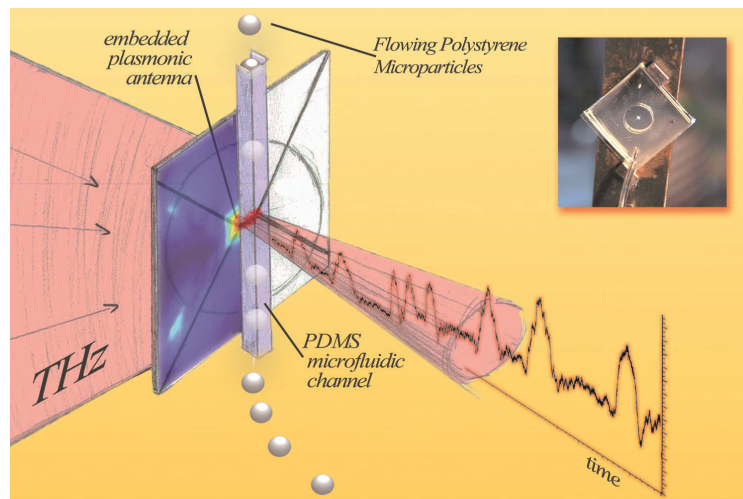


Figure 1.

Sketch of the on-chip bowtie plasmonic antenna system. A plasmonic antenna consists of a subwavelength metal pattern designed for a specific wavelength in the proper polarization. In presence of electromagnetic radiation (prefocalized beam) polarized parallel to the axis of the bowtie (parallel to the channel represented in the figure), the radiation is coupled down to a small region of volume below the corresponding free space wavelength. In the figure the microfluidic channel is also schematically represented passing through the focal point.

In our proof-of-concept experiment, the capability of distinguishing two species was actually just based on their respective size, leading to a weaker or stronger transmission. Clearly, potential bio-applications would rather target in the future quantitative differences in the spectroscopic THz response, for instance arising from differences in composition, molecular resonances, etc. From an experimental standpoint, the measurement is anyway equivalent, since it is exclusively based on the analysis of the THz-signal peak intensity. Of course, in the case of sharp resonances, more detailed information could be obtained resorting to a tunable source and investigating the spectral dependence of the signal.

Our data prove the applicability of this technology to recognition and sensing even in the dynamic fast-transit configuration that is required for instance by sorting and/or large-statistics applications. We believe it paves the way to the development of THz-based spectroscopy of biomolecules at the cell level, with exciting perspectives for label-free diagnostics.

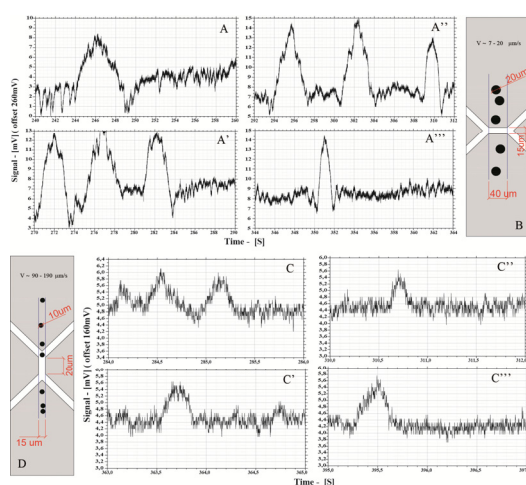


Figure 2.

The figure shows measurements of polystyrene microspheres of 20  $\mu\text{m}$  diameter (A) to (A''') and 10  $\mu\text{m}$  diameter flowing in the channel across the antenna. The respective chip configuration is schematized in (B) and (D). The peak in THz transmission is due to the lower absorption of Polystyrene with respect to surrounding water. The baseline is shifted as indicated to increase the ADC resolution of the Lockin amplifier (PerkinElmer).

### Contact person

Alessandro Tredicucci (alessandro.tredicucci@unipi.it)

### Reference

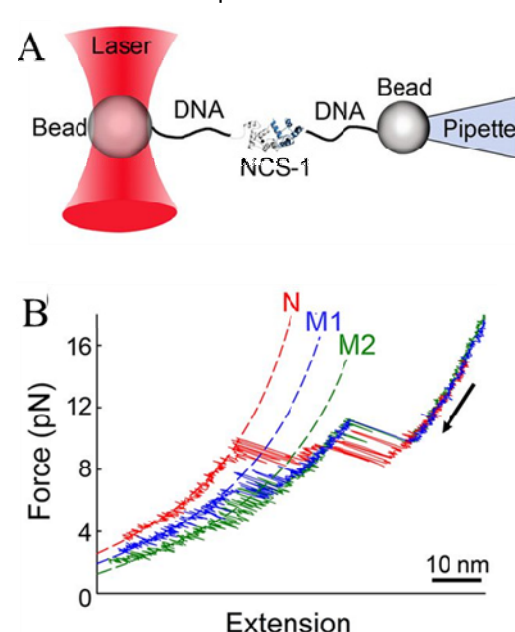
- [1] *Terahertz probe of individual subwavelength objects in a water environment*. L. Masini, S. Meucci, J. H. Jihua, R. Degl'Innocenti, F. Castellano, H. E. Beere, D. Ritchie, D. Balduzzi, R. Puglisi, A. Galli, F. Beltram, M. S. Vitiello, M. Cecchini, and A. Tredicucci. *Laser & Photonics Rev* 8, 734-742 (2014).



## DIRECT OBSERVATION OF CALCIUM-DEPENDENT MISFOLDING IN SINGLE NEURONAL CALCIUM SENSOR-1 MOLECULES

Protein misfolding has attracted significant attention due to its well-established link to neurodegenerative diseases. However, detecting misfolded states has been quite difficult and little is known regarding the early molecular rearrangements that promote their formation. Sparse populations and their weak associated signals limit the use of traditional bulk methods for monitoring the early events of misfolding and relatively few systems have been studied in detail. Single-molecule manipulation techniques, such as optical tweezers, have lately proven to be a new powerful approach to detect and characterize misfolded states, and investigate their link to neurodegenerative diseases.

We have used single-molecule optical tweezers to observe misfolding events and derive their mechanisms of formation for the neuronal calcium sensor 1 (NCS-1), a multi-specific EF-hand protein involved in neurotransmitter release and linked to severe neurological disorders. In addition to the native folding pathways, we directly observed two alternative trajectories leading to kinetically trapped distinctly misfolded conformations [1], Figure 1. Both trajectories start from an on-pathway intermediate state and compete with native folding in a calcium-dependent manner. The misfolding behaviour of NCS-1 could be selectively controlled by modulating the relaxation rate of the applied force. Through constant-force experiments and hidden Markov model analysis, we reconstructed the free energy landscape of the misfolding transitions under both physiological and pathophysiological calcium concentrations.



Remarkably for a calcium sensor, we found that higher calcium concentrations increased the lifetimes of the misfolded conformations and slowed NCS-1 folding to the native state. We proposed a multi-dimensional energy landscape for NCS-1 and speculate on a direct link between protein misfolding, calcium dysregulation, and neurodegeneration.

Figure 1.

A) Experimental setup. A single molecule of NCS-1 is manipulated between polystyrene beads by means of DNA molecular handles. B) During refolding the protein can follow its native folding pathway leading to the native state, N, (red trace), or two alternative misfolding pathways leading to two distinct misfolded conformations, M1 and M2 (blue and green traces). From Ref [1].

### Contact person

Ciro Cecconi (ciro.cecconi@unimore.it)

### Reference

[1] *Direct single-molecule observation of calcium-dependent misfolding in human neuronal calcium sensor-1.* P. O. Heidarsson, M. M. Naqvi, M. R. Otazo, A. Mossa, B. B. Kragelund, and C. Cecconi. PNAS 111, 13069 (2014).





## Selected publications

A list of publications from journals with  $IF \geq 7.512$  (i.e., *Physical Review Letter's* IF in 2014) ordered by their JCR 2014 IF is given. A full and updated list of publications is available on the Institute website at the page "Publications" (<http://www.nano.cnr.it/?mod=men&id=103>). Publications marked with © earned a cover in the corresponding journal. Covers are displayed at the end of this section.

### 2014

Silicon-Germanium Nanowires: Chemistry and Physics in Play, from Basic Principles to Advanced Applications.

M. Amato, M. Palummo, R. Rurali, and S. Ossicini. *Chem Rev.* **114**, 1371-1412 (2014).

Photodetectors based on graphene, other two-dimensional materials and hybrid systems.

F. H. L. Koppens, T. Mueller, Ph. Avouris, A. C. Ferrari, M. S. Vitiello, and M. Polini. *Nat Nanotechnol* **9**, 780–793 (2014).

Nanoscale spin rectifiers controlled by the Stark effect.

F. Rossella, A. Bertoni, D. Ercolani, M. Rontani, L. Sorba, F. Beltram, and S. Roddaro. *Nat Nanotechnol* **9**, 997-1001 (2014).

Long-range charge transport in single G-quadruplex DNA molecules.

G. I. Livshits, A. Stern, D. Rotem, N. Borovok, G. Eidelstein, A. Migliore, E. Penzo, S. J. Wind, R. Di Felice, S. Skourtis, J. C. Cuevas, L. Gurevich, A. B. Kotlyar, and D. Porath. *Nat Nanotechnol* **9**, 1040-1046 (2014).

Coherent ultrafast charge transfer in an organic photovoltaic blend.

S. M. Falke, C. A. Rozzi, D. Brida, M. Maiuri, M. Amato, E. Sommer, A. De Sio, A. Rubio, G. Cerullo, and E. Molinari. *Science* **344**, 1001-1005 (2014).

Ultimate classical communication rates of quantum optical channels.

V. Giovannetti, R. Garcia-Patron, N. J. Cerf, and A. S. Holevo. *Nat Photonics* **8**, 796-800 (2014).

Ultrafast multi-terahertz nano-spectroscopy with sub-cycle temporal resolution.

M. Eisele, T. L. Cocker, M. A. Huber, M. Plankl, L. Viti, D. Ercolani, L. Sorba, M. S. Vitiello, and R. Hober. *Nat Photonics* **8**, 841-845 (2014).

A generalization of the entropy power inequality to bosonic quantum systems.

G. De Palma, A. Mari, and V. Giovannetti. *Nat Photonics* **8**, 958-964 (2014).

Quantum channels and memory effects.

F. Caruso, V. Giovannetti, C. Lupo, and S. Mancini. *Rev Mod Phys* **86**, 1203-1259 (2014).

Investigating charge dynamics in halide perovskite-sensitized mesostructured solar cells.

V. Rofati, S. Colella, G. Lerario, L. De Marco, A. Rizzo, A. Listorti, and G. Gigli. *Energ Environ Sci* **7**, 1889-1894 (2014).

S. Zanotto, F. P. Mezzapesa, F. Bianco, G. Biasiol, L. Baldacci, M. S. Vitiello, L. Sorba, R. Colombelli, and A. Tredicucci. *Nat Phys* 10, 830-834 (2014).

Nanoliter-Droplet Acoustic Streaming via Ultra High Frequency Surface Acoustic Waves.

R. J. Shilton, M. Travaglini, F. Beltram, and M. Cecchini. *Adv Mater* 26, 4941-4946 (2014).

© Distributed Feedback Imprinted Electrospun Fiber Lasers.

L. Persano, A. Camposeo, P. Del Carro, V. Fasano, M. Moffa, R. Manco, and S. D'Agostino. *Adv Mater* 26, 6542-6547 (2014).

© Cooperativity in the Enhanced Piezoelectric Response of Polymer Nanowires.

L. Persano, C. Dagdeviren, C. Maruccio, L. De Lorenzis, and D. Pisignano. *Adv Mater* 26, 7574-7580 (2014).

Multipoint-Emitting Optical Fibers for Spatially Addressable In Vivo Optogenetics.

F. Pisanello, L. Sileo, I. A. Oldenburg, M. Pisanello, L. Martiradonna, J. A. Assad, B. L. Sabatini, and M. De Vittorio. *Neuron* 82, 1245-1254 (2014).

Stark Effect in Perovskite/TiO<sub>2</sub> Solar Cells: Evidence of Local Interfacial Order.

V. Roiati, E. Mosconi, A. Listorti, S. Colella, G. Gigli, and F. De Angelis. *Nano Lett* 14, 2168-2174 (2014).

Unintentional High-Density p-Type Modulation Doping of a GaAs/AlAs Core-Multishell.

J. Jadcak, P. Plochocka, A. Mitioglu, I. Breslavetz, M. Royo, A. Bertoni, G. Goldoni, T. Smolenski, P. Kossacki, A. Kretinin, H. Shtrikman, and D. K. Maude. *Nano Lett* 14, 2807-2814 (2014).

An Advanced Lithium-Ion Battery Based on a Graphene Anode and a Lithium Iron Phosphate Cathode.

J. Hassoun, F. Bonaccorso, M. Agostini, M. Angelucci, M. G. Betti, R. Cingolani, M. Gemmi, C. Mariani, S. Panero, V. Pellegrini, and B. Scrosati. *Nano Lett* 14, 4901-4906 (2014).

Two interconvertible folds modulate the activity of a DNA aptamer against transferrin receptor.

D. Porciani, G. Signore, L. Marchetti, P. Mereghetti, R. Nifosì, and F. Beltram. *Mol Ther Nucleic Acids* 3, e144 (2014).

Polarity-Driven Polytypic Branching in Cu-Based Quaternary Chalcogenide Nanostructures.

R. R. Zamani, M. Ibanez, M. Luysberg, N. Garcia-Castello, L. Houben, J. D. Prades, V. Grillo, R. E. Dunin-Borkowski, J. R. Morante, A. Cabot, and J. Arbiol. *ACS Nano* 8, 2290-2301 (2014).

Heat-Generating Iron Oxide Nanocubes: Subtle "Destructurators" of the Tumoral Microenvironment.

J. Kolosnjaj-Tabi, R. Di Corato, L. Lartigue, I. Marangon, P. Guardia, A. K. A. Silva, N. Luciani, O. Clement, P. Flaud, and J. V. Singh. *ACS Nano* 8, 4268-4283 (2014).

Edge Structures for Nanoscale Graphene Islands on Co(0001) Surfaces.

D. Prezzi, D. Eom, K. T. Rim, H. Zhou, S. Xiao, C. Nuckolls, T. F. Heinz, G. W. Flynn, and M. S. Hybertsen. *ACS Nano* 8, 5765-5773 (2014).

Bundling of GaAs Nanowires: A Case of Adhesion-Induced Self-Assembly of Nanowires.

S. Carapezzi, G. Priante, V. Grillo, L. Montes, S. Rubini, and A. Cavallini. *ACS Nano* 8, 8932-8941 (2014).

Physically Transient Photonics: Random versus Distributed Feedback Lasing Based on Nanoimprinted DNA.

A. Camposeo, P. Del Carro, L. Persano, K. Cyprych, A. Szukalski, L. Sznitko, J. Mysliwiec, and D. Pisignano. *ACS Nano* 8, 10893-10898 (2014).

Surface Packing Determines the Redox Potential Shift of Cytochrome c Adsorbed on Gold. L. Zanetti-Polzi, I. Daidone, C. A. Bortolotti, and S. Corni. *J Am Chem Soc* 136, 12929-12937 (2014).

Organic Nanofibers Embedding Stimuli-Responsive Threaded Molecular Components. V. Fasano, M. Baroncini, M. Moffa, D. Iandolo, A. Camposeo, A. Credi, and D. Pisignano. *J Am Chem Soc* 136, 14245-14254 (2014).

Surface investigation on  $Gd_4M_8$  ( $M=Zn, Ni$ ) Single Molecule Coolers. V. Corradini, A. Ghirri, A. Candini, R. Biagi, U. del Pennino, V. De Renzi, G. Dotti, E. Otero, T. N. Hooper, R. Inglis, E. K. Brechin, and M. Affronte. *Adv Funct Mater* 24, 4782-4788 (2014).

Polymorphism in Crystalline Microfibers of Achiral Octithiophene: The Effect on Charge Transport, Supramolecular Chirality and Optical Properties. F. Di Maria, E. Fabiano, D. Gentili, M. Biasiucci, T. Salzillo, G. Bergamini, M. Gazzano, A. Zanelli, A. Brillante, M. Cavallini, F. Della Sala, G. Gigli, and G. Barbarella. *Adv Funct Mater* 24, 4943-4951 (2014).

Optical Gain in the Near Infrared by Light-Emitting Electrospun Fibers. G. Morello, M. Moffa, S. Girardo, A. Camposeo, and D. Pisignano. *Adv Funct Mater* 24, 5225-5231 (2014).

A quantum diffractor for thermal flux. M. J. Martínez-Perez and F. Giazotto. *Nat Commun* 5, 3579 (2014).

Quantum state majorization at the output of bosonic Gaussian channels. A. Mari, V. Giovannetti, and A. S. Holevo. *Nat Commun* 5, 3826 (2014).

Exciton-dominated optical response of ultra-narrow graphene nanoribbons. R. Denk, M. Hohage, P. Zeppenfeld, J. Cai, C. A. Pignedoli, H. Söde, R. Fasel, X. Feng, K. Müllen, S. Wang, D. Prezzi, A. Ferretti, A. Ruini, E. Molinari, and P. Ruffieux. *Nat Commun* 5, 4253 (2014).

Exponential rise of dynamical complexity in quantum computing through projections. D. K. Burgarth, P. Facchi, V. Giovannetti, H. Nakazato, S. Pascazio, and K. Yuasa. *Nat Commun* 5, 5173 (2014).

Anomalous low-temperature Coulomb drag in graphene-GaAs heterostructures. A. Gamucci, D. Spirito, M. Carrega, B. Karmakar, A. Lombardo, M. Bruna, L. N. Pfeiffer, K. W. West, A. C. Ferrari, M. Polini, and V. Pellegrini. *Nat Commun* 5, 5824 (2014).

Photonic quasi-crystal terahertz lasers. M. S. Vitiello, M. Nobile, A. Ronzani, A. Tredicucci, F. Castellano, V. Talora, L. Li, E. H. Linfield, and A. G. Davies. *Nat Commun* 5, 5884 (2014).

Probing short-range protein Brownian motion in the cytoplasm of living cells. C. Di Rienzo, V. Piazza, E. Gratton, F. Beltram, and F. Cardarelli. *Nat Commun* 5, 5891 (2014).

Experimental basis for a new allosteric model for multisubunit proteins.

C. Viappiani, S. Abbruzzetti, L. Ronda, S. Bettati, E. R. Henry, A. Mozzarelli, and W. A. Eaton. PNAS 111, 12758-12763 (2014).

Direct single-molecule observation of calcium-dependent misfolding in human neuronal calcium sensor-1.

P. O. Heidarsson, M. M. Naqvi, M. R. Otazo, A. Mossa, B. B. Kragelund, and C. Cecconi. PNAS 111, 13069-13074 (2014).

Probing the mechanism for graphene nanoribbon formation on gold surfaces through X-ray spectroscopy.

A. Batra, D. Cvetko, G. Kladnik, O. Adak, C. Cardoso, A. Ferretti, D. Prezzi, E. Molinari, A. Morgante, and L. Venkataraman. Chem Sci 5, 4419-4423 (2014).

Generation of Nondiffracting Electron Bessel Beams.

V. Grillo, E. Karimi, G. C. Gazzadi, S. Frabboni, M. R. Dennis, and R. W. Boyd. Phys Rev X 4, 011013 (2014).

Frequency-Comb-Assisted Terahertz Quantum Cascade Laser Spectroscopy.

S. Bartalini, L. Consolino, P. Cancio, P. De Natale, P. Bartolini, A. Taschin, M. De Pas, H. Beere, D. Ritchie, M. S. Vitiello, and R. Torre. Phys Rev X 4, 021006 (2014).

Assessing the Nonequilibrium Thermodynamics in a Quenched Quantum Many-Body System via Single Projective Measurements.

L. Fusco, S. Pigeon, T. J. G. Apollaro, A. Xuereb, L. Mazzola, M. Campisi, A. Ferraro, M. Paternosto, and G. De Chiara. Phys Rev X 4, 031029 (2014).

Combined nano- and micro-scale topographic cues for engineered vascular constructs by electrospinning and imprinted micro-patterns.

M. Moffa, A. G. Sciancalepore, L. G. Passione, and D. Pisignano. Small 10, 2439-2450 (2014).

© Terahertz probe of individual subwavelength objects in a water environment.

L. Masini, S. Meucci, J. H. Jihua, R. Degl'Innocenti, F. Castellano, H. E. Beere, D. Ritchie, D. Balduzzi, R. Puglisi, A. Galli, F. Beltram, M. S. Vitiello, M. Cecchini, and A. Tredicucci. Laser & Photonics Rev 8, 734-742 (2014).

© Random lasing in an organic light-emitting crystal and its interplay with vertical cavity feedback.

A. Camposeo, M. Polo, P. Del Carro, L. Silvestri, S. Tavazzi, and D. Pisignano. Laser & Photonics Rev 8, 785-791 (2014).

Biological Applications of LbL Multilayer Capsules: From Drug Delivery to Sensing.

L. L. del Mercato, M. M. Ferraro, F. Baldassarre, S. Mancarella, V. Greco, R. Rinaldi, and S. Leporatti. Adv Colloid Interface Sci 207, 139-154 (2014).

Enhancing Dye-Sensitized Solar Cell Performances by Molecular Engineering: Highly Efficient pi-Extended Organic Sensitizers.

R. Grisorio, L. De Marco, R. Agosta, R. Iacobellis, R. Giannuzzi, M. Manca, P. Mastrorilli, G. Gigli, and G. P. Suranna. ChemSusChem 7, 2659-2669 (2014).

Relaxation Oscillations in the Formation of a Polariton Condensate.

M. De Giorgi, D. Ballarini, P. Cazzato, G. Deligeorgis, S. I. Tsintzos, Z. Hatzopoulos, P. G. Savvidis, G. Gigli, F. P. Laussy, and D. Sanvitto. Phys Rev Lett 112, 113602 (2014).

Ab Initio Simulation of Optical Limiting: The Case of Metal-Free Phthalocyanine.

C. Cocchi, D. Prezzi, A. Ruini, E. Molinari, and C. A. Rozzi. Phys Rev Lett 112, 198303 (2014).

Quantum Discord Determines the Interferometric Power of Quantum States.  
D. Girolami, A. M. Souza, V. Giovannetti, T. Tufarelli, J. G. Filgueiras, R. S. Sarthour, D. O. Soares-Pinto, I. S. Oliveira, and G. Adesso. Phys Rev Lett 112, 210401 (2014).

Tunable Nonequilibrium Luttinger Liquid Based on Counterpropagating Edge Channels.  
M. G. Prokudina, S. Ludwig, V. Pellegrini, L. Sorba, G. Biasiol, and V. S. Khrapai. Phys Rev Lett 112, 216402 (2014).

Optimal Persistent Currents for Interacting Bosons on a Ring with a Gauge Field.  
M. Cominotti, D. Rossini, M. Rizzi, F. Hekking, and A. Minguzzi. Phys Rev Lett 113, 025301 (2014).

Ultrafast Control and Rabi Oscillations of Polaritons.  
L. Dominici, D. Colas, S. Donati, J. P. R. Cuartas, M. De Giorgi, D. Ballarini, G. Guirales, J. C. Carreno, A. Bramati, G. Gigli, E. del Valle, F. P. Laussy, and D. Sanvitto. Phys Rev Lett 113, 226401 (2014).

Corbino Disk Viscometer for 2D Quantum Electron Liquids.  
A. Tomadin, G. Vignale, and M. Polini. Phys Rev Lett 113, 235901 (2014).

## 2015

Highly confined low-loss plasmons in graphene-boron nitride heterostructures.  
A. Woessner, M. B. Lundberg, Y. Gao, A. Principi, P. Alonso-González, M. Carrega, K. Watanabe, T. Taniguchi, G. Vignale, M. Polini, J. Hone, R. Hillenbrand, and F. H. L. Koppens. Nat Mater 14, 421-425 (2015).

Rectification of electronic heat current by a hybrid thermal diode.  
M. J. Martínéz-Perez, A. Fornieri, and F. Giazotto. Nat Nanotechnol 10, 303-307 (2015).

Frictional transition from superlubric islands to pinned monolayers.  
M. Pierno, I. Bruschi, G. Mistura, G. Paolicelli, A. di Bona, S. Valeri, R. Guerra, A. Vanossi, and E. Tosatti. Nat Nanotechnol 10, 714-718 (2015).

Graphene, related two-dimensional crystals, and hybrid systems for energy conversion and storage.  
F. Bonaccorso, L. Colombo, G. H. Yu, M. Stoller, V. Tozzini, A. C. Ferrari, R. S. Ruoff, and V. Pellegrini. Science 347, 1246501 (2015).

Active polymer nanofibers for photonics, electronics, energy generation and micromechanics.  
L. Persano, A. Camposeo, and D. Pisignano. Prog Polym Sci 43, 48-95 (2015).

Superconducting transistors: A boost for quantum computing.  
F. Giazotto. Nat Phys 11, 527-528 (2015).

Structured quantum waves.  
J. Harris, V. Grillo, E. Mafakheri, G. C. Gazzadi, S. Frabboni, R. W. Boyd, and E. Karimi. Nat Phys 11, 629-634 (2015).



#### Black Phosphorus Terahertz Photodetectors.

L. Viti, J. Hu, D. Coquillat, W. Knap, A. Tredicucci, A. Politano, and M. S. Vitiello. *Adv Mater* 27, 5567–5572 (2015).

#### Atomic Scale Structure and Reduction of Cerium Oxide at the Interface with Platinum.

P. Luches, L. Giordano, V. Grillo, G. C. Gazzadi, S. Prada, M. Campanini, G. Bertoni, C. Magen, F. Pagliuca, G. Pacchioni, and S. Valeri. *Adv Mater* 2, 1-10 (2015).

#### Human Neuronal SHSY5Y Cells on PVDF: PTrFE Copolymer Thin Films.

I. Tonazzini, E. Bystrenova, B. Chelli, P. Greco, D. De Leeuw, and F. Biscarini. *Adv Energy Mater* 17, 1051-1056 (2015).

#### Pb/InAs Nanowire Josephson Junction with High Critical Current and Magnetic Flux Focusing.

J. Paajaste, M. Amado, S. Roddaro, S. F. Bergeret, D. Ercolani, L. Sorba, and F. Giazotto. *Nano Lett* 15, 1803-1808 (2015).

#### InAs/GaAs Sharply Defined Axial Heterostructures in Self-Assisted Nanowires.

D. Scarpellini, C. Somaschini, A. Fedorov, S. Bietti, C. Frigeri, V. Grillo, L. Esposito, M. Salvalaglio, A. Marzegalli, F. Montalenti, E. Bonera, P. G. Medaglia, and S. Sanguinetti. *Nano Lett* 15, 3677-3683 (2015).

#### Suppression of Low-Frequency Electronic Noise in Polymer Nanowire Field-Effect Transistors

F. Lezzi, G. Ferrari, C. Pennetta, and D. Pisignano. *Nano Lett* 15, 7245-7252 (2015).

#### Pyramid-Shaped Wurtzite CdSe Nanocrystals with Inverted Polarity.

S. Ghosh, R. Gaspari, G. Bertoni, M. C. Spadaro, M. Prato, S. Turner, A. Cavalli, L. Manna, and R. Brescia. *ACS Nano* 9, 8537-8546 (2015).

#### Exciton-Plasmon Coupling Enhancement via Metal Oxidation.

F. Todisco, S. D'Agostino, M. Esposito, A. I. Fernandez-Dominguez, M. De Giorgi, D. Ballarini, L. Dominici, L. Tarantini, M. Cuscuna, F. Della Sala, G. Gigli, and D. Sanvitto. *ACS Nano* 9, 9691-9699 (2015).

#### Probing the Influence of Citrate-Capped Gold Nanoparticles on an Amyloidogenic Protein.

G. Brancolini, A. Corazza, M. Vuano, F. Fogolari, M. C. Mimmi, V. Bellotti, M. Stoppini, S. Corni, and G. Esposito. *ACS Nano* 10, 2600-2613 (2015).

#### Metal-Enhanced Near-Infrared Fluorescence by Micropatterned Gold Nanocages.

A. Camposeo, L. Persano, R. Manco, Y. Wang, P. Del Carro, C. Zhang, Z. Y. Li, D. Pisignano, and Y. Xia. *ACS Nano* 9, 10047-10054 (2015).

#### 'Darker-than-Black' PbS Quantum Dots: Enhancing Optical Absorption of Colloidal Semiconductor Nanocrystals via Short Conjugated Ligands.

C. Giansante, I. Infante, E. Fabiano, R. Grisorio, G. P. Suranna, and G. Gigli. *J Am Chem Soc* 137, 1875-1886 (2015).

#### Molecular-Level Switching of Polymer/Nanocrystal Non-Covalent Interactions and Application in Hybrid Solar Cells.

C. Giansante, R. Mastria, G. Lerario, L. Moretti, I. Kriegel, F. Scotognella, G. Lanzani, S. Carallo, M. Esposito, M. Biasiucci, A. Rizzo, and G. Gigli. *Adv Funct Mater* 25, 111-119 (2015).

#### Alignment of Rod-Shaped Single-Photon Emitters Driven by Line Defects in Liquid Crystals.

L. Pelliser, M. Manceau, C. Lethiec, D. Coursault, S. Vezzoli, G. Lemenager, L. Coolen, M. De

Vittorio, F. Pisanello, L. Carbone, A. Maitre, A. Bramati, and E. Lacaze. *Adv Funct Mater* 25, 1719-1726 (2015).

Charge Separation Dynamics and Opto-Electronic Properties of a Diaminoterephthalate-C-60 Dyad.

S. Pittalis, A. Delgado, J. Robin, L. Freimuth, J. Christoffers, C. Lienau, and C. A. Rozzi. *Adv Funct Mater* 25, 2047-2053 (2015).

Rapid and Controllable Digital Microfluidic Heating by Surface Acoustic Waves.

R. J. Shilton, V. Mattoli, M. Travagliati, M. Agostini, A. Desii, F. Beltram, and M. Cecchini. *Adv Funct Mater* 25, 5895-5901 (2015).

Experimental evidence of replica symmetry breaking in random lasers.

N. Ghofraniha, I. Viola, F. Di Maria, G. Barbarella, G. Gigli, L. Leuzzi, and C. Conti. *Nat Commun* 6, 6058 (2015).

Triple-helical nanowires by tomographic rotatory growth for chiral photonics.

M. Esposito, V. Tasco, F. Todisco, M. Cuscunà, A. Benedetti, D. Sanvitto, and A. Passaseo. *Nat Commun* 6, 6484 (2015).

Electronic cooling via interlayer Coulomb coupling in multilayer epitaxial grapheme.

M. T. Mihnev, J. R. Tolsma, C. J. Divin, D. Sun, R. Asgari, M. Polini, C. Berger, A. de Heer, A. H. MacDonald, and T. B. Norris. *Nat Commun* 6, 8105 (2015).

Magnetic crystals and helical liquids in alkaline-earth fermionic gases.

S. Barbarino, L. Taddia, D. Rossini, L. Mazza, and R. Fazio. *Nat Commun* 6, 8134 (2015).

Inhibition of glycolysis by using nanolipid bromopyruvic chitosan carrier is a promising tool to prevent HCC invasiveness.

N. A. N. Hanafy, M. L. De Giorgi, C. Nobile, G. Giannelli, A. Quarta, and S. Leporatti. *J Hepatology* 62, S401-S401 (2015).

Facet selectivity in gold binding peptides: exploiting interfacial water structure.

L. B. Wright, J. P. Palafox-Hernandez, P. M. Rodger, S. Corni, and T. R. Walsh. *Chem Sci* 6, 5204-5214 (2015).

A novel mechano-enzymatic cleavage mechanism underlies transthyretin amyloidogenesis.

J. Marcoux, P. P. Mangione, R. Porcari, M. T. Degiacomi, G. Verona, G. W. Taylor, S. Giorgetti, S. Raimondi, S. Sanglier-Cianferani, and J. L. P. Benesch. *EMBO Mol Med* 7, 1337-1349 (2015).

© Nanofibers: Ratiometric Organic Fibers for Localized and Reversible Ion Sensing with Micrometer-Scale Spatial Resolution.

L. L. Del Mercato, M. Moffa, R. Rinaldi, and D. Pisignano. *Small* 11, 6417-6424 (2015).

Effect of lithium intercalation on the photovoltaic performances of photovoltachromic cells.

F. Malara, A. Cannavale, and G. Gigli. *Prog Photovoltaics* 23, 290-301 (2015).

Holographic Generation of Highly Twisted Electron Beams.

V. Grillo, G. C. Gazzadi, E. Mafakheri, S. Frabboni, E. Karimi, and R. W. Boyd. *Phys Rev Lett* 114, 034801 (2015).

Acoustic Black Hole in a Stationary Hydrodynamic Flow of Microcavity Polaritons.

H. S. Nguyen, D. Gerace, I. Carusotto, D. Sanvitto, E. Galopin, A. Lemaitre, I. Sagnes, J. Bloch, and A. Amo. *Phys Rev Lett* 114, 036402 (2015).

Very Large Thermophase in Ferromagnetic Josephson Junctions.

F. Giazotto, T. T. Heikkilä, and F. S. Bergeret. Phys Rev Lett 114, 067001 (2015).

First-Principles Photoemission Spectroscopy and Orbital Tomography in Molecules from Koopmans-Compliant Functionals.

N. L. Nguyen, G. Borghi, A. Ferretti, I. Dabo, and N. Marzari. Phys Rev Lett 114, 166405 (2015).

Accessing Phonon Polaritons in Hyperbolic Crystals by Angle-Resolved Photoemission Spectroscopy.

A. Tomadin, A. Principi, J. C. W. Song, L. S. Levitov, and M. Polini. Phys Rev Lett 115, 087401 (2015).

Localized Majorana-Like Modes in a Number-Conserving Setting: An Exactly Solvable Model.

F. Iemini, L. Mazza, D. Rossini, R. Fazio, and S. Diehl. Phys Rev Lett 115, 156402 (2015).

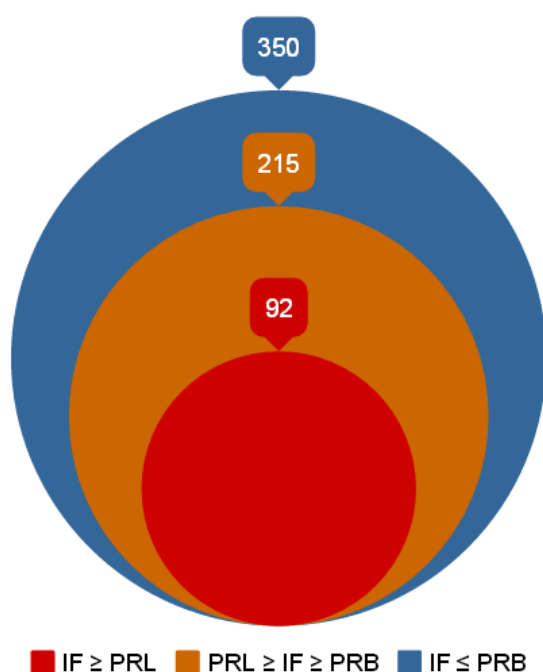
Interplay of Surface and Dirac Plasmons in Topological Insulators: The Case of  $\text{Bi}_2\text{Se}_3$ .

A. Politano, V. M. Silkin, I. A. Nechaev, M. S. Vitiello, L. Viti, Z. S. Aliev, M. B. Babanly, G. Chiarello, P. M. Echenique, and E. V. Chulkov. Phys Rev Lett 115, 216802 (2015).

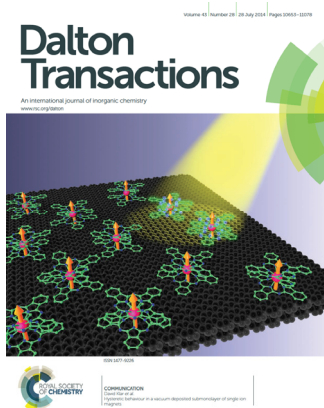
Necessity of Eigenstate Thermalization.

G. De Palma, A. Serafini, V. Giovannetti, and M. Cramer. Phys Rev Lett 115, 220401 (2015).

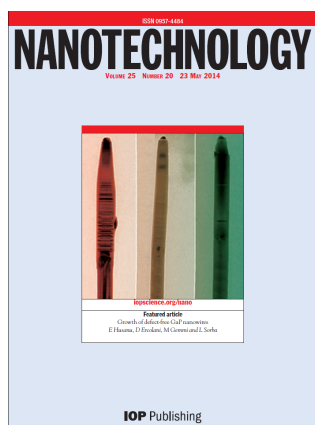
### Total number of publications (657) in 2014-2015 sorted by their 2014 IFs.



## covers



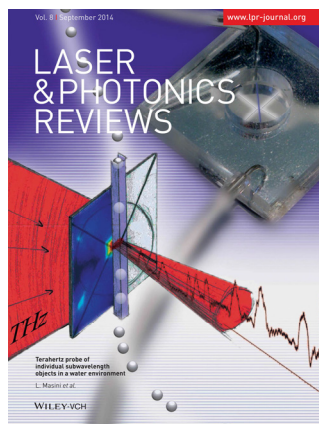
Dalton Transaction 43, 10686 (2014) [inside front cover]



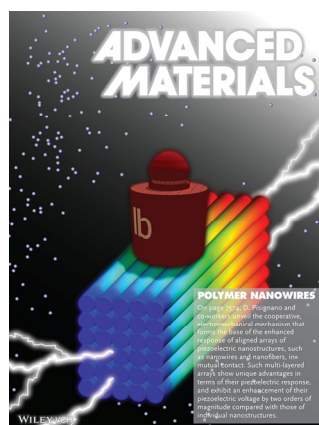
Nanotechnology 25, 205601 (2014)



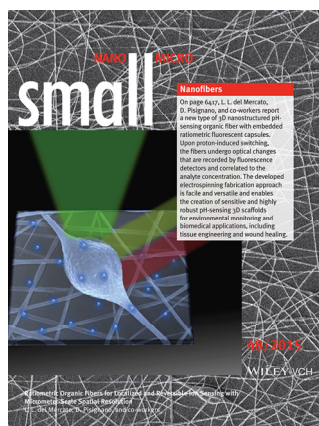
Biophys J 109, 113 (2015)



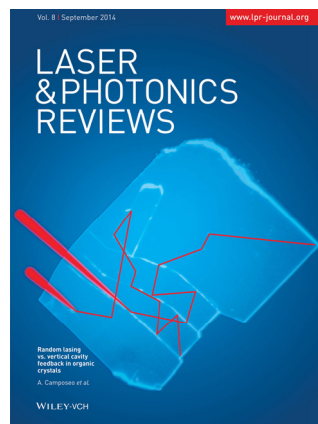
Laser & Photonics Rev 8, 734 (2014) [inside front cover]



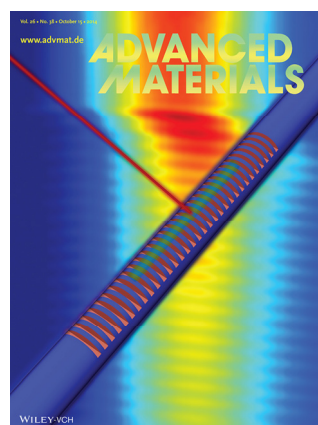
Adv Mater 26, 7574 (2014) [frontispiece]



Small 11 (48), 6417 (2015) [frontispiece]

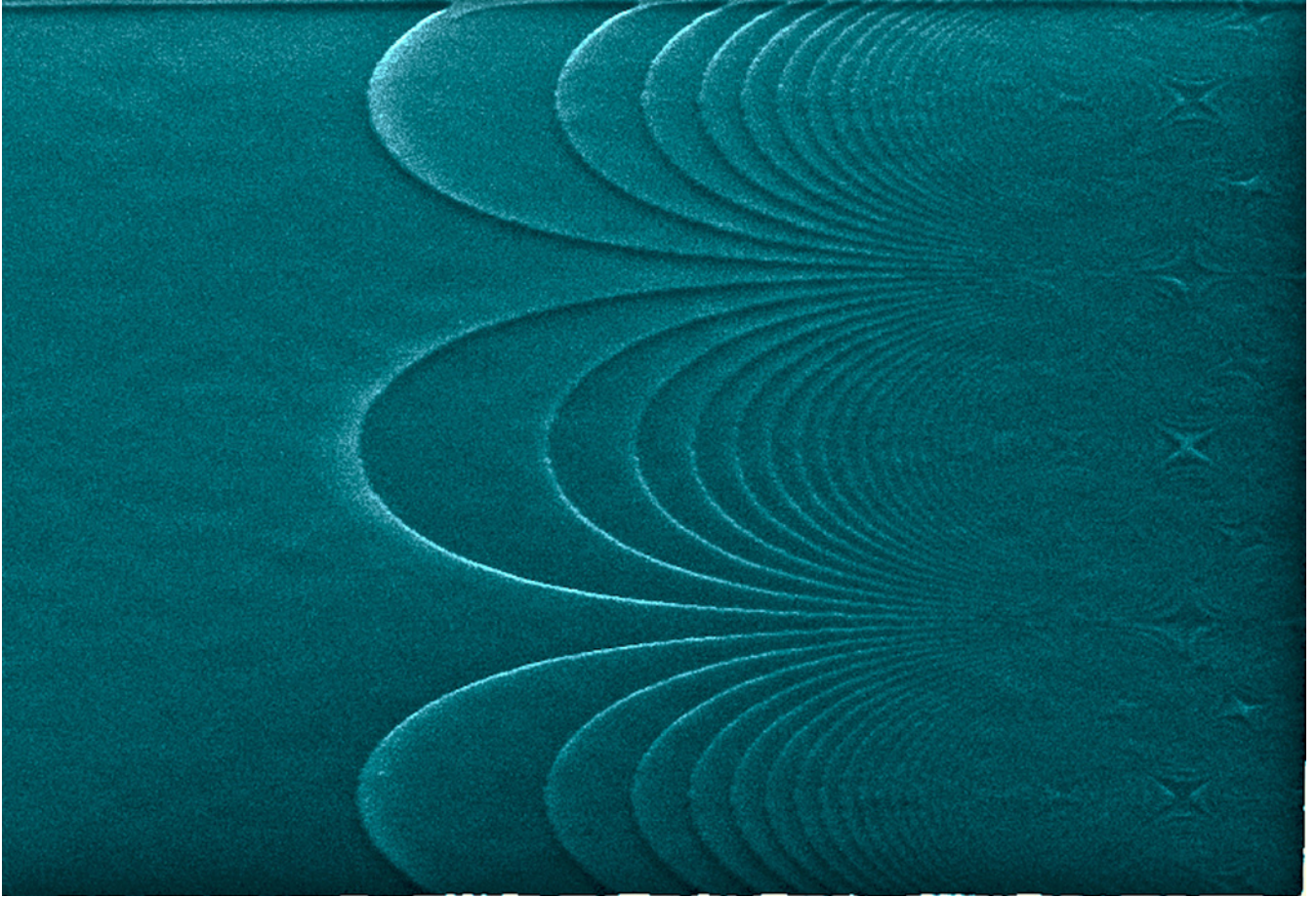


Laser & Photonics Rev 8, 785 (2014) [back cover]



Adv Mater 26, 6542 (2014) [back cover]






## **Projects & grants**

Cnr Nano research activity is mainly supported by funding obtained through competitive calls at different levels, from international to local.

Projects running in 2014-2015 are listed below with following details: project name, type of call, coordinator, Cnr Nano principal in investigator (if different), start and ending years, website (if available). Starred projects are currently run by former Cnr Nano scientists in their new Cnr Institute.

## European projects

 **AFM4NanoMed&Bio.** European network on applications of Atomic Force Microscopy to NanoMedicine and Life Sciences. COST Action TD1002. CNRS Marcoule, FR (P. Parot); Cnr Nano Modena (P. Facci). 2010-2014. <http://www.afm4nanomedbio.eu/home.aspx>

**COMANCHE.** Coherent manipulation and control of heat in solid-state nanostructures: the era of coherent caloritronics. FP7-IDEAS-ERC ERC-2013-CoG. Cnr Nano Pisa (F. Giazotto). 2014-2019.



**CRONOS.** Time dynamics and Control in nanostructures for magnetic recording and energy applications. UE FP7 NMP.2011.2.1-2. Trinity College Dublin, IE (S. Sanvito); Cnr Nano Modena (C. A. Rozzi). 2012-2015. <http://www.cronostheory.eu/>



**FLAGSHIP GRAPHENE.** Graphene-Based Revolutions in ICT and Beyond. FP7-ICT-2013.9.9. Chalmers Tekniska Högskola AB, SE (J. Kinaret); Cnr Nano Pisa (V. Tozzini). 2013-2016. <http://grapheneflagship.eu/>

**GRAFLEX** Graphene curvature, flexibility and reactivity control by means of external fields; theory and computer simulations. H2020-MSCA-IF-2014. Cnr Nano Pisa (V. Tozzini). 2015-2017.

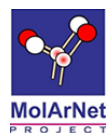
**INDEX.** Indirect Excitons: Fundamental Physics and Applications. FP7-PEOPLE-2011-ITN. CNRS. Cnrs & Université du Montpellier, FR (M. Vladimirova); Cnr Nano Modena (M. Rontani). 2011-2015. <http://indexitn.ges.univmontp2.fr/>

**\*IT-LIVER.** UE FP7-PEOPLE-2012-ITN. Fundacio Institut D'investigacio Biomedica De Bellvitge, ES (I. Fabregat); [former] Cnr Nano Lecce (S. Leporatti). 2013-2016.



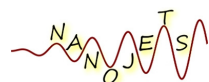
**MaX.** Materials design at the exascale. H2020-EINFRA-2015-1. Cnr Nano Modena (E. Molinari). 2015-2018. <http://www.max-centre.eu/>

**MODENADYNA.** MODeling Electron Non-Adiabatic DYNAMics. FP7-PEOPLE-2013-IIF. Cnr Nano Modena (C. A. Rozzi). 2015-2017.



**MOLARNET.** Molecular Architectures for QCA-inspired Boolean Networks. FP7-ICT-2011.9.6. Cnr Nano Lecce (R. Rinaldi). 2012-2016. <http://www.molarnet.eu/>

**MOQUAS.** Molecular Quantum Spintronics. FP7-ICT-2013.9.7. Cnr Nano Modena (M. Affronte). 2013-2016. <http://www.moquas.eu/>



**NANO-JETS.** Next-generation polymer nanofibers: from electrified jets to hybrid optoelectronics. FP7-IDEAS-ERC ERC-SG-PE8. Cnr Nano



Lecce (D. Pisignano). 2013-2018. <http://www.nanojets.eu/>



NANOREG. A common European approach to the regulatory testing of nanomaterials. FP7-NMP-2012-LARGE-6. Ministerie van Infrastructuur en Milieu-Dip. SCTM, NL (T. van Teunenbroek); Cnr Nano Pisa (G. M. Ratto). 2013-2016. <http://www.nanoreg.eu/>

\*POLAFLOW. Polariton condensates: from fundamental physics to quantum based devices. UE FP7-IDEAS-ERC ERC-SG-PE2. [former] Cnr Nano Lecce (D. Sanvitto). 2012-2017.

PHOSPHUN. Phosphorene functionalization: a new platform for advanced multifunctional materials. ERC Advanced Grant 2014 PE5. Cnr Iccom (M. Peruzzini) and Cnr Nano Pisa (S. Heun) 2015-2019.



Q-NET. Quantum-Nano-Electronics Training. FP7-PEOPLE-2010-ITN. Institut Néel-UJF, FR (H. Courtois); Cnr Nano Pisa (F. Giazotto). 2011-2015. <http://www.quantum-net.org/>



REDOX. Reducible oxide chemistry, structure and functions. COST ACTION CM1104. Universität Osnabrück, DE (M. Reichling); Cnr Nano S3 (P. Luches). 2012-2016. <http://www.cost-redox.nano.cnr.it/>

SOULMAN. Sound-Light Manipulation in the Terahertz. UE FP7-IDEAS-ERC ERC-AG-PE3. Università di Pisa, IT; Cnr Nano Pisa (A. Tredicucci). 2013-2018.

SuperMag. Cooperation between Superconductivity and Magnetism in Mesoscopic Systems: towards Majorana States. H2020-MSCA-IF-2014. Cnr Nano Pisa (F. Giazotto). 2015-2017.



TherMiQ. Thermodynamics of Mesoscopic Quantum Systems. FP7-ICT-2013-C. The Queen's University of Belfast, IE (M. Paternostro); Cnr Nano Pisa (G. M. Palma). 2014-2016. <http://www.thermiq2.eu/>

ULTRAQCL. Ultrashort Pulse Generation from Terahertz Quantum Cascade Lasers. UE H2020-FETOPEN-2014-2015-RIA. CNRS-LPA, FR (S. Dhillon); Cnr Nano Pisa (M. S. Vitiello). 2015-2018. <http://www.ultraqcl.eu/>

Understanding and Controlling Nano and Mesoscale Friction. MPNS COST ACTION MP1303. Università degli Studi di Milano, IT (N. Manini); Cnr Nano Modena (G. Paolicelli). 2013-2017. <http://www.nanofriction.org/>

## National projects

Assessing protein system dynamics and thermodynamics: a novel NMR approach at single-residue resolution. PRIN 2012. Università degli Studi di Udine (G. Esposito); Cnr Nano Modena (S. Corni). 2014-2017.

Caloritronica coerente in sistemi mesoscopici a superconduttore. FIRB FR 2013. Cnr Nano Pisa (C. Oriol Altimiras Martin). 2014-2017.

Computer modeling and simulation of nucleic acids structure and dynamics. MAE Progetti Canaletto Italia-Polonia. Cnr Nano Pisa (V. Tozzini). 2013-2015.

Dispositivi ibridi a base di grafene e nanomagnetici molecolari per la lettura del singolo spin. MIUR FIRB Futuro in ricerca 2012. Cnr Nano Modena (A. Candini). 2014-2017.

Effetti della manipolazione della via di trasduzione ERK sulla plasticità strutturale della via cortico-striatale in vivo mediante microscopia a due fotoni. PRIN 2008. Cnr Nano Pisa (G. M. Ratto). 2010-2014.

\*EFOR. Energie da fonti rinnovabili. Progetto interdipartimentale Cnr. [former] Cnr Nano Lecce (G. Gigli). 2011-2014.

FLASHit. Unraveling ultra-fast photo-induced phenomena at the nanoscale: a joint theoretical and experimental approach. RBFR12SWOJ. MIUR Firb Futuro in Ricerca 2012. University of Rome Tor Vergata (A. Marini); Cnr Nano Modena (D. Prezzi). 2013-2016.

FRONTERA. Ricerca fondamentale sui dispositivi fotonici innovativi operanti nella regione spettrale Terahertz. Firb Futuro In Ricerca 2010. Cnr Nano Pisa (M. S. Vitiello). 2012-2015.

GRAF. Frontiere della ricerca sul grafene: comprensione e controllo di funzionalità avanzate. PRIN 2010-2011. University of Trieste (A. Morgante); Cnr Nano Pisa (V. Pellegrini). 2013-2016.

MEMO. Imaging Metallorganic Molecules: Scanning tunneling spectroscopy and many-body theory. PRIN 2012. Università del Salento (G. Maruccio); Cnr Nano Modena (M. Rontani). 2014-2017.

MERIT. Nanofibre biomedicali per ingegneria tissutale basata su cellule staminali renali. FIRB MERIT. Cnr Nano Lecce (D. Pisignano). 2011-2014.

MILES. Mild Infrared Laser System. MIUR-FAR Cnr Pisa (M. Tonelli) 2012-2015.

Nanoelettronica quantistica per le tecnologie delle informazioni. MAE Italia-Canada. Cnr Nano Pisa (S. Heun). 2014-2015.

Nanofibre polimeriche attive multifunzionali per la fotonica e l'elettronica. FIRB Futuro in Ricerca 2008. Cnr Nano Lecce (D. Pisignano). 2010-2014.

Nuove sfide nel nanomagnetismo molecolare (RBFR12RRPD1). MIUR Firb Futuro in Ricerca 2012. University of Parma (S. Carretta); Cnr Nano Modena (A. Ghirri). 2013-2016.

Ossidi nanostrutturati: multifunzionalità e applicazioni (RBAP115AYN). MIUR FIRB. University of Milano Bicocca (G. Pacchioni); Cnr Nano Modena (S. Valeri). 2012-2015.

PLASMOGRAPH. Plasmons and Terahertz devices in graphene. FIRB Futuro in Ricerca 2010. Cnr Nano Pisa (M. Polini). 2011-2014. <http://www.plasmograph.it/>

## Cnr projects

Nano Brain. Progetto Bandiera Nanomax, Cnr Nano Pisa (G. M. Ratto). 2014-2016.

Organic Electronics for innovative research instrumentation. Progetto premiale Cnr. Cnr Nano Modena (A. Calzolari). 2012-2015.

QUANTOM. Quantum-opto-mechanics. Progetto premiale Cnr. Cnr Nano Pisa (A. Tredicucci). 2012-2015.

Abnanotech. Atom-based Nanotechnology. Progetto premiale Cnr. Cnr Nano Pisa (M. Polini). 2012-2015.

High Mobility Graphene monolayer for novel quantum devices bilateral project. Cnr Bilateral projects. CNR JSPS, JP; Cnr Nano Pisa (S. Heun). 2014-2015.

SPM Investigations of superconducting hybrid systems. Cnr Bilateral Projects. CNR-CNRS, FR; Cnr Nano Pisa (F. Giazotto). 2015-2016.

Semiconductor Nanowires: from fundamental studies to innovative devices. Cnr Bilateral Projects. CNR-RFBR, RU; Cnr Nano Pisa (L. Sorba). 2015-2017.

Tuning correlated transport and localization in low dimensional electron systems with spin orbit interaction. Cnr Bilateral Projects. CNR-RFBR, RU; Cnr Nano Pisa (S. Roddaro). 2015-2017.

## Regional projects

AMIDERHA. Sistemi avanzati mini-invasivi di diagnosi e radioterapia. MIUR MSE PON FSE. Cnr Nano Pisa (R. Rinaldi). 2012-2015.

\*BEYOND-NANO. Materials and processes BEYOND the NANO scale. MIUR MSE PON FSE. [former] Cnr Nano Lecce (G. Gigli). 2012-2014. <http://www.ponrec.it/open-data/progetti/scheda-progetto?ProgettoID=5362>

FLIMFLOW. Fluorescence lifetime multiplex flow cytometry system. Biophotonics Plus Joint Initiative. Regione Toscana. Seco S.r.l.; Cnr Nano Pisa (R. Bizzarri). 2014-2016. <http://www.biophotonicsplus.eu/>

GR-2011-0235-1049. Min. Salute: Bando 2011-2012 Progetti Giovani Ricercatori. Regione Toscana. Cnr Nano Pisa (R. Bizzarri). 2014-2017.

\*MAAT. Molecular Nanotechnology for Health and Environment. MIUR MSE PON FSE. Dhithec; [former] Cnr Nano Lecce (G. Gigli). 2012-2015.

\*NAMISTE. Nanomateriali per l'edilizia sostenibile. MIUR MSE POR FSE. Lorusso Vergara; [former] Cnr Nano Lecce (G. Ciccarella). 2012-2014.

RINOVATIS. Activating RINOVATIS: Ingegneri Innovatori/Imprenditori specializzati in tecnologie e metodologie della Tissue Engineering. MIUR MSE PON FSE. Dhithec; Cnr Nano Lecce (R. Rinaldi). 2012-2015. <http://www.ponrec.it/open-data/progetti/scheda-progetto?ProgettoID=5804>

SAFE & SMART. Nuove tecnologie abilitanti per la food safety e l'integrità delle filiere agro-alimentari in uno scenario globale. PON. Dipartimento Agroalimentare CNR; Cnr Nano Lecce (R. Rinaldi). 2013-2015.

SAFEMEAT. Innovazioni di processo e di prodotto per incrementare i profili di sicurezza e per diversificare la gamma dei prodotti (freschi e stagionati) a base di carne suina. Regione Puglia. Cnr Dipartimento Agroalimentare; Cnr Nano Lecce (R. Rinaldi). 2011-2014.

SOCIAL-NANO. Cluster di innovazione sociale mediante piattaforma nanotecnologica cross-disciplinare per il monitoraggio ambientale e l'healthcare. PON Start-up. Cnr Nano Lecce (L. Persano). 2013-2015.

\*VINCENTE. Un ambiente virtuale di "Collective Intelligence" abilitante lo sviluppo di ecosistemi per l'impreditorialità tecnologica sostenibile. MIUR MSE PON FSE

PON02\_00563\_3470993. Dhithec; [former] Cnr Nano Lecce (G. Gigli). 2012-2015. <http://www.ponrec.it/open-data/progetti/schedaprogetto?ProgettoID=5805>

## Other funding agencies

Meccanismi biomolecolari nella malattia di Krabbe: utilizzo di tecniche nano-biofisiche innovative per l'individuazione di nuovi target terapeutici. Fondazione Cassa di Risparmio di Lucca. Cnr Nano Pisa (M. Cecchini). 2012-2016.

Quantum Properties of Molecular Nanomagnetism. AOARD. Cnr Nano Modena (M. Affronte). 2013-2015.

Role of dysregulated astrocyte-GABAergic interneuron interactions in the control of seizures in monogenic models of epilepsy. Fondazione Telethon. Cnr Nano Pisa (G. M. Ratto). 2012-2015.

Sviluppo di materiali e trattamenti/ricoprimenti superficiali per componenti metalliche esposte ad ambienti aggressivi. Fondazione Cassa di Risparmio di Modena "Bando Ricerca Applicata 2013/2014". Cnr Nano Modena (S. Valeri). 2014-2016.

Unravelling the Rett syndrome: effects of MeCP2 mutations on synaptic function. Fondazione Telethon. Cnr Nano Pisa (G. M. Ratto). 2013-2016. <http://www.telethon.it/en/funding-research/fundedprojects/details/unravelling-the-rett-syndrome-effects-of-mecp2-mutations-on-synaptic-function>

**2014-2015 funding chart.**  
**Incoming funding sorted as from different kind of grants (in €).**



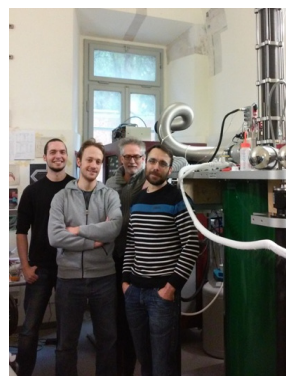




## Cnr Nano events in 2014

### January | COMANCHE awarded with ERC Grant

Francesco Giazotto from Cnr Nano Pisa has been awarded an ERC Consolidator Grants, the European Research Council funding frame dedicated to mid-career excellent researchers. Giazotto's project COMANCHE (COherent MANipulation and Control of HEat in solid-state nanostructures) aims at investigating the effects of control, measure, distribution and conversion of heat in nanoscale devices. The researcher proposes an original approach to set the experimental ground for the investigation and implementation of a new branch of science, the “coherent caloritronics”, which wants to take advantage of quantum circuits to phase-coherently manipulate and control the heat current in solid-state nanostructures.



### February-June | Meet the scientists

A successful science-café series, “Scienza in Centro” (Science Downtown), started with a renewed schedule and topics: a chance for the general public to meet researchers and experts in a non-academic way and to informally share curiosity, experience and knowledge. Organized by Cnr Nano Lecce, talks topics ranged from cosmic rays, to Higgs boson, to genetic diseases and hosted, in different public spaces, Cnr Nano scientists and renowned external experts.



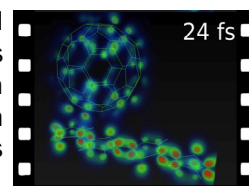
### March | Coffee with graphene

A unique dissemination event took place in Genoa in a very unusual place: a pastry shop. Valentina Tozzini and Vittorio Pellegrini from Cnr Nano Pisa met the general public for a Science Café to illustrate graphene's superior properties. They also had the opportunity to grow public awareness on the Graphene Flagship, a new European-funded initiative of unprecedented scale, that intends to bring graphene out of the realm of academic laboratories into everyday life.



### May | When light turns into electricity

How does the transformation of sunlight into electrical current work in an organic solar cell? Cnr Nano researchers and collaborators created a movie of this pivotal process in real time, on an unprecedented scale: millionths of a billionth of a second. The news was broadcasted on national news channels. [Science 344, 1001 (2015)].





## June | FareFisica 2014

The one-week full-time summer school FareFisica took place at the Department of Physics of the University of Modena and Reggio Emilia and the Cnr Nano laboratories, allowing about 100 high-school students to attend guided activities at the research laboratories, lectures, educational seminars and meetings with both researchers and professionals in the main industrial sectors. Living in close contact with campus life and carrying out short research projects, participants had the opportunity to get in contact with a real "science research experience" and become familiar with the main research techniques.



## July | Single molecule cooler: how cool!

The work from a Cnr Nano team in collaboration with University of Modena, using the SOLEIL-Synchrotron DEIMOS beamline to investigate Gadolinium based materials (Gd4M8) deposited on a gold surface, was highlighted on the SOLEIL Synchrotron Facility newsletter. Researchers report a really efficient cooling systems at cryogenic temperatures, i.e., below  $-150^{\circ}\text{C}$ . They observed that the deposition process did not alter the electronic, magnetic and thermodynamic properties of the molecules, opening the way for exploitable cooling processes at molecular level.

## July | At school in beautiful Erice



The International school on the Physics of Indirect Excitons took place in Ettore Majorana Foundation and Centre for Scientific Culture (EMFCSC) in Erice (IT), from July 26 to August 1, 2014. The event, organized by Cnr Nano in the frame of the Marie Curie ITN Index, addressed topics as the fundamental physics of cold bosons in solid state materials, novel principles for optoelectronic devices, new systems with indirect excitons. It was attended by more than 40 PhD students from Europe and US. Lectures were held by Cnr Nano researchers, such as M. Rontani, E. Molinari, V. Pellegrini, and some of the most prominent professors in the field. The students were also given the chance to visit this beautiful part of Sicily.

## August | Giuseppe Occhialini Prize



The Italian Physical Society (SIF) and the Institute of Physics (IOP) awarded Alessandro Tredicucci from Cnr Nano and the University of Pisa with the "Giuseppe Occhialini" Prize. Dr Tredicucci received the prize "for his innovative contributions to the realisation of terahertz heterostructure devices". The prize is announced on an annual basis alternatively by the SIF and IOP, to award a physicist based in Italy or in the UK-Ireland, in recognition of distinguished work in Physics research carried out within the past 10 years.

## September | Nanotechnologies go to school

From research laboratories to the school labs, nanoscience goes to school. The book “Alla scoperta delle nanotecnologie” (Discovering nanotechnologies, Zanichelli editore), written by Guido Goldoni and Valentina De Renzi of the University of Modena and Reggio Emilia and Cnr Nano, along with Annamaria Lisotti, high-school teacher and PhD, is the first Italian school book that introduces nanoscale physics in the curricula of high schools. A real innovative educational project proposing experiments with gold nanoparticles, shape-memory metals and liquid marbles based on a fully 'hands-on' approach.



## September | Researchers' Night in Lecce



Cnr Nano Lecce took part in the Researchers' Night, the widest European popular science event, with a number of activities. On Sept. 26 from 6 to 12 pm, in the historical former convent Olivetani, researchers from Cnr Nano presented to a non-specialized audience their activities and the latest research results in nanotechnology developed in our labs.

## October | Meet me at MoQuaS

On October 22 scientists active in MoQuaS, a FP7 FET-OPEN project dedicated to molecular quantum spintronics, met in Modena for the project's first annual meeting. The MoQuaS coordinator Prof. Affronte and the partners discussed their ongoing works in the field of Molecular Quantum Spintronics.

## Cnr Nano events in 2015

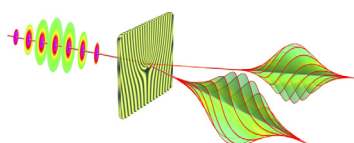
### January | Yambo Hands on the code

The third edition of the hands-on tutorial dedicated to Yambo, an open-source ab-initio code now adapted for massively-parallel computing architectures, took place in Lausanne (CH) from 13 to 17 April. The 5-day Cecam school event, organized and tutored by Cnr Nano and other European research centres, provided training to more than 30 students in the theory and practice of computing electronic and optical excitations within density functional and Green's function approaches as well as the application of these techniques to the study of realistic and challenging systems using the Yambo code.



### February | Electron beam with a twist

V. Grillo, S. Frabboni, and G. C. Gazzadi's PRL paper has been selected by Physics, the daily selection of papers from the APS journal collection. Their article 'Big Twist for Electron Beam' explains how the Cnr Nano researchers and others generated an electron beam with very high orbital angular momentum, suitable to study magnetism in materials and for other fundamental research. [PRL 114, 034801 (2015)].



## February | Talking of ourselves

By this time of the year two series of seminars called "Colloquia 2015" were in full swing both in the Pisa and Modena units. Cnr Nano Colloquia are delivered periodically by our researchers in order to inform their colleagues in the Cnr Nano scientific community about their ongoing research, in order to foster collaborations, develop new connections and boost the sense of belonging to a lively and groundbreaking scientific institute. Seminars are always video broadcasted to the other Cnr Nano units, so that they can help the spreading of new ideas and common projects.

## March | SPIE award

Congratulations to Miriam S. Vitiello for winning the prestigious annual Early Career Achievement Award of SPIE, the international society for optics and photonics. The award recognizes outstanding individual and team technical accomplishments. Miriam's Early Career Achievement Award motivation recognizes "her outstanding results in research on semiconductor laser sources and electronic high frequency nanodetectors which have opened new frontiers in the Terahertz photonics and optoelectronics fields".



## June | Accademia dei Lincei young physicists award



Accademia dei Lincei has awarded Alessandro Pitanti from Cnr Nano with the annual "Alfredo Di Braccio" award, dedicated to young physics researchers with outstanding curricula and publications. Alessandro, PhD in Physics, after a post-doc at the Scuola Normale Superiore and Cnr Nano, spent two years (2012-2014) as a Marie Curie Fellow at Caltech (in professor Oskar Painter's group) in the framework of Nemo project. He is now back at Cnr Nano and his research is focused on the study of interaction and control of nanomechanical devices with electromagnetic fields through radiation pressure.

## July | Nano goes social

In order to collect results and discuss the future development of the interdisciplinary project of technological innovation SOCIAL-NANO, the workshop Nanotechnology for environmental monitoring and healthcare, was organized on July 29 in Lecce. In the first two years of activity the goal of SOCIAL-NANO was to organize an interdisciplinary team of government agencies and companies, able to find new production areas in the field of nanotechnology relevant for social and economic growth of the territory. The project coordinated by Cnr Nano developed a nanotechnology platform for the environmental particle monitoring and for the controlled release of chemotherapeutic drugs based on advanced nanotechnology.





### July | A successful Fosforene Day

A successful Fosforene Day was held in Florence on July 17, when a workshop dedicated to Phosphorene, the novel material similar to graphene, brought together more than fifty physicists and chemists to discuss research and innovation opportunities related to the "youngest" among the two-dimensional graphene's cousin materials. Despite a scorching day, a large and eager audience attended the meeting in which researchers reviewed the Italian activities on Phosphorene in order to inspire new collaborations. The meeting showed the Italian research community's advanced skills in this field.



### September | A bright night in Flatland



"Benvenuti a Flatlandia" (Welcome to Flatland) was written of the booth dedicated to graphene and 2D-materials set up by Cnr Nano researchers in downtown Pisa for the Researchers' Night event. From September 16 to 22, the Flatlandia booth was crowded with citizens, families and kids who had the chance to be introduced to graphene's incredible features by Cnr Nano, Scuola Normale Superiore and IIT researchers. This event was organized in the frame of the European Researchers' Night.

### September | Bessel award to Vincenzo Grillo

Cnr Nano researcher Vincenzo Grillo is one of the recipients of the prestigious international research award Friedrich Wilhelm Bessel. Grillo was honoured with the award for his studies on phase holograms, in particular his research on the development of new HRTEM and STEM-HAADF techniques. The Friedrich Wilhelm Bessel award, annually granted by the Alexander von Humboldt Foundation, is addressed to mid-career researchers whose ideas have a relevant future development potential. The award includes a 6 to 12 month research grant to spend in a research institution in Germany.



**Alexander von Humboldt**  
Stiftung / Foundation

### December | Driving the future materials design



Its name is MaX, it is coordinated by Cnr Nano in Modena (prof. E. Molinari), and it is the new European infrastructure for the simulation and supercomputing dedicated to designing new materials. On December 14-15 at MaX (Materials at the eXascale) kick off all 13 partners met to start working on the Centre's task: the design and development of a new application and data ecosystem, aimed at serving industrial and academic community through end-user oriented actions. MaX is one of the 8 European Centers of Excellence for HPC applications supported by the EU under its H2020 e-INFRA-2015 call.



**People**

## **Cnr Nano researchers**

Alessandra Aloisi  
Valerio Bellini  
Stefania Benedetti  
Andrea Bertoni  
Ranieri Bizzarri  
Francesco Bonaccorso  
Giorgia Brancolini  
Arrigo Calzolari  
Andrea Camposeo  
Andrea Candini  
Riccardo Castagna  
Fabrizio Castellano  
Alessandra Catellani  
Marco Cecchini  
Giovanni Checcucci  
Stefano Corni  
Valdis Corradini  
Fabio Della Sala  
Antonio Della Torre  
Alessandro di Bona  
Rosa Di Felice  
Eduardo Fabiano  
Paolo Facci  
Riccardo Farchioni  
Andrea Ferretti  
Gian Carlo Gazzadi  
Francesco Ghetti  
Alberto Ghirri  
Francesco Giazotto  
Vincenzo Grillo  
Stefan Heun  
Paola Luches  
Maria Moffa  
Daniel Navarro Urrios  
Riccardo Nifosì  
Guido Paolicelli  
Daniela Parisi

Teresa Pellegrino  
Luana Persano  
Marco Pieruccini  
Alessandro Pitanti  
Stefano Pittalis  
Marco Polini  
Deborah Prezzi  
Gian Michele Ratto  
Stefano Roddaro  
Massimo Rontani  
Carlo Andrea Rozzi  
Antonella Sgarbossa  
Lucia Sorba  
Elia Strambini  
Fabio Taddei  
Andrea Tomadin  
Valentina Tozzini  
Filippo Troiani  
Daniele Varsano  
Stefano Veronesi  
Alessandro Vezzani  
Miriam Serena Vitiello

## **Cnr Nano post-docs**

Zoobia Ameer  
Sara Antonini  
Tony John G. Apollaro  
Valentina Arcadio  
Andrea Arcangeli  
Lorenzo Baldacci  
Daniel Balleza Mejia  
Matteo Barborini  
Antonella Battisti  
Federica Bianco  
Christophe Blanc  
Giovanni Borghi  
Maria Camarasa Gomez  
Vito Dario Camiola

Matteo Carrega  
Domizia Chericoni  
Silvia Colella  
Piero Cosseddu  
Sophie D'Ambrosio  
Francesco De Feo  
Pompilio Del Carro  
Alain Delgado Gran  
Antonella De Pasquale  
Riccardo Di Corato  
Flavia Viola Di Girolamo  
Marco Esposito  
Omid Faizy Namarvar  
Paolo Fantuzzi  
Gianmarco Ferri  
Gabriel José Gil Perez  
Enrico Gualtieri  
Valentino L. P. Guerra  
Karina A. Guerrero Becerra  
Elena Husanu  
Radoslaw Jurga  
Khatuna Kakhiani  
Silvia Landi  
Savio Laricchia  
Giacomo Levita  
Nadia Ligato  
Rita Manco  
Andrea Mari  
Simone Marocchi  
Margherita Marsili  
M. Jose Martinez Perez  
Leonardo Martini  
Luca Masini  
Rosanna MASTRIA  
Giovanni Morello  
Yuya Murata  
Jonna Marika Paajaste  
Riccardo Parra  
Claudia M. Pereira Cardoso



Iolanda Pio	Annalisa Bonfiglio	Stefano Ossicini
Silvio Pipolo	Paolo Bordone	Gioacchino Massimo Palma
Nicola Poccia	Carlo Augusto Bortolotti	Vittorio Pellegrini
Elisabetta Primiceri	Rossella Brunetti	Pasqualantonio Pingue
Maria Clelia Righi	Marilia Junqueira Caldas	Dario Pisignano
Luigi Romano	Franco Carillo	Vincenzo Resta
Alberto Ronzani	Alberto Carlini	Angelo Rettori
Habib Rostami	Giovanni Carlotti	Rosaria Rinaldi
Alberto Rota	Carlo Cavazzoni	Davide Rossini
José Francisco Saenz Cogollo	Ciro Cecconi	Alice Ruini
Anna Giovanna Sciancalepore	Francesco Ciccarello	Marco Sola
Ilaria Siloi	Giancarlo Cicero	Thomas Szkopek
Szymon Smiga	Roberto Cingolani	Alessandra Toncelli
Giulia Lia B. Spampinato	Renato Colle	Mauro Tonelli
Davide Spirito	Sergio D'Addato	Giovanni Tosi
Barbara Storti	Valentina De Renzi	Alessandro Tredicucci
Sebastian Sulis Sato	Elena Degoli	Sergio Valeri
Wenming Sun	Umberto del Pennino	Tiziano Verri
Aleksandrs Terentjevs	Alberto Di Lieto	Cristiano Viappiani
Chiara Cristina Toma	Daniele Ercolani	Michele Virgilio
Karsten Leding Vendelbjerg	Rosario Fazio	Giampaolo Zuccheri
Leonardo Viti	Mauro Ferrario	
Shudong Wang	Stefano Frabboni	
Jihua Xu	Alessandro Fraleoni Morgera	
Laura Zanetti Polzi	Anna Maria Garbesi	
Valentina Zannier	Guillaume Gervais	
Alessandra Zizzari	Vittorio Giovannetti	
Alessandra Zucca	Guido Goldoni	

### Affiliated researchers

Stefania Abbruzzetti	Sara Invitto	Gerardo Abbandonato
Marco Affronte	Carlo Jacoboni	Pietro Artoni
Andrea Alessandrini	Alessandro Lascialfari	Luca Bellucci
Carles Oriol Altimiras Martin	Stefano Luin	Enrico Benassi
Mario Amado Montero	Rita Magri	Marco Brondi
Fabio Beltram	Franca Manghi	Michele Campisi
Carlo Maria Bertoni	Diego Marchetto	Alessandro Cannavale
Roberto Biagi	Claudia Menozzi	Claudia Carlucci
	Elisa Molinari	Pino D'Amico
	Umberto Muscatello	Mariagrazia Di Luca
		Lorenzo Dominici
		Elena Favilla
		Salvatore Gambino
		Andrea Gamucci
		Andrea Iagallo

### Affiliated post-docs

Andrea Listorti  
Alberto Lodi Rizzini  
Laura Marchetti  
Elisabetta Marulli  
Leonardo Mazza  
Domenico Montemurro  
Victor Mukherjee  
Michele Nobile  
Francesca Pederzoli  
Francesco M. D. Pellegrino  
Francesco Rossella  
Miguel Royo Valls  
Cayetano Sanchez-Fabres C.  
Elisabetta Tarentini  
Ilaria Tonazzini  
Valerio Voliani  
Shaohua Xiang  
Simone Zanotto

### **Affiliated PhD students**

Matteo Agostini  
Gaelle Françoise Arnaud  
Michael Ontita Atambo  
Simone Barbarino  
Martina Basini  
Francesco Benedetti  
Luca Bergamini  
Alberto Biella  
Claudio Bonizzoni  
Luca Bursi  
Mariafrancesca Cascione  
Tommaso Cavallucci  
Luigi Cigarini  
Marzio De Corato  
Giacomo De Palma  
Ambra Del Grosso  
Alessandro Farace  
Gabriele Gasperi

Umesh Prasad Gomes  
Federico Grasselli  
Michele Guerrini  
Stefano Guiducci  
Nicholas Hemsworth  
Abhishek Kumar  
Simone Ierinò  
Stefano Lumetti  
Erfan Mafakheribashmagh  
Giulia Marianetti  
Maria Celeste Maschio  
Cecilia Masciullo  
Francesco Mazza  
Guido Menichetti  
Sandro Meucci  
Mohsin Mubarak Naqvi  
Jacopo Stefano Pelli Cresi  
Alberto Portone  
Enrico Pracucci  
Lorenzo Romeo

Marta Rosa  
Mattia Sacchi  
Elisabetta Serpini  
Punam Sonar  
Maria Chiara Spadaro  
Marco Travagliati  
Francesco Trovato  
Ilaria Valenti  
Stefano Valentini  
Federico Venturi  
Anna Vianelli  
Azzurra Volpi

### **Administrative staff**

Maria Grazia Angelini  
Sara Barsotti  
Elisa Bolognesi  
Tommaso De Carlo

Luca Del Prete  
Sandro Guerrazzi  
Carmela Iannotta  
Diletta Miceli  
Patrizia Pucci  
Anna Grazia Stefani  
Ciro Urso

### **Technical staff**

Davide Calanca  
Giorgio Casalini  
Mariangela Margarito  
Luisa Neri  
Riccardo Pallini  
Silvia Rizzo  
Maddalena Scandola

### **Former NNL members**

Gianluca Accorsi  
Francesco Amato  
Valentina Arima  
Dario Ballarini  
Eleonora Bellini  
Monica Bianco  
Mariano Biasiucci  
Laura Blasi  
Francesco Calabi  
Agostina Lia Capodilupo  
Davide Caputo  
Sonia Carallo  
Luigi Carbone  
Paolo Cazzato  
Maria Serena Chiriaco  
Giuseppe Ciccarella  
Barbara Cortese  
Pantaleo Davide Cozzoli  
Massimo Cuscunà

Eliana D'Amone  
 Stefania D'Amone  
 Maria Luisa De Giorgi  
 Milena De Giorgi  
 Gianvito De Iaco  
 Loretta L. del Mercato  
 Massimo De Vittorio  
 Stefano Donati  
 Gianmichele Epifani  
 Marzia Maria Ferraro  
 Antonio Fieramosca  
 Vittorio Federico Fiorelli  
 Antonio Gaballo  
 Carlo Giansante  
 Antonio Domenico Gigante  
 Giuseppe Gigli  
 Nemany A. Nemany Hanafy  
 Stefano Leporatti  
 Giovanni Lerario  
 Vincenzo Maiorano  
 Federica Mangione  
 Diego Mangiullo

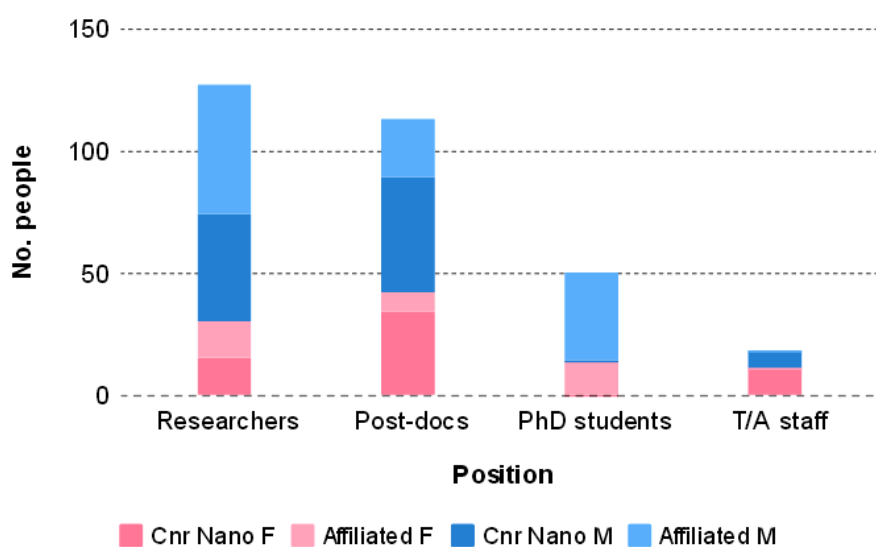
Giuseppe Maruccio  
 Sofia Masi  
 Marco Mazzeo  
 Concetta Nobile  
 Ilaria Elena Palamà  
 Adriana Grazia Passaseo  
 Elisabetta Perrone  
 Alessandra Quarta  
 Aurora Rizzo  
 Maria Giovanna Santoro  
 Daniele Sanvitto  
 Concita Sibilia  
 Blanca Silva Fernandez  
 Daniela Simeone  
 Vittorianna Tasco  
 Maria Teresa Todaro  
 Francesco Todisco  
 Viviana Vergaro  
 Valeria Videtta  
 Ilenia Viola  
 Antonella Zacheo  
 Alessandro Zammillo

Gabriella Zammillo

### Support staff in Genova

Matilde Bolla  
 Barbara Cagnana  
 Enrico Camauli  
 Marco Campani  
 Paola Corezzola  
 Monica Dalla Libera  
 Roberta De Donatis  
 Fabio Distefano  
 Francesca Fortunati  
 Maria Carla Garbarino  
 Giuseppe Genovese  
 Danilo Imperatore  
 Tatiana Marescalchi  
 Elisabetta Narducci  
 Marco Punginelli  
 Liliana Sciaccaluga  
 Simone Spinozzi

### Gender balance in Cnr Nano people 2014-2015



# Contacts



Piazza San Silvestro, 12

I-56127 Pisa, Italy

ph. +39 050 509525



Piazza San Silvestro, 12

I-56127 Pisa, Italy

ph. +39 050 509525



Via Arnesano

I-73100 Lecce, Italy

ph. +39 0832 298205



Via Campi, 213A

I-41125 Modena, Italy

ph. +39 059 2055629

## Credits

Cover image	GaAs nanowires grown by chemical beam epitaxy. Courtesy of Valentina Zannier (Cnr Nano Pisa); artwork Lucia Covi.
Pag. 5	Graphene nanoribbon device for scanning gate microscopy studies. Courtesy of Lennart Bours and Stefan Heun (Cnr Nano Pisa).
Pag. 31	Nanofabricated phase hologram mask. Courtesy of Gian Carlo Gazzadi (Cnr Nano Modena); artwork Lucia Covi.
Pag. 63	Human neuroblastoma cells (tubulin in green, actin in red, nuclei in blue). Courtesy of Ilaria Tonazzini (Cnr Nano Pisa).
Pag. 95	Nanofabricated phase hologram mask. Courtesy of Gian Carlo Gazzadi (Cnr Nano Modena); artwork Lucia Covi.

